Doctoral school: Science of Matter, Radiation and Environment
Discipline: Optics and Lasers, Physical Chemistry, Atmosphere

Doctoral dissertation

Characterization of wood pellets combustion for clean energy generation

By

Xiangyu ZHU

Reviewers:

Sylvana De Iullis, Research director, National Research council-CNR, Milan, Italy

Jean-François Brilhac, Professor, University of Haute-Alsace, France

Examiners:

Guillaume Legros, Professor, University of Orléans, France (president of the jury)

Sébastien Caillat, Doctor, Fives Stein, Maisons-Alfort, France

Moinul Hossain, Assistant Professor, University of Kent, UK

Supervisors:

Eric Therssen, Professor, University of Lille, France

Céline Morin, Professor, University of Polytechnique Hauts-de-France, France

Yong Yan, Professor, University of Kent, UK

Invited member:

Eric Delacourt, Assistant Professor, University of Polytechnique Hauts-de-France, France

Laboratory of Physico-Chemistry of Combustion Processes and the Atmosphere (PC2A) - France

Laboratory of Automation, Mechanics and Industrial and Human Computing (LAMIH) – France

School of Engineering - University of Kent - UK

Defended the 12th May 2023

École doctorale : Sciences de la Matière, du Rayonnement et de l'Environnement
Spécialité: Optique et Lasers, Physico-Chimie, Atmosphère

Thèse de doctorat

Caractérisation de la combustion de pellets de bois pour la production d'énergie propre

Par

Xiangyu ZHU

Rapporteur et Rapportrice:

Sylvana De Iullis, Directeur de recherche, Conseil National de la Recherche-CNR, Milan, Italie

Jean-François Brilhac, Professeur, Université de Haute-Alsace, France

Examinateurs:

Guillaume Legros, Professeur, Université de Orléans, France (président du jury)

Sébastien Caillat, DocteuThèse de doctoratr, Fives Stein, Maisons-Alfort, France

Moinul Hossain, Maître Assistant, Université de Kent, UK

Directeurs et Directrice:

Eric Therssen, Professeur, Université de Lille, France

Céline Morin, Professeur, Université de Polytechnique Hauts-de-France, France

Yong Yan, Professeur, Université de Kent, UK

Membre invité:

Eric Delacourt, Maître Assistant, Université de Polytechnique Hauts-de-France, France

Laboratoire de Physico-Chimie des Processus de Combustion et de l'Atmosphère (PC2A) - France

Laboratoire d'Automatique, de Mécanique et d'Informatique Industrielles et Humaines (LAMIH) - France

École d'ingénieurs - Université de Kent - UK

Soutenue le 12 mai 2023

Acknowledgements

I would like to offer my gratitude and appreciation to everyone who have helped me with this study in various ways.

First of all, I would like to thank the I-SITE Université Lille Nord-Europe for funding this Ph.D. project.

I would like to thank Prof. Eric Therssen, Prof. Yong Yan and Prof. Céline Morin. I am honored to be one of their Ph.D. students. I appreciate all of their contributions of time, ideas and their guidance to this work. This work would not have been done without their dedication and support.

Special thanks go to Dr. Eric Delacourt and Francois Delcourt for their selfless help and valuable advice during the experiments, for all the scientific discussions, and for all their support over the past three years.

Big thanks to Prof. Benjamin Hanoune (director of the PC2A lab.) and Prof. Laurent Dubar (director of the LAMIH lab.) for all the help concerning the administrative procedures, and for all the useful advice.

Many thanks to Fabrice Cazier, Dorothée Dewaele and Paul Genevray from CCM for their help with emissions measurements in the flame and data processing.

Many thanks to Denis Petitprez, Sylvie Gosselin and Valentine Bizet from PC2A for their help with the SMPS measurement.

Thanks to Amaury Lahccen, Maximilien Blanc, Pin Chen, and Qin Li for helping me so many times.

I'd like to thank all the people in the laboratory LAMIH, PC2A and Instrumentation and Control Group at the University of Kent. Without them, I would never have been able to complete this thesis.

Finally, I would like to thank my friends and family who silently supported me, because of you, I could persist in completing this research. Thanks to my parents for their understanding and tolerance. Thanks to my wife for her help and encouragement. Thanks also to my two lovely daughters, Alice and Chloé.

Abstract

As the 4th largest global primary energy carrier following fossil fuels (coal, oil and natural gas), biomass is the most abundant renewable energy source on earth. Among all the biomass conversion technologies, the direct burning of biomass for heat and power generation is the most common and cost-effective route to turn biomass into energy. Natural wood biomass is widely used as an alternative to fossil fuels to reduce atmospheric emissions from heat and power generation in the UK, France and the rest of the world. Meanwhile, black pellets are recently produced from various woody biomass or agricultural residues through a thermal process, called torrefaction. Black pellets are regarded as high-grade solid biofuels with stable, homogeneous and greater energy density and calorific value than the original biomass. It is believed that torrefied biomass offers a cost-effective route to significantly increase the use of biomass as a renewable energy source and at the same time to lower greenhouse gas and particulate emissions from heat and power generation.

However, there are very limited systematic and comprehensive evaluations of the combustion characteristics and environmental benefits of these two types of biomass fuels.

The aim of this thesis is to quantify the combustion characteristics and associated pollutant emissions of natural wood pellets. To achieve this goal, A modified 10 kW boiler was used as the burner in our research. The characterization of the combustion of natural wood pellets is carried out using advanced equipment (measurement of gaseous emissions by analyzers and study of particulate emissions by LII and SMPS). In addition, a calibration method has been improved to directly deduce the soot volume fraction from the LII signal using the absolute radiance emitted from a light source having black body. In parallel, SMPS technology is also used to measure the particle size distribution of particulate matter emissions. Emissions of gaseous and particulate pollutants were studied for two conditions, with and without secondary air.

Keywords: Combustion, biomass, wood pellets, gaseous emissions, soot particles, laser diagnostics, laser-induced incandescence, soot volume fraction, primary air, secondary air.

Résumé

En tant que 4ème vecteur mondial d'énergie primaire après les combustibles fossiles (charbon, pétrole et gaz naturel), la biomasse est la source d'énergie renouvelable la plus abondante sur terre. Parmi toutes les technologies de conversion de la biomasse, la combustion directe de la biomasse pour la production de chaleur et d'électricité est la voie la plus courante et la plus rentable pour transformer la biomasse en énergie. La biomasse de bois naturel est largement utilisée comme alternative aux combustibles fossiles pour réduire les émissions atmosphériques provenant de la production de chaleur et d'électricité au Royaume-Uni, en France et dans le reste du monde. Pendant ce temps, des granulés noirs sont récemment produits à partir de diverses biomasses ligneuses ou de résidus agricoles grâce à un procédé thermique, appelé torréfaction. Les granulés noirs sont considérés comme des biocombustibles solides de haute qualité avec une densité énergétique et une valeur calorifique stables, homogènes et supérieures à celles de la biomasse d'origine. On pense que la biomasse torréfiée offre une voie rentable pour augmenter considérablement l'utilisation de la biomasse comme source d'énergie renouvelable et en même temps pour réduire les émissions de gaz à effet de serre et de particules provenant de la production de chaleur et d'électricité.

Cependant, il existe très peu d'évaluations systématiques et complètes des caractéristiques de combustion et des avantages environnementaux de ces deux types de biocombustibles.

Dans le cadre de ce travail de thèse, nous visons à quantifier les caractéristiques de combustion et les émissions polluantes associées des granulés de bois naturel. Pour atteindre cet objectif, une chaudière modifiée de 10 kW sera utilisée comme brûleur dans nos recherches. La caractérisation de la combustion des granulés de bois naturel est réalisée à l'aide d'équipements avancés (mesure des émissions gazeuses par analyseurs et étude des émissions particulaires par LII et SMPS). De plus, une méthode d'étalonnage a été améliorée pour déduire directement la fraction volumique de suie du signal LII en utilisant la luminance absolue émise par une source lumineuse à corps noir. En parallèle, la technologie SMPS est également utilisée pour mesurer la distribution granulométrique des particules émissions. Les émissions de polluants gazeux et particulaires ont été étudiées pour deux conditions, avec et sans air secondaire.

Mots clés : Combustion, biomasse, pellets de bois, émissions gazeuses, particules de suie, diagnostic laser, incandescence induite par laser, fraction volumique de suie, air primaire, air secondaire.

List of acronyms

CHP : Combined heat and power

CPC : Condensation particle counter

DMA : Differential mobility analyzer

GC / MS : gas chromatography coupled with mass spectrometry

HTU : Hydrothermal upgrading

IEA : International Energy Agency

LHV : Lower heating value

LII : Laser-Induced Incandescence

MCP : Microchannel plate

MTOE : Million Tonnes of Oil Equivalent

NMVOC : Non-Methane Volatile Organic Compounds

PA : Primary air

PAHs : Polycyclic aromatic hydrocarbon

PM : Particulate matter

PMT : Photomultiplier tube

SA : Secondary air

SCR : Selective catalytic reduction

SNCR : Selective non-catalytic reduction

SPM : Secondary particulate matter

TBP's : Torrefied biomass pellets

TES : Total energy supply

TFC : Total final consumption

THC : Total hydrocarbons

VOCs : Volatile organic compounds

Nomenclature

list of alphabets

c	Speed of light (3×10^8 m s^{-1})
C_i	Mole fraction of pollutant
C_p	Molar heat capacity of air at constant pressure (J $mol^{-1}K^{-1}$)
C_p^{CO}	Heat capacity of CO (J $mol^{-1}K^{-1}$)
C_s	Particle specific heat (J $kg^{-1}K^{-1}$)
C_v	Molar heat capacity of air at constant volume (J $kg^{-1}K^{-1}$)
C_{water}	Specific heat of water (J $kg^{-1}K^{-1}$)
d_p	Particle diameter (m)
$E(m)$	Refractive index function
E_{bb}	Emittance of an elementary surface (W)
e_{air}	Air excess
e	Euler's number (2.71828)
f_v	Soot volume fraction
G	Function of the heat capacity ratio
ΔH_{ann}	Enthalpy of annealing (J mol^{-1})
ΔH_{ox}	Enthalpy of the CO formation (J mol^{-1})
ΔH_s	Enthalpy of formation of the sublimed carbon clusters (J mol^{-1})
h	Planck constant (6.626×10^{-34} J s)
$I_l(t)$	Time-dependent irradiance of the incident beam (W m^{-2})
k_a	Thermal conductivity of the bath gas (W $m^{-1}K^{-1}$)
k_{ann}	Rate constant of annealing (s^{-1})
k_B	Boltzmann constant (1.38×10^{-23} J K^{-1})
L	Mean free path (m)
$L°$	Luminance (W.m^{-2} Sr^{-1})

l_{window}	Length of the window (m)
M	Particle mass (kg)
M_{air}	Mole mass of air (kg mol^{-1})
M_{pellet}	Mole mass of pellets (kg mol^{-1})
M_s	Molecular weight of the sublimed carbon clusters (kg mol^{-1})
M_c	Molecular weight of a carbon atom (kg mol^{-1})
m	Complex index of refraction
$\dot{m}_{air}$	Mass flow rate of inlet air (kg s^{-1})
m_e	Electron mass (kg)
$\dot{m}_{pellets}$	Mass flow rate of pellets (kg s^{-1})
$\dot{m}_{water}$	Mass flow rate of water (kg s^{-1})
N_A	Avogadro constant (6.0221×10^{23} mol^{-1})
N_d	Number of defect sites in the particle
N_p	Number of soot particle
p_V	Saturation partial pressure of the sublimed carbon clusters (Pa)
ρ_s	Particle density (kg m^{-3})
$\dot{Q}$	Power (W)
$\dot{Q}_{abs}$	Absorptive heating rate (W)
$\dot{Q}_{ann}$	Annealing heating rate (W)
$\dot{Q}_{cond}$	Conductive cooling rate (W)
Q_{input}	Input power of the boiler (W)
Q_{output}	Output power of the boiler (W)
$\dot{Q}_{oxi}$	Oxidative heating rate (W)
$\dot{Q}_{raq}$	Radiative cooling rate (W)
$\dot{Q}_{sub}$	Evaporation cooling rate (W)
$\dot{Q}_{therm}$	Thermionic cooling rate (W)
S_{LII}	LII signal

$S_{sphere\ orifice}$	Sphere orifice (Sr^{-1})
$S_{PMT\ (\lambda)}$	PMT signal
T	Particle temperature (K)
T_{in}	Inlet water temperature (K)
T_{out}	Outlet water temperature (K)
t	Time (s)
U_{int}	Internal energy of particle (J)
V_m	volume of measurement (m^3)
X_{CO2}	Mole fraction of CO_2
X_{O2}	Mole fraction of O_2

list of Greek letters

$\alpha(\lambda, T)$	Absorption coefficient
α_M	Mass accommodation coefficient
α_T	Thermal accommodation coefficient
β	Detection efficiency
γ	Heat-capacity ratio
$\varepsilon(\lambda, T)$	Emission coefficient
λ	Wavelength (m)
$\Delta\lambda$	Emission spectral range (m)
Φ_{laser}	Diameter of laser (m)
ϕ	Work function (J)
φ	Equivalence ratio
Ω	solid angle
$\Gamma(5)$	Value of the gamma function of 5 (24)
$\zeta(5)$	Value of the Riemann zeta function of 5 (1.0363)

Contents

List of figures

List of tables

Chapter 1

Introduction

This thesis was realized in co-supervision between 3 laboratories (LAMIH and PC2A in France and University of Kent in UK). In this chapter, some comparisons between the two countries will be introduced.

1.1 Global situation

Since the beginning of the 21st century, the environmental impact of energy production has been identified as one of the most critical issues to be addressed in the world. The effects of climate change can be felt more strongly now than 30 years ago. The tangible effects of this problem justify the urgency of finding solutions and push us to take consistent decisions to accelerate an energy transition.

From the statistics of Enerdata as illustrated in Figure 1-1, the world's energy consumption is continuously increasing. Global energy consumption grew significantly (+2.3%) in 2018, spurred by the sustained economic growth and rising demand in China, the world's largest energy consumer since 2009. Global energy consumption growth declined by 4% in 2020 due to lockdown measures and transport restrictions, in the context of the global pandemic [1]. (MTOE: Million Tonnes of Oil Equivalent)

The global dependence on different fuels in 2020 was shown in Figure 1-2. 80% of the global energy demand is met by fossil fuels such as coal, gas and oil, only 10% comes from biomass, and 10% comes from electricity generated by renewable resources like wind, hydro and solar. There is a general agreement that fossil fuels be depleted or at least become too expensive to produce within this century [2].

Moreover, energy generation by combustion is also a source of environmental problems. The environmental impact of energy generation by combustion has been identified as one of the most critical issues to be solved in the world in the 21st century. The need for energy due to industrial growth is constantly increasing, and consequently impacts the environment with greenhouse gas emissions. These emissions cause an increase of several degrees Celsius in the Earth's average temperature.

Therefore, accelerating an energy transition to meet the growing energy consumption while minimizing the environmental impact caused by the combustion of fossil fuels has become one of the major challenges for today's scientists.

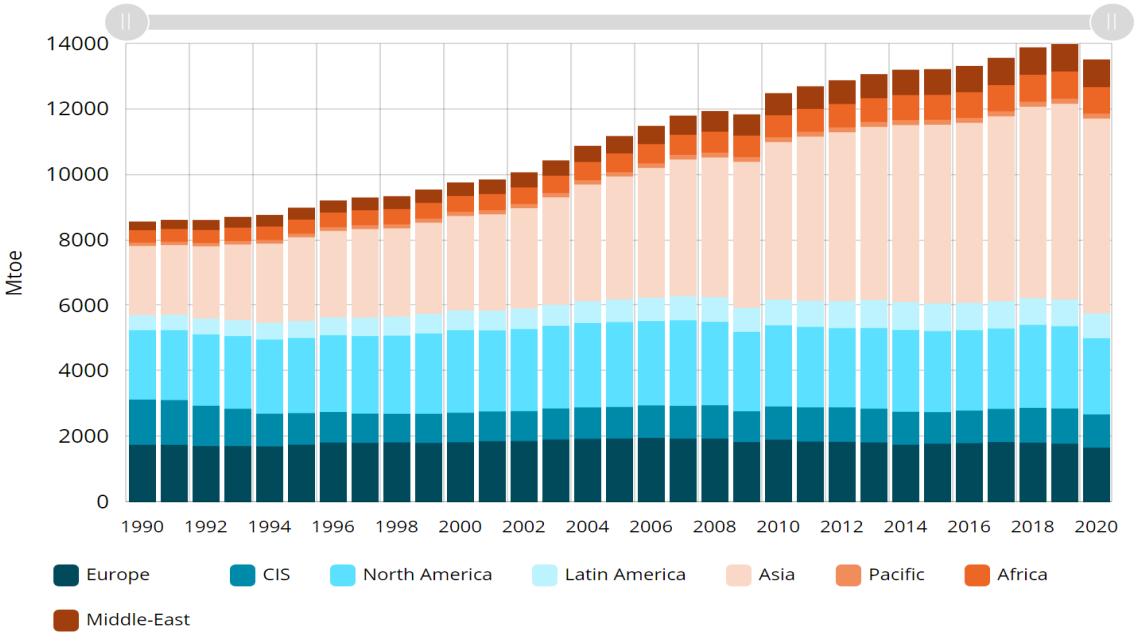

Figure 1-1 Global energy consumption million tonnes of oil equivalent (Mtoe) versus years from 1990 up to 2020 [1]

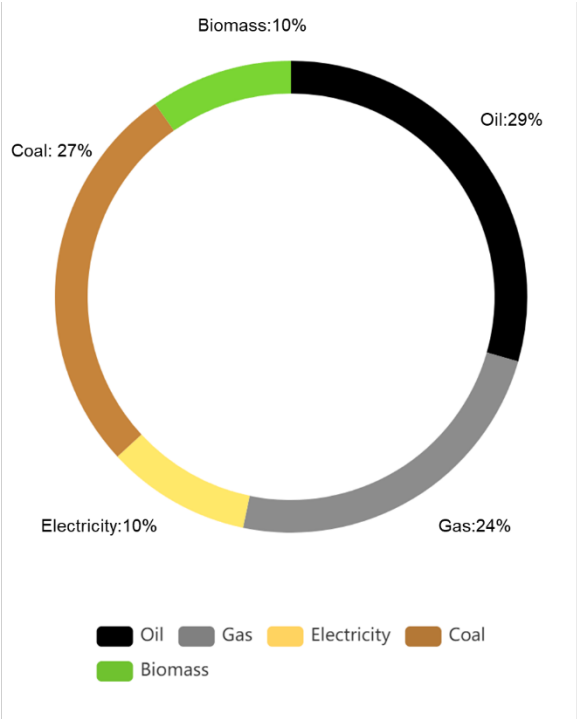

Figure 1-2 The global dependence of different fuels in 2020 [1]

1.2 Energy consumption in France and UK

1.2.1 Energy consumption in France

Since 2005, both the total energy supply and total final energy consumption in France have been decreasing. On the energy supply side, coal, oil, and natural gas account for 2 5%, 27.9%, and 15.8% of the total energy supply in 2020 as shown in Figure 1-3. On the energy consumption side in 2020, 0.8% of total energy consumption comes from coal, 43.9% from oil products, and 19.6% percent from natural gas as shown in Figure 1-4. Biofuels and waste only account for 7.5% of the total energy supply and 8.2% of the total energy consumption. It shows that although France does not produce coal, oil or natural gas, these three energy sources correspond to over 60% of the energy consumption in the country. The majority of the energy deficit in France is therefore filled by fossil fuels. The country remains dependent on these fossil fuels which are imported and used for conventional applications in order to meet its energy needs.

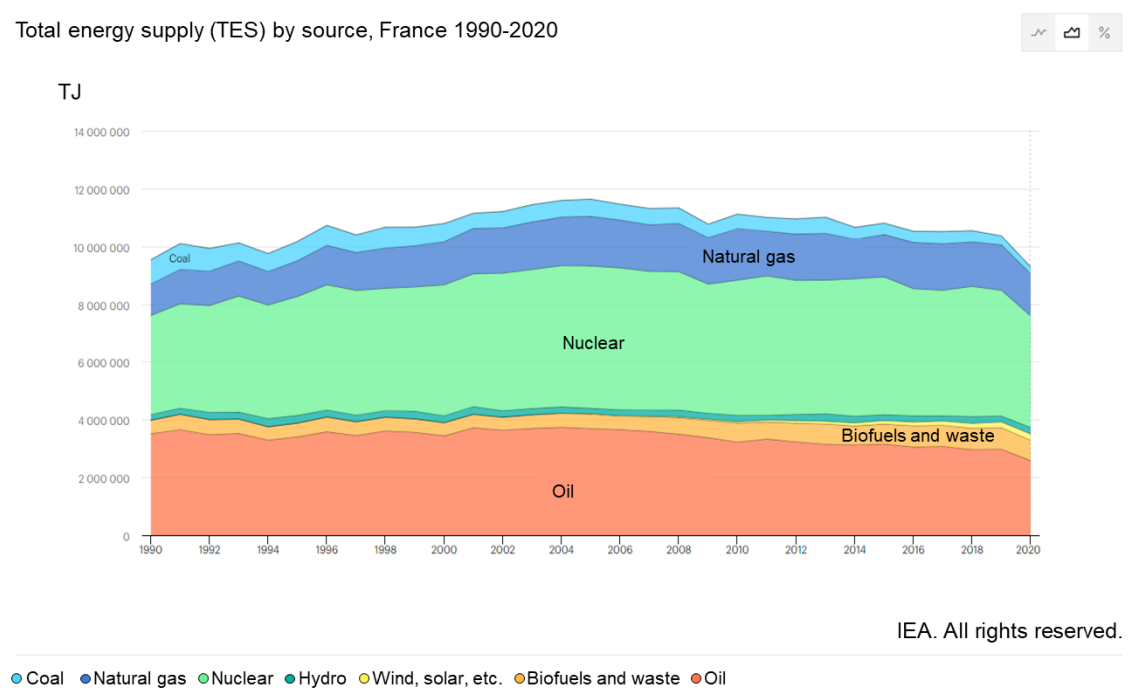

Figure 1-3 Total energy supply (TES) by source, France TJ versus years 1990-2020 [3]

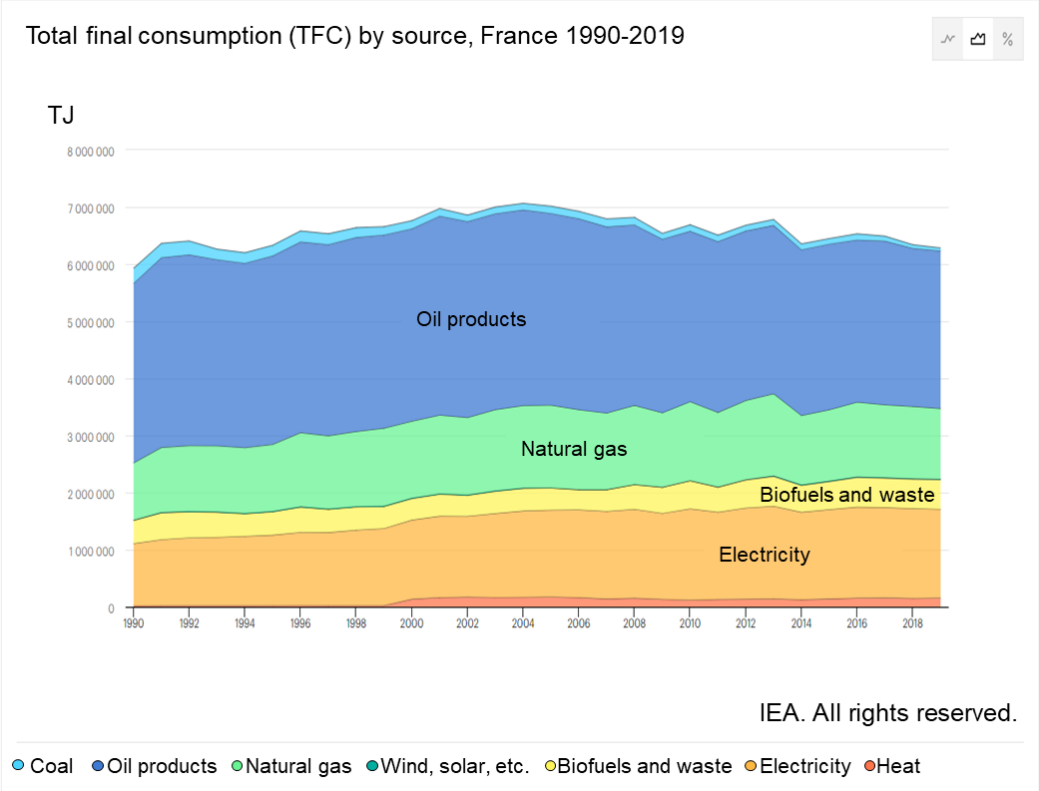

Figure 1-4 Total final consumption (TFC) by source, France TJ versus years 1990-2019 [3]

Figure 1-5 provides the details about the total energy consumption by sector. The total energy consumption peaked in 2005 and fell slightly in the following years. The residential sector and the transport sector have always been the most important energy consumers. Their share in total energy consumption has always been more than 50%. The transport sector is increasingly predominant: its share in total energy consumption has increased from 27.1% in 1990 to 30.1% in 2019. The residential sector share peaked at 27.7% in 2010 and then began to decrease to 24.9% in 2019. The industrial sector fell from 22.2% to 18.3%. Conversely, the commercial and public service sector rise from 13.3% to 14.4 %.

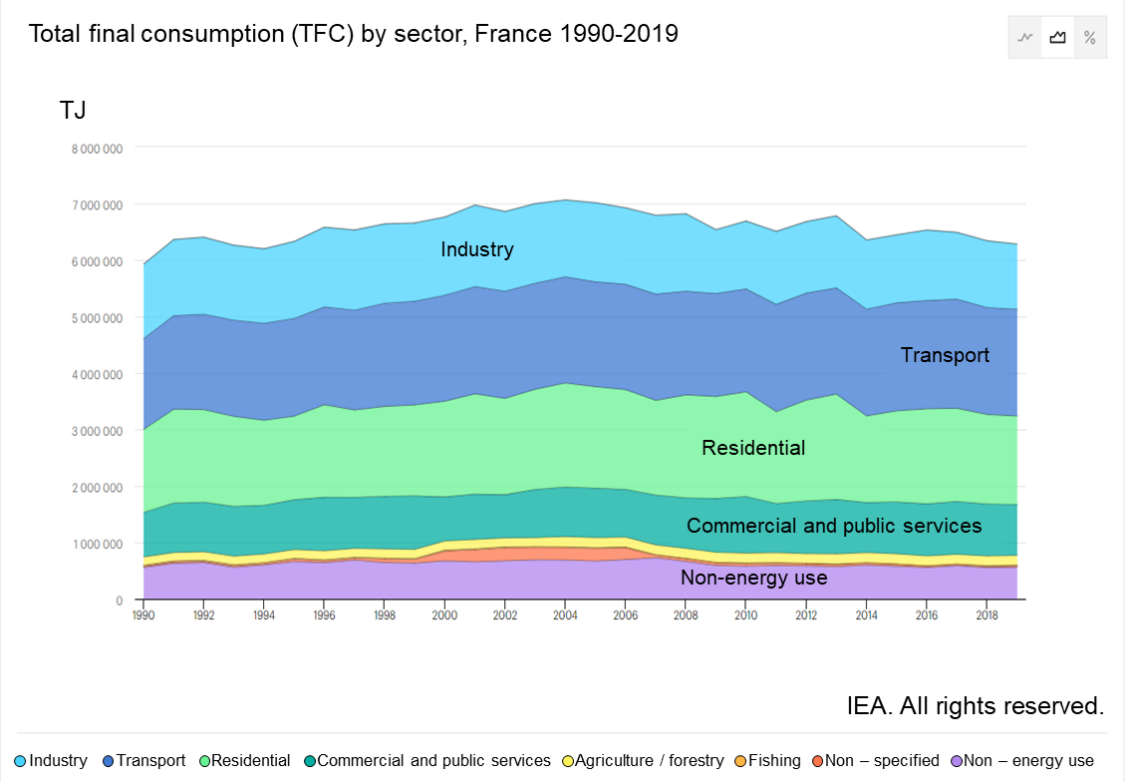

Figure 1-5 Total final consumption (TFC) by sector, France TJ versus years 1990-2019 [3]

1.2.2 Energy consumption in the UK

UK and France share similar energy trends. The total energy supply in the UK has been decreasing since 2005. For total final energy consumption, the downward trend even started in 2000. On the energy supply side, 0.8% of the total energy supply comes from coal, 31.9% from oil, and 41.2% percent from natural gas in 2019 as shown in Figure 1-6. On the energy consumption side, coal, oil products and natural gas account for 1.6%, 42.2% and 31.2% of the total energy supply in 2019 as shown in Figure 1-7. Biofuels and waste only account for 9.9% of the total energy supply and 4.1% of the total energy consumption. Compared with France, the UK's fossil fuel accounts for a higher proportion of the total energy consumption, which is as high as over 70% of total energy consumption. In contrast, the share of biofuels and waste in total energy consumption is twice lower as it is in France. This shows that the UK is more reliant on fossil fuels to meet its energy needs than France.

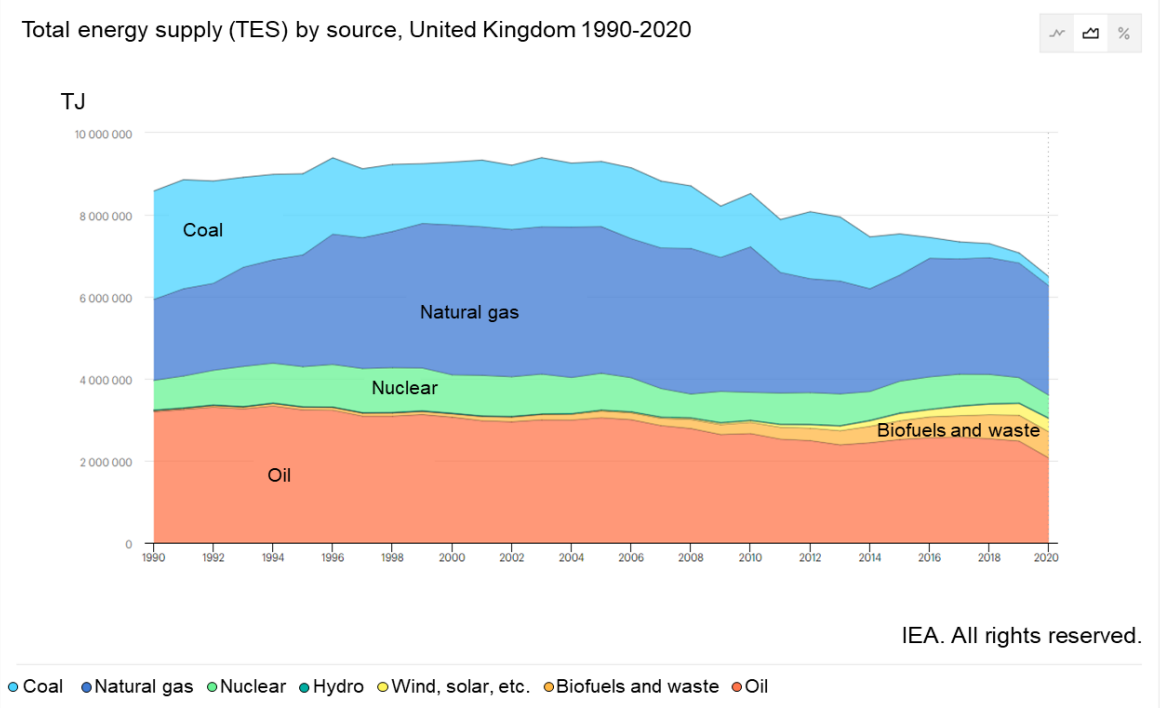

Figure 1-6 Total energy supply (TES) by source, United Kingdom TJ versus years 1990-2020 [3]

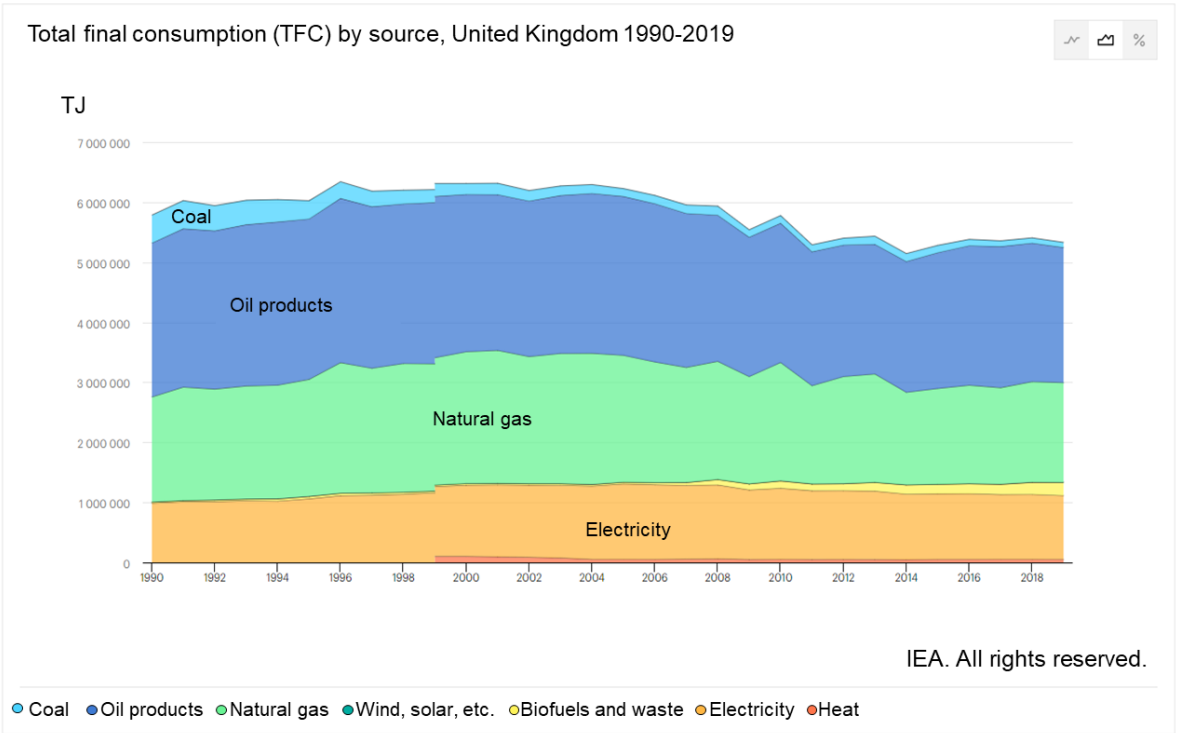

Figure 1-7 Total final consumption (TFC) by source, United Kingdom TJ versus years 1990-2019 [3]

The details about the total energy consumption by sector was shown in Figure 1-8. The total energy consumption peaked in 2000 and fell in the following years. Similar to France, the residential sector and the transport sector have always been the most important energy consumers. More than 60% of the total energy consumption is contributed by these two sectors in 2019. The transport sector's share in total energy consumption has increased from 28.4% in 1990 to 32.3% in 2019. The residential sector share peaked at 32.9% in 2010 and then began to decrease to 29.9% in 2019. The share of industrial sector energy consumption was decreasing while the share of commercial and public service sector was increasing, which is similar to France.

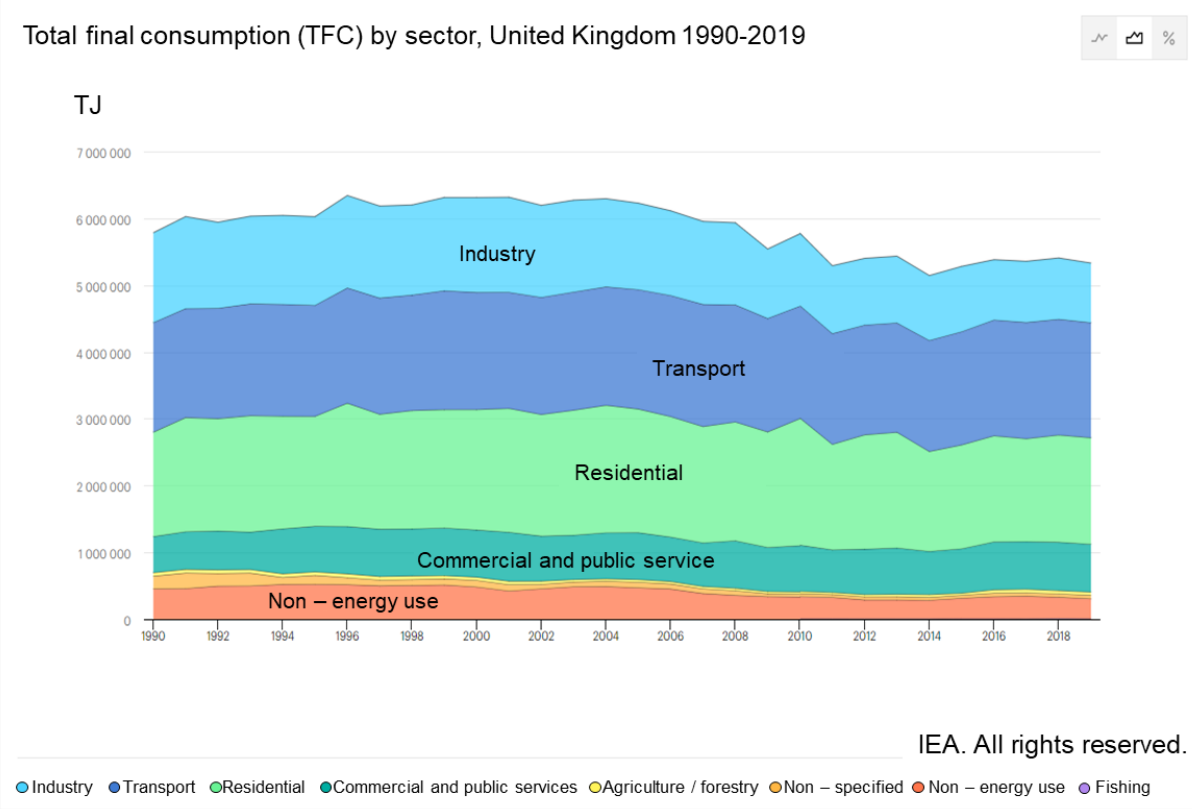

Figure 1-8 Total final consumption (TFC) by sector, United Kingdom TJ versus years 1990-2019 [3]

1.3 Renewable energy

Renewable energy is energy that is collected from renewable resources that are naturally replenished on a human timescale. It includes sources such as sunlight, wind, rain, tides, waves, geothermal heat and bioenergy [3].

Renewable energy will play a key role in the decarbonization of our energy systems in the coming decades. In 2019, around 11% of global primary energy came from renewable technologies [4]. Hydropower accounted for the largest share of renewables in the global renewable energy generation, i.e., 57.7% in 2019. The wind comes second with 21.4%, followed by solar at 11.5% and other renewables at 9.4% as shown in Figure 1-9. Here the 'Other renewables' refers to renewable sources including geothermal, biofuels, waste, waves and tidal. Traditional biomass (wood fuels, agricultural by-products …) is not included.

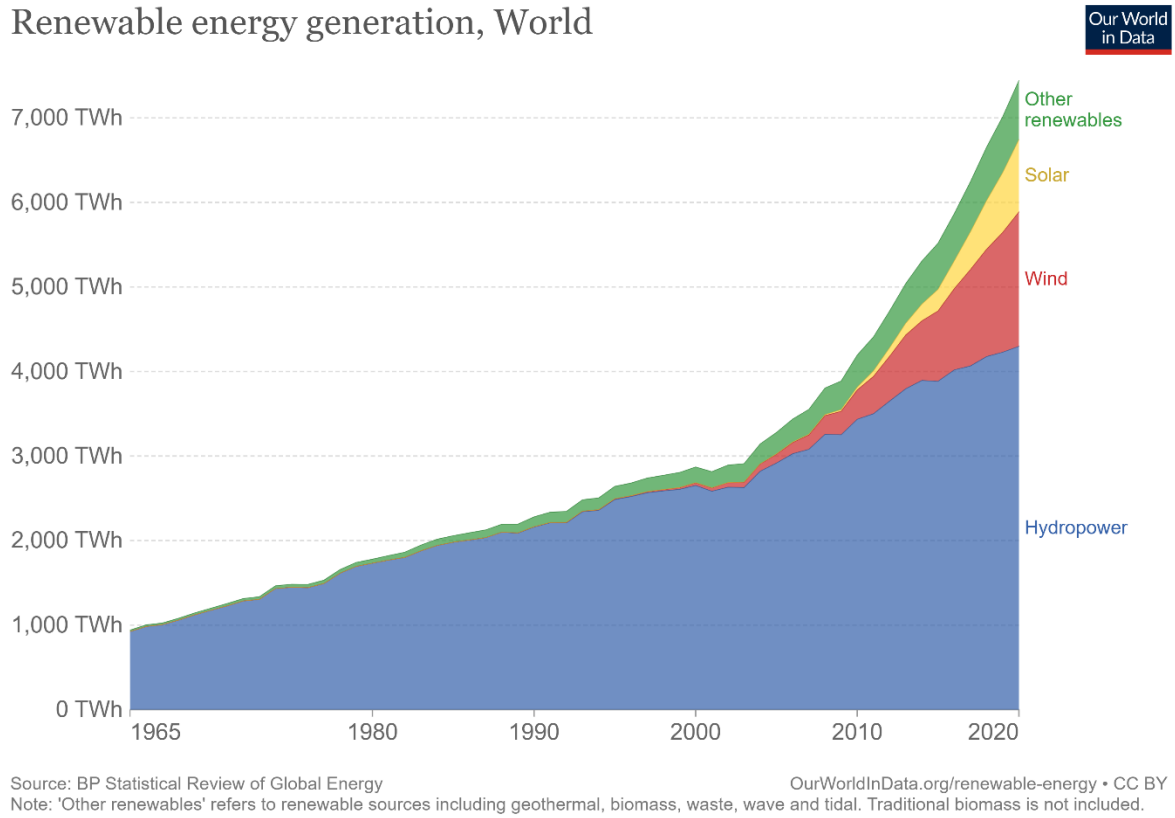

Figure 1-9 Renewable energy generation in the world – TWh versus year [5]

However, among the renewable energy sources, one of the most promising is biomass which is not included in Figure 1-9. Modern biofuels mainly include bioethanol and biodiesel. These fuels are typically made from crops such as corn,

sugarcane, hemp, and cassava. So modern biofuels could be considered to compete with other primary needs of humanity like food, health, etc.

Figure 1-10 shows global renewable energy consumption over the long term. As observed, renewable energy consumption has been dominated by traditional biofuels.

Biomass mainly includes the combustion of fuelwood, forestry products, animal and agricultural wastes. The traditional biomass was an important energy source for a long period of human history. Since the 2000s, other sources of renewable energy are developing rapidly and the use of traditional biomass is finally giving way to new resources.

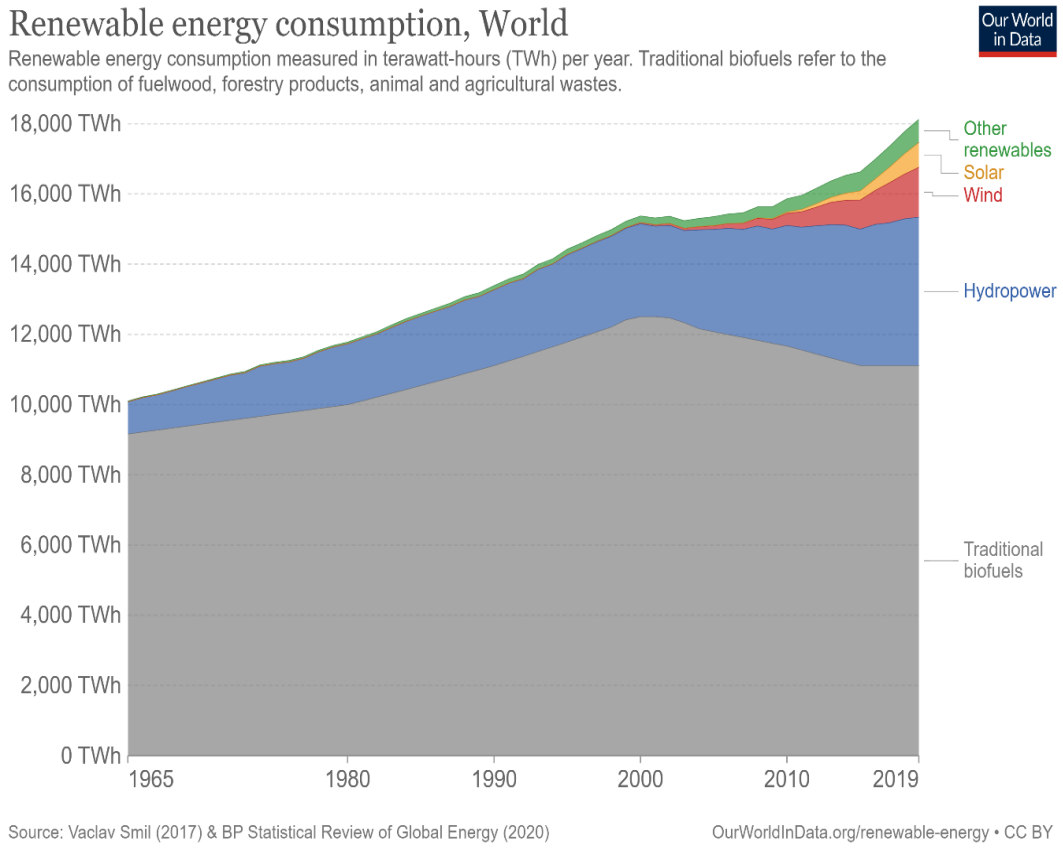

Figure 1-10 World renewable energy consumption TWh versus year [5]

Traditional biomass is still the main component of renewable energy today, accounting for 60% to 70% of global renewable energy consumption. Traditional biomass energy is a local energy source, which is readily available to meet the energy needs of a significant proportion of the population – particularly the poor in rural areas of the developing world [5]. Traditional biomass energy is low cost and it does not require processing before use. The combustion of biomass,

therefore, remains the most common method of use compared to other energy sources. However, traditional biomass use has significant drawbacks which is the air pollution from biomass combustion in unvented bio-fuel stoves.

The share of renewable energy in final energy consumption in France amounts to 19.1% in 2020. The growth of renewable energies in France has been significant since 2005, in particular with the development of biofuels, solid biomass, heat pumps, wind power, and photovoltaic solar energy. In 2020, the share of renewable energies increase sharply, by 1.9 points. Figure 1-11 shows the proportion of the final consumption of renewable energies in 2020. The main renewable energies used in France are listed below.

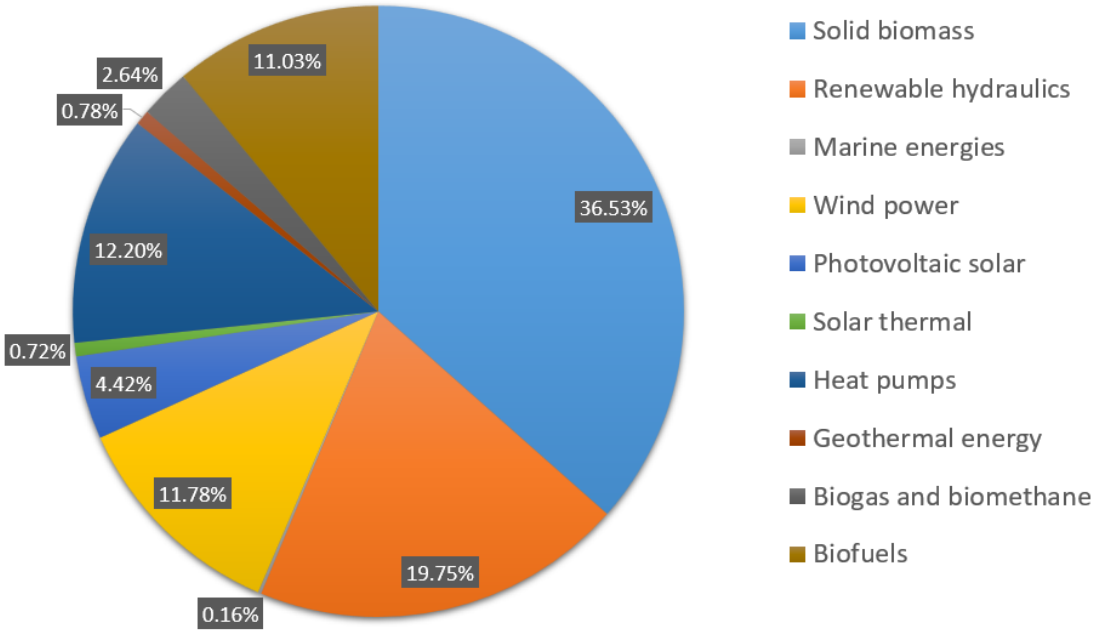

Figure 1-11 Proportion of final consumption of renewable energies in France, 2020 [3]

• Solid biomass:

Solid biomass is mainly used to produce heat and a minimal part is used to produce electricity. It is the most common renewable energy in France in the residential sector. Solid biomass represents 36.5% of the final renewable energy consumption in France in 2020.

• Renewable hydraulics:

France has more than 2,000 hydraulic installations, which makes it one of the main producers of hydraulic energy in the European Union. The energy produced

by the hydraulic source remains variable due to changes in river flow, which very depend on the influence of rainfall and global warming which appears these last years. Hydropower represents 50.6% of total renewable electricity production in France in 2020. In 2020, hydraulic production increased slightly compared to 2019.

• Heat pumps:

The stock of heat pumps installed in France continues to grow, in particular thanks to the sale of air-air units. In 2020, 37.5 TWh of renewable heat was produced by heat pumps, a figure up 10% compared to the previous year. This also makes heat pumps the third-largest renewable energy source in France.

• Wind power:

Since the 2000s, wind power generation has been steadily increasing. In 2020, total production reached 36.2 TWh, an increase of 11.6% compared to 2019. This increase is explained by very favorable weather conditions and by an increase in the number of installations. Most of the production is done in the north of France.

• Biofuels:

Biofuels are the 5th renewable source in France. It should be noted that biodiesel represents 78.9% of biofuel consumption, against 21.1% for bioethanol in 2020.

• Photovoltaic solar:

From 2009, the photovoltaic solar sector progressed at a brisk pace. In 2020, production amounted to 13.6 TWh, a figure up by 11.1% compared to 2019. The fall in the price of photovoltaic modules in recent years can in particular explain this enthusiasm. Unsurprisingly, it is in the southwest and southeast of France, the geographical areas that benefit from the greatest sunshine, that production is highest.

• Biogas and biomethane:

Biogas is mainly used to produce electricity and heat. In 2020, 8.1 TWh of biomethane obtained by biogas purification was injected into the natural gas networks. This represents an increase of 17% compared to 2019.

• Geothermal energy:

Geothermal energy is produced in particular in Ile-de-France, New Aquitaine, and the Rhine basin. In 2020, 0.1 TWh of electric geothermal energy and 2.3 TWh of thermal geothermal energy were recorded.

• Solar thermal:

The solar thermal sector grew by 2.8% in 2020 to reach 2.2 TWh. This sector is particularly developed in the overseas departments, and specifically in the Reunion.

• Marine energy:

Marine energy is the last renewable energy source in France. In 2020, only 0.1 TWh of renewable electricity was produced by the marine energy source.

1.4 Biomass energy

Biomass, according to the definition of the International Energy Agency (IEA), refers to various organisms formed through photosynthesis, including all animals, plants and microorganisms.

Biomass energy is the energy derived from the reaction between CO_2 in the air, water, and sunlight via photosynthesis stored in biomass in the form of chemical energy. If the chemical energy stored in the biomass can be extracted efficiently, the carbon is oxidized to produce CO_2 and water. The process is cyclical, as the CO_2 is then available to produce new biomass [6]. So, it is widely accepted that biomass is CO_2 neutral. It has always been one of the most important energy sources for human survival. It is the fourth largest energy source in the world after coal, oil, and natural gas which plays an important role in the system.

Among various renewable energy sources, large-scale hydropower has potential ecological and environmental risks, wind energy, geothermal energy, and solar energy are restricted by regional resources. Their development has been restricted. However, biomass is considered the renewable energy source with the highest potential to contribute to the energy needs of modern society for both developed and developing economies worldwide [7].

Biomass can be converted into useful energy (heat or electricity) or energy carriers (comparable to coal, oil or gas) by thermochemical and biochemical conversion technologies. The actual choice of a process depend on the type and quantity of available biomass feedstock, the end-use of the energy, environmental standards, economic conditions, and other factors [8]. Figure 1-12 shows the thermochemical and biochemical conversion of biomass. Combustion, gasification and pyrolysis are the main processes used in thermal conversion to recover energy from biomass. The next is biochemical conversion where microorganisms during fermentation, anaerobic digestion, and esterification release energy from the

biomass. Finally, there is the mechanical extraction technology capable of producing energy in the form of biodiesel [9]. The thermochemical conversion of biomass was given special attention as it is the subject of this thesis.

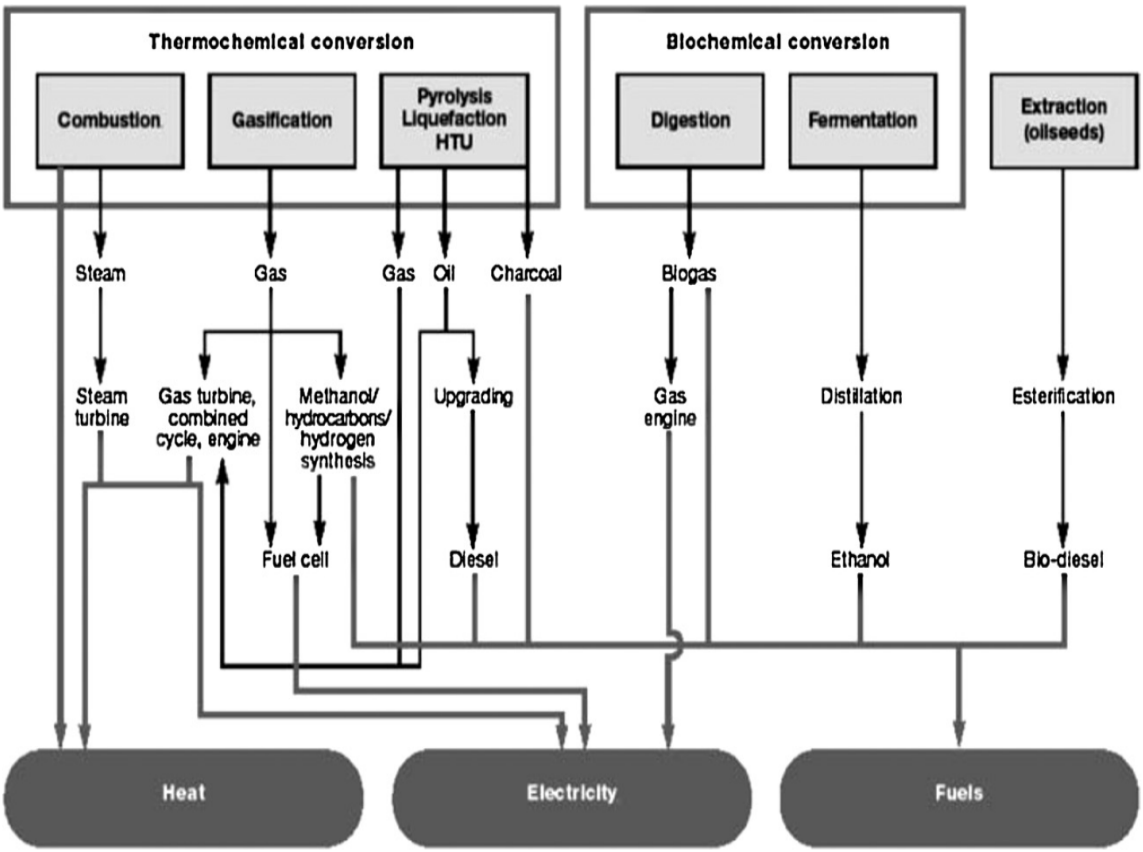

Figure 1-12 Thermochemical and biochemical conversion of biomass

Three main processes are used for the thermochemical conversion of biomass: gasification, pyrolysis, and combustion. There are also some lesser-used options like hydrothermal upgrading (HTU), liquefaction and torrefaction.

• Gasification:

Gasification is the conversion of biomass into a combustible gas mixture by the partial oxidation of biomass at high temperatures, typically in the range of 800-900 °C [10]. The gas mixture usually called syngas or synthesis gas, which can be used for the production of energy (heat and/or electricity generation), chemicals (ammonia), and biofuels. Furthermore, a solid residue after biomass conversion (char) is generally found [11]. Syngas consists of a mixture of CO, H_2, CO_2, CH_4 (primary components) and H_2O, H_2S, NH_3, tar, and other trace species (secondary

components), with a composition dependent on feedstock type and characteristics, operating conditions, and gasification technology. Syngas can be used to generate electricity, produce liquid or gaseous fuels such as methanol, ethanol, dimethyl ether, Fischer-Tropsch Synthesis, hydrogen, and synthetic natural gas, and produce chemicals [12].

• Pyrolysis:

Pyrolysis is the conversion of biomass to liquid (termed bio-oil or bio-crude), solid and gaseous fractions, by heating the biomass in the absence of air to around 500°C [10]. The main products of biomass pyrolysis depend on the temperature, heating rate, particle size, and catalyst used[13]. The typical gas composition of woody biomass pyrolysis includes CO, CO_2, CH_4, and H_2 as major products along with other organic compounds [14]. Pyrolysis can be used to produce predominantly bio-oil if flash pyrolysis is used, enabling the conversion of biomass to bio-crude with an efficiency of up to 80%. Bio-oil is an important pyrolysis product that can be used to generate electricity, heat, transport fuel, and produce chemicals [13].

• Combustion:

Combustion of biomass in the air is widely used in various items of process equipment to convert chemical energy stored in biomass into heat, mechanical or electrical energy, e.g. stoves, furnaces, boilers, steam turbines, turbo-generators, etc. The scale of combustion plants ranges from very small-scale simple batch-operated designs in domestic up to large-scale complex biomass-fired power stations. Biomass combustion essentially depends on the particle size and properties of the feedstock, temperature, and combustion atmosphere [15]. The high emission of NO_x, CO_2, and particulate matter is the most technical problem to be solved in biomass combustion.

Biofuels are generally divided into three generations. First-generation biofuels include ethanol and biodiesel and are directly related to biomass that is more than often edible. Second-generation fuels are produced from the conversion of lignocellulosic materials or wood/agriculture waste, biomass that mainly contains cellulose, hemicellulose, and lignin. The third-generation biofuels are fuels that would be produced from algal biomass. Therefore, the major difference between the second and third generations is the feedstock. Compared to first-generation fuels, second-generation and third-generation fuels have an advantage because they avoid competing with other basic human needs such as food [16].

• Other processes:

HTU converts biomass in a wet environment at high pressure to partly oxygenated hydrocarbons. Liquefaction is the conversion of biomass into a stable liquid hydrocarbon using low temperatures and high hydrogen pressures. Torrefaction involves heating the biomass to a moderate temperature in the absence of oxygen and under atmospheric pressure.

The research in this thesis focuses on the combustion of wood biomass. This is because wood biomass is currently the most commercialized and most cited. When considering an energy source as an alternative to conventional fossil fuel, it must meet several criteria. Firstly, the energy must be renewable. Secondly, its impact on the environment must be limited. Finally, it should not compete with other primary needs of humanity like food, health, etc.

1.5 Aim and objectives of this thesis

This co-supervision PhD thesis aims to quantify the combustion characteristics and associated pollutant emissions of the natural wood pellets. The main objectives of this research are to review the state of the art of biomass combustion techniques, to build a test bench with advanced diagnostic and emission monitoring equipment, to analyze the effect of different air flow rates and air supply conditions on gaseous and particulate emissions, to measure the absolute soot volume fraction using the two-color laser induced incandescence (LII) method, and to provide professional advice to heating and combustion engineers on the most economical and environmentally friendly use of biomass pellets.

This work is composed of five chapters. The first chapter gives the practical and scientific context of the thesis. The second chapter provides a review and literature research on the technologies related to biomass combustion and the pollutants produced by biomass combustion. The third chapter describes in details all experimental techniques and set-ups employed in this work. The fourth chapter mainly shows and analyzes the results obtained from wood pellet combustion experiments. Finally, the main results of the thesis are summarized, and some general conclusions and perspectives are proposed in chapter 5.

1.6 Contributions to this research

This research is an international collaborative project. The plan was to spend two years in France by analyzing the characteristics of biomass combustion and

one year in the UK by studying and modelling the combustion mechanism of individual pellets. However, due to the impact of the Covid 19, the progress of the experiment has been greatly delayed, resulting in only enough time to complete the characteristic analysis part of the biomass combustion experiment, and not to engage in the research and modelling of the combustion mechanism of individual pellets.

Some chemical measurements investigated by the laboratory Common Center of Measurements (CCM, Dunkerque) to characterize the different operating conditions of the boiler (ignition, steady state, extinction) were obtained before the beginning of the thesis. All other results were obtained during the PhD thesis.

Chapter 2

State of the art

2.1 Introduction

Combustion is one of the most important discoveries in human history and it is a cornerstone which our modern society is built upon. Even more, it can be argued that without combustion there would have been no modern civilized society. During the first industrial revolution, the energy produced by coal combustion provided power for the steam engine. This was the first leaping of human productivity. Nowadays, combustion is still a most important process, especially in energy generation, transportation, and other industrial fields like metallurgy and papermaking. Substantial work has been carried out in the domain of biomass combustion. In order to define the state-of-the-art of biomass combustion, fully understanding of the basic research strategies and the development of the existing techniques is useful.

2.2 Biomass combustion technology and boiler

2.2.1 Biomass combustion process and technology

Combustion is a high-temperature exothermic redox chemical reaction between a reductant (fuel) and an oxidant (usually atmospheric oxygen) that produces oxidized (usually gaseous products) and releases heat. While the activation energy must be overcome to initiate combustion, the heat from a flame may provide enough energy to make the reaction self-sustaining.

In the specific case of the combustion of solids, several phenomena occur simultaneously. Drying and heating process removes moisture from biomass fuel. Then biomass fuel decompose into volatiles, tar and char through pyrolysis process. The combustion of volatiles is homogeneous combustion where the reaction takes place in the gaseous phase (gas-gas). The combustion of char is heterogeneous combustion which occurs in the presence of different phases (solid-gas). The combustion process of biomass can be divided into several processes (figure 2-1):

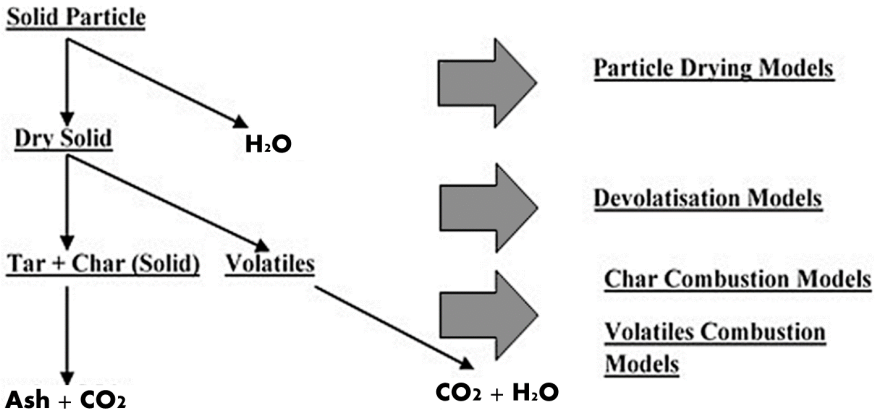

Figure 2-1 Combustion process of biomass

• Drying and heating:

Typically, biomass being fired into any combustor contain some moisture at ambient temperature. To initiate combustion, the first stage involves the removal of H_2O from the biomass fuel particle and the heating of the particle to vaporization temperature. This process can be represented as follows:

$$\text{Wet fuel particle} + \text{heat} \rightarrow \text{dry fuel particle} + H_2O \qquad \text{Equation } 2-1$$

• Pyrolysis:

Pyrolysis occurs just as the biomass particle reaches the particle vaporization temperature in the absence of oxygen, signifying the release of volatiles from the biomass particle. The three classes of products of pyrolysis are volatiles, tar, and char. This process can be represented by the following equation:

$$C_aH_bO_c + \text{heat} \rightarrow$$
$$H_2O + CO_2 + H_2 + CO + CH_4 + C_2H_6 + CH_2O + \cdots + \text{tar} + \text{char} \qquad \text{Equation } 2-2$$

Pyrolysis involves both chemical and physical changes. The physical changes include the potential for particle shrinkage, and the thermodynamic and transport properties of the fuel particle to be more insulative [17]. The dominant influences on the residence times required to complete pyrolysis are combustor temperature, fuel particle type, and fuel particle size [18].

• Volatile combustion:

The volatiles released during pyrolysis creates a source for gaseous combustion. Volatiles carry most of the energy for biomass combustion with the volatiles consisting mostly of CO, CO_2, H_2O, CH_4, H_2, and other inorganic products [19]. This process can be represented as follows by using the general lumped form of volatiles:

$$CH_bO_c + \left(1 + \frac{b}{2} - \frac{c}{4}\right)O_2 \rightarrow CO_2 + \frac{b}{2}H_2O \qquad \text{Equation } 2-3$$

• Char combustion:

Char combustion involves the consumption of biomass particles by heterogeneous gas-solids reactions. The char is mainly the carbon fraction of the biomass particle left after devolatilization. Char combustion occurs at higher temperatures thus the particle temperature must be higher than the vaporization temperature to activate this reaction. This heterogeneous combustion takes place close to the char surface and can be represented as follows by the simple global equations[20]:

$$C + CO_2 \rightarrow CO \qquad \text{Equation } 2-4$$

$$C + \frac{1}{2}O_2 \rightarrow CO \qquad \text{Equation } 2-5$$

$$C + H_2O \rightarrow CO + H_2 \qquad \text{Equation } 2-6$$

As mentioned above, biomass combustion can be achieved on many different scale boilers, from domestic boilers to large industrial facilities. The choice and design of any biomass combustion system are mainly determined by the characteristics of the fuel to be used, the environmental legislation, the costs and performance of equipment, and the energy produced.

The different types of combustion technologies depend mainly on the characteristics of the fuel, the scale, and the application to meet technological and ecological requirements.

A combustion unit is mainly composed of four main systems: fuel supply system, air supply system, combustion chamber, and ash discharge system (ash may also be collected from the boiler). Additionally, there may be the flue gas recirculation (FGR) system, the heat exchange system, and the automatic control system. The information found in the following sections is mainly drawn from the work [21]. References no longer be cited for each piece of information discussed for simplicity.

• Type of burner:

There are mainly three types of burners: fixed bed, moving grate, and burning plate (volcano type).

Almost all pellet boilers and wood-log boilers use fixed bed burners. The most common fixed bed burner is the horizontal feeding type.

The moving grate design is preferred in some chip boilers and pellet-and-chip boilers. The moving grate becomes increasingly preferable as the power of the unit increases, especially for boilers with capacities greater than 40 kW. The burning plate design involves constant fuel addition. This is due to the design of the moving grate which prevents the accumulation of cinders on the grate surface and maintains an almost constant boiler performance.

The fuel fed into the burning bed from below the plate through a pipe. The new fuel pushes the partially combusted particles outward until the ash falls from the plate.

• Types of ignition systems:

Almost all the modern boilers use automatic ignition systems (some wood log boilers still use a manual plug ignition). The main technologies are a hot-air generator (ceramic ignition electrode) which dries the first load of fuel on the combustion bed and then heats it to above the spontaneous ignition temperature of 400 °C.

• Types of feeding systems:

Burners are classified as bottom-fed burners, horizontal-fed burners, and top-fed burners according to their feeding systems. It is noted that most log burners are manually fed horizontally. Top-fed burners were developed for pellet combustion. Pellets are fed from the top and dropped down to the bed. The main advantage is that it allows better control of the amount of fuel fed. The disadvantage is that the falling pellets may collide with existing pellets or splash dust on the bed, increasing the amount of unburned products and dust.

• Automatic control system:

The modern boilers on the market have an automatic control system. This control is very important for guaranteeing the best possible performance and the lowest possible emissions in every situation. The system controls the air supply through the oxygen mole fraction measured by the lambda probe to adjust the oxygen levels to ensure complete combustion.

•Ash removal and heat exchange cleaning:

Some boilers have ash removal. Both the ash deposited in the burner and the fly ash from the combustion chamber is collected in-store boxes that are inserted in the boiler. The ash is eliminated automatically with specific mechanisms such as vibratory grates, shakers, vibrators, hinge devices, swing grates, and so on.

There are mainly two types of completely different technologies: mechanical systems and flow recirculation systems. In a mechanical system, the heat exchanger is provided by mechanical devices located in the flue gas passage such as springs, tubulating blades, levers, vibrating devices, and helicoidal screw augers to remove ash and slag. In flow recirculation systems, the ash and slag are removed by high-speed combustion gases forced through the heat exchanger.

2.2.2 Biomass boilers

Large-scale systems can be classified as a function of the relative velocity between the gas flow and fuel particles into packed beds, fluidized beds, and pulverized fuel systems[22]. The characteristics of the biomass influence the type of technology to be used, usually, the large-scale systems use low-quality fuels including high moisture content, particle size, and non-uniform ash melting behavior. The combustion technology applied on a large scale has the characteristics of strong adaptability to biomass fuel and low comprehensive cost. Older combustion technologies have been proven to fail emissions compliance when dealing with heterogeneous biomass fuels. Current new fuel preparation, combustion, and flue gas cleaning technologies are more efficient, cleaner, and more cost-effective than previous systems for large-scale biomass combustion. Large-scale biomass combustion is not the focus of this thesis and is not described in detail below.

Small-scale domestic biomass boiler has been chosen for this experimental work. So, its related technologies were introduced in detail. The market provides a wide range of different combustion appliances for the domestic biomass boiler. Usually, small-scale combustion appliances are designed for the utilization of

specific biomass fuel types, although wood pellets and wood chips both consist of the same raw material the fuel properties relevant for combustion vary [21]. The most common biomass combustion appliances for domestic are described in more detail in the following sections.

• Wood-burning stove:

A wood-burning stove is a heating or cooking appliance capable of burning wood fuel and wood-derived biomass fuel, such as sawdust bricks. The stove consists of a solid closed firebox which is generally covered with fire-resistant materials. Some stoves are equipped with ash grids at the bottom of the firebox on which the wood rests. In this case, the ashes are collected in an ashtray placed under the grid. Keeping the air flowing correctly through a wood-burning stove is essential for the safe and efficient operation of the stove. As the fire burns, the smoke must be allowed to rise through the stovepipe and exit through the chimney.

A wood-burning stove is a historic burning device. It belongs to the fixed bed burner and generally manual ignition and feeding. Some stoves install dampers into the stove, flue, and stove pipes to control the air. In newer stoves, a second combustion chamber is added with the injection of secondary air to complete the combustion of the gases. Indoor air pollution and carbon monoxide leaks are both safety concerns for this type of stove.

• Heat storage stoves:

Heat storage stoves usually are wood-burning stoves with an element of heat storage. The heat storage elements cannot make the stove more efficient. However, it delivers a fairly constant heat throughout the ignition-extinguishing-reignition cycle. Additionally, it can continue to deliver its stored heat for many hours afterward after the extinguishing. In this case, a heat storage stove can be cost-effective equipment for maintaining a higher ambient temperature over a much longer period. The ever-increasing cost of energy and environmental concerns have encouraged much better natural stone heat storage elements than traditional cast iron. Finnish soapstone stoves usually have a considerably high mass of between 700 kg to 3000 kg, and sometimes even more. It can therefore store a lot of energy and then keep released heat into the surrounding space for 1 to 2 days.

• Logwood boilers:

Logwood boilers can be classified into three categories according to the path of the gases in the combustion chamber. The first is an updraft boiler in which the

primary air is injected under the wood, the secondary air above the wood and the airflow is natural (no extractor or fan). The second is horizontal combustion boilers where the primary air is injected from the bottom of the wood, and only the bottom part of the wood stack burns. A separate combustion chamber with a secondary air injector is placed on the side of the fireplace. The airflow could be often natural or forced. Finally, the most advanced is the downdraft boiler. The primary air is injected at the top of the combustion chamber and flows down through the wood on a grid. Under this grid is a subsequent mixing zone with an injection of secondary air followed by the post-combustion chamber. Such boilers are usually operated with a forced draft, by application of ventilators for the air inlet and/or for the flue gas exhaust.

Figure 2-2 shows the structure of a typical downdraft boiler. It is an automatic boiler with a lambda sensor and microprocessor controller. The system controls the flue gas suction fan to adjust the oxygen levels to ensure complete combustion. Under typical operation conditions, boilers with the downdraft principle allow significantly lower emissions than updraft boilers.

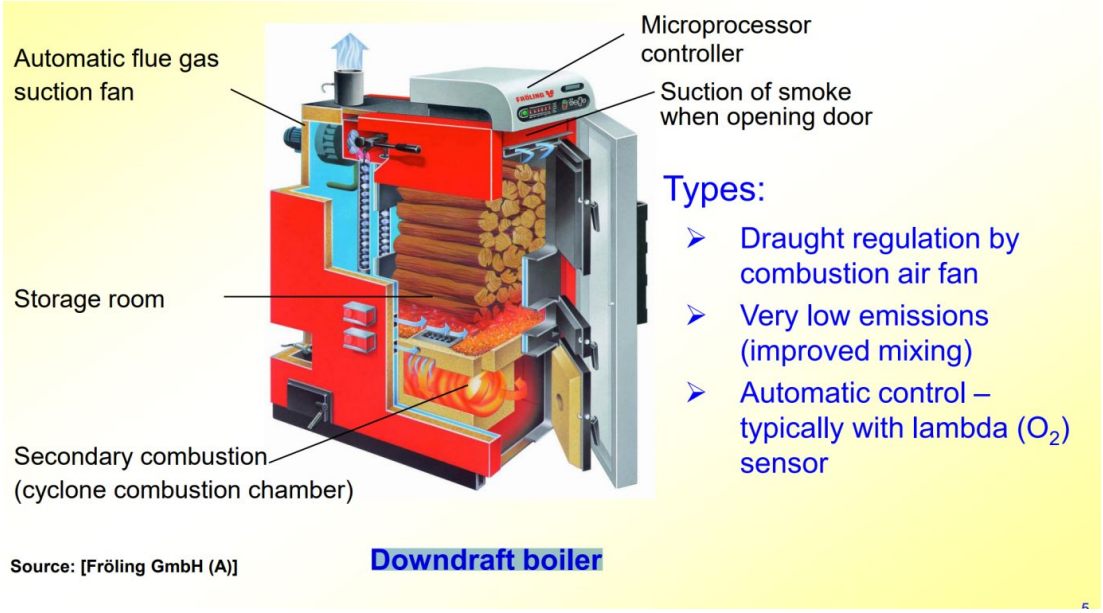

Figure 2-2 Structure of a downdraft boiler[23]

• Wood chips boilers:

Wood chips boilers are simply boilers that can be operated by burning wood chips. The majority of these boilers are classified as multi-fuel boilers as they are

also able to run on pellets or energy crops like grain. It usually has a large capacity fuel store, allowing them to run fully automatically without the need for manual fuel loading every day like logwood boilers. The only thing that needs to be handled manually is the emptying of the ash box. There is an auger that runs straight from the boiler into the center of the fuel store. When the boiler requires fuel, the auger turn and then takes the fuel to the boiler. Wood chip is typically 20 to 30% cheaper than wood pellets per kWh, but due to the bulk density and calorific value， a given volume of wood pellets hold around 3.5 times the energy of the same volume of chips. This means that larger fuel stores are required with chips boilers.

Figure 2-3 shows the structure of a modern wood chip and pellet boiler. It is a moving grate boiler with many new combustion technologies. It adjusts fully automatically according to the quality or features of the fuel through an automatic control system. With the ash removal and heat exchange cleaning functions, it can clean itself during ongoing operations even the heat exchanger cleans itself and removes its own ash.

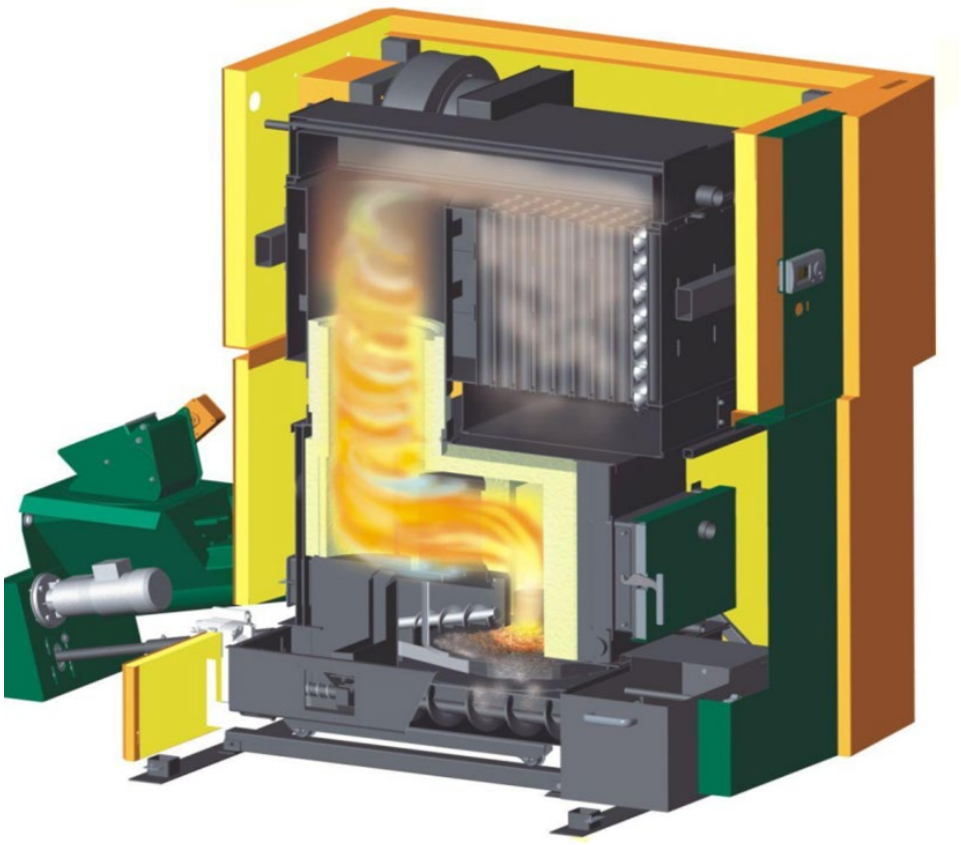

Figure 2-3 Structure of a modern wood chip and pellet boiler[23]

• Pellets boilers:

A pellet boiler is a heating system that burns pellets. Pellet boilers are typically used in central heating systems for single-family homes and larger residential, commercial, or institutional. The use of pellets for domestic heating is quite recent. Pellets boilers were developed in the 1980s. But the significant market penetration of pellet boilers has only taken place in the past two decades with rising oil prices.

Pellet boilers can achieve high-efficiency and low-emission combustion. The best pellet systems can achieve efficiencies of over 80% with very low emissions. Modern pellet boiler uses temperature or flame space sensor in combination with a suck-blow fan or a lambda probe to achieve complete combustion.

The heat output of domestic pellet boilers is usually less than 25 kW. Depending on the feeding systems, three different types of burners can be identified, as shown in Figure 2-4.

Underfed burner (Figure 2-4 part A) - The pellets are pressed from below into retort furnaces by an auger where they are burnt and the ash that remains falls over the edge of the plate into the ash pan below. The characteristic of this feeding system is that the emission is relatively stable.

Horizontally fed burners (Figure 2-4 B) - The technology functions similarly to underfed combustion, except that the fuel is forced from the side onto the burner plate by an auger. At the same time, the combustion plate and air supply can be configured to match part of the performance.

Overfed burners (Figure 2-4 part C) - Pellets slide down a drop into a grate furnace. Combustion can be precisely controlled by controlling the amount of pellets and the area where they slide down. This feeding system provides the least ash compared with other systems.

The application of advanced combustion technology and excellent burner design contributes to reducing emissions.

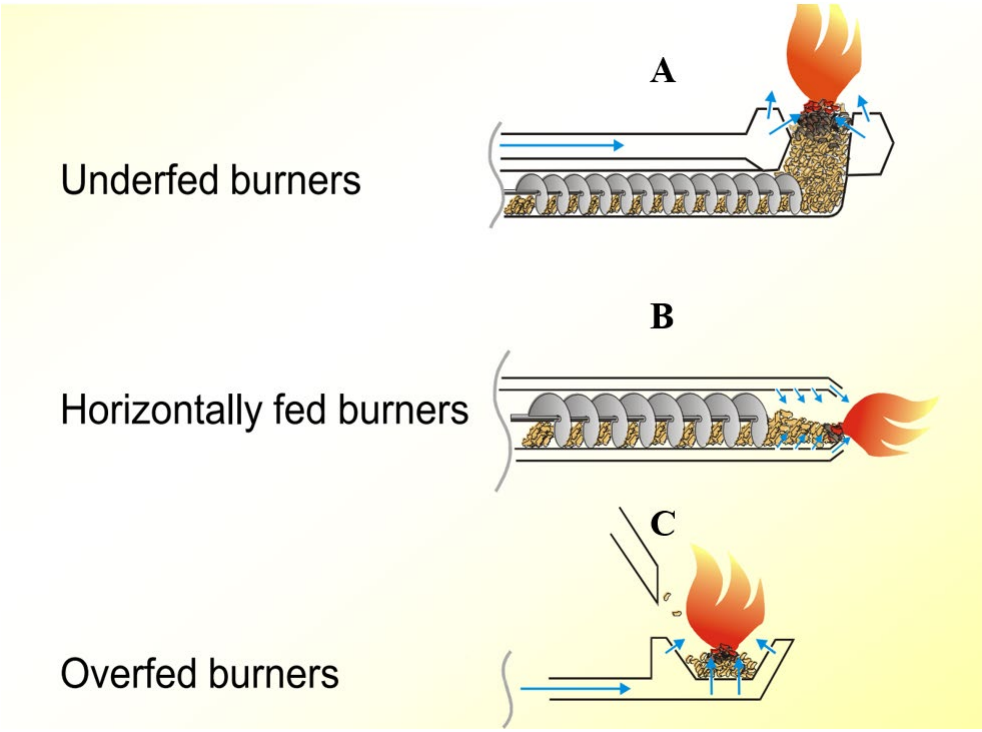

Figure 2-4 Three different types of feeding systems[23]

2.3 Wood biomass and torrefied black biomass

As mentioned above, biomass fuel has some advantages as a sustainable alternative fuel to coal and other fossil fuels as they are renewable and CO_2 neutral. They are often compared to coal and are assumed to behave like low-rank coals [24]. Relative to coal, biomass generally has less carbon, more oxygen, higher hydrogen content, larger volatile component, more silica and potassium, less aluminum and sometimes calcium, titanium, and iron [25]. The main problems related to the use of biomass fuel for energy production are linked to its lower heating value, high moisture content, and heterogeneity, which create difficulties in handling, transport, and storage [26]. Low energy density means that the transportation cost per energy unit is higher, and more storage space is required, which makes biomass logistics expensive. The high moisture content reduces the heating value of the biomass. The wetter the biomass is, the less energy that can be obtained from its combustion. The heterogeneity of biomass can also cause problems in the final conversion stage.

A recent trend to remedy the critical issues of using biomass for combustion is densification and standardization. Compressing raw materials to obtain denser

fuels with homogeneous properties and dimensions, is also characterized by higher energy density [27].

Among the various densification processes available, pelletizing is currently the most extended one. Biomass use in form of pellets generates a biofuel that is more cost-effective than the direct use of non-modified biomass residues for energy production [28]. Pelletizing process involves applying high pressure and high temperature to the pretreated semi-dry biomass and passing it through holes of a specific size to produce cylinders, which are then cut and cooled. This process increases the bulk density of biomass, thus reducing handling, transport, and storage costs [29]. Particle quality is affected by several parameters such as the properties of the raw material such as moisture content, particle size distribution, and chemical composition, and fabrication conditions such as temperature, pressure, and holding time [30].

2.3.1 Wood pellets

Although pellets can be produced from various raw materials such as wastes obtained from forestry, agriculture, or a combination of the latter, wood represents the main feedstock for pellet production. Wood pellets are often seen as a solution to alleviate the disadvantages of using biomass as a sustainable alternative fuel. Wood pellets have a higher energy density, higher calorific value, and lower moisture content than woodchips or untreated biomass. They are made uniform in size and more homogenous regarding fuel quality.

However, wood pellets still have some disadvantages. Despite the low moisture content of the wood pellets, it still retains the hygroscopicity of the wood pellets and is susceptible to water. The possibility of biological degradation can cause storage problems and implies that special precautions need to be taken in the logistics chain in general [24]. Another disadvantage is that wood pellets production has traditionally been limited to only a few types of feedstocks, mainly sawdust, shavings, and bark, which are by-products of the wood processing industry and have limited supplies to meet the increasing demand for wood pellets [31].

Non-woody biomass, such as agricultural residues, is one of the most important alternative raw materials for pelleting. This biomass has the advantages of large availability, low price, and recyclability. However, the quality of agricultural pellets is usually not as good as wood pellets, due to the low bulk density, high ash content, and low calorific value [32]. Another quality-improving

solution is post-processing of the pellets such as torrefaction, the next section describe this process and the characteristics of black particles.

2.3.2 Torrefied black pellets

Torrefaction is a thermal conversion technology that can increase the energy density of biomass, which involves heating the biomass to a moderate temperature in the absence of oxygen and under atmospheric pressure [33].

During the torrefaction process, biomass starts to decompose and releases combustible volatile matter with moisture. Considerable energy densification can be achieved by torrefaction. Research shows that the remaining solid typically contains up to 90% of the initial energy content but only 70% of the initial weight of the biomass [34].

The combination of both torrefaction and pelletizing process results in the torrefied biomass pellets (TBP's), an energy-dense biomass solid fuel. TBP’s is high bulk and energy density, high calorific value, hydrophobic nature, and improved grindability compared to untreated biomass [35].

• **Torrefaction process:**

The torrefaction process could be divided into distinct six phases: initial heating, pre-drying, post-drying, intermediate heating, torrefaction, and solids cooling. Figure 2-5 shows the general process of torrefaction combined with pelletizing.

Firstly, the biomass is subjected to initial heating until the drying temperature is obtained and the biomass humidity starts to evaporate. The pre-drying stage involves the free water present on biomass evaporating at 100 °C (constant temperature). At the post-drying and intermediate heating stages, the temperature is increased until it reaches 200 °C. The remaining water present in biomass chemical bonds is completely evaporated. This phase is responsible for mass loss due to the evaporation of light fractions of the biomass. Thereafter, the torrefaction process occurs at the maximum torrefaction temperature and the major loss in biomass mass occurs at this stage. The torrefaction temperature is given by the maximum stable temperature used during the process. The last stage involves the final product being cooled down to the ambient temperature. If the torrefaction process is combined with pelletizing, the product is cooled after size reduction and pelletizing.

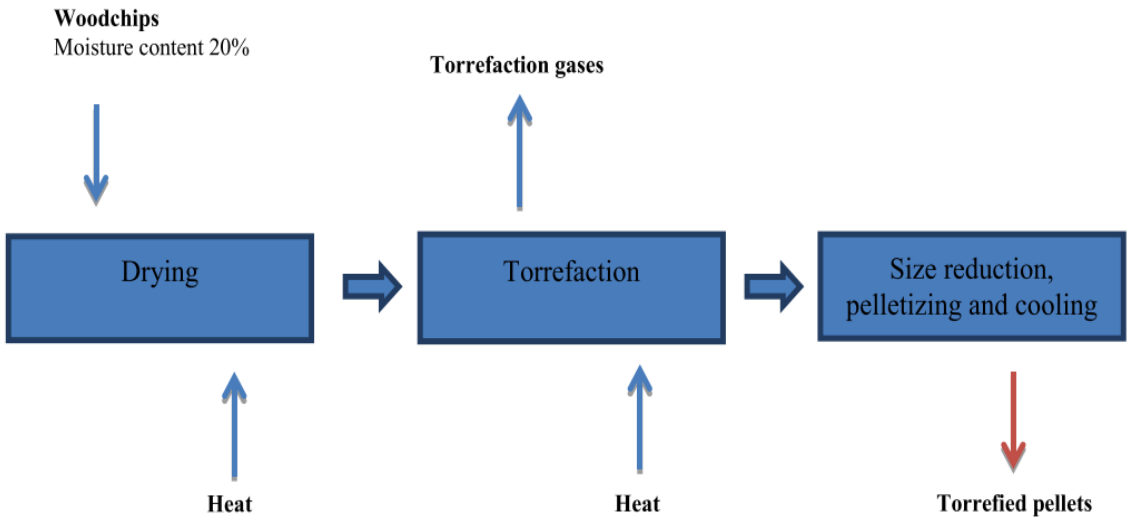

Figure 2-5 Combined torrefaction and pelletizing process [35]

• Influence of torrefaction process parameters:

During the torrefaction process, some parameters influence the final product characteristics. These parameters include the torrefaction temperature and residence time, heating rate, operating atmospheric composition, controlling of the torrefaction process instability, and the type of reactor.

In most of these studies, the effect of torrefaction temperature was paramount in determining the yield and better properties of torrefied biomass followed by reaction time and heating rate. The ideal torrefaction process should try to maximize the quality of the torrefied biomass production by optimizing these parameters or at least determining their combination. The transformation of biomass properties because of torrefaction is graphically presented in Figure 2-6.

• Torrefaction temperature:

The temperature at which the torrefaction is investigated has a significant influence on the composition of biomass especially the volatile matter and the fixed carbon. As the temperature increases, the volatile matter content of biomass decreases, and the ash content and fixed carbon content increase. This is related to the increased thermal degradation of hemicellulose and cellulose in biomass with increasing temperature [36].

• Residence time:

The residence time influences the composition and properties of the torrefaction products, although the influence is not as significant as the torrefaction temperature. The fiber structure of biomass can continue to disintegrate when the torrefaction time is increased. This results in an increase in the fixed carbon content and calorific value of the torrefied biomass. Residence time also affects other biomass properties such as grindability and surface area. The higher the residence time, the higher the grindability and the larger the surface area [37].

• Heating rate:

The heating rate is another important factor that affects the torrefaction products. Higher heating rates typically lower the effects of heat and mass transfer limitations in the biomass particles [38].

• Influence of torrefaction treatment on biomass:

Torrefaction can significantly improve the chemical and physical properties of biomass. Compared with the regular biomass materials, torrefaction can offer the following advantages such as no biological activity, hydrophobic nature, higher durability, excellent grindability, higher bulk density, more homogenous product, and higher calorific value [39].

These factors not only benefit the storage and long-distance transport of torrefied biomass or the production of solid fuel pellets but also positively influence other thermochemical conversion technologies such as pyrolysis, gasification, combustion, and co-firing. Torrefaction weakens the inherent structural chemistry of biomass, making it more susceptible to thermal degradation by other thermochemical conversion techniques [40]. The following section mainly introduces the application related to combustion.

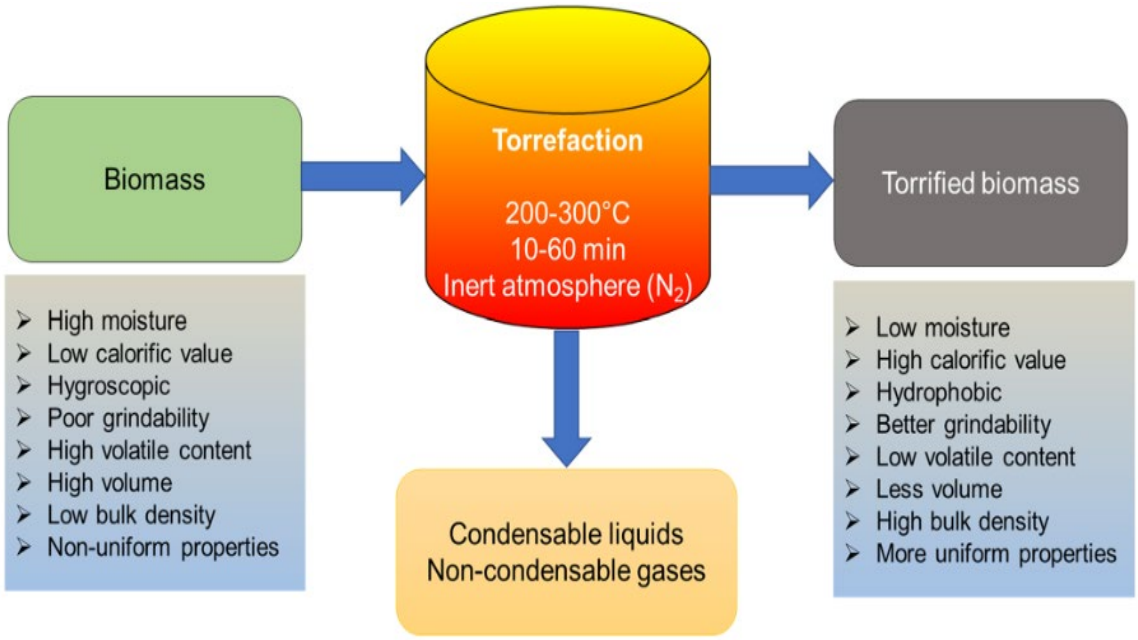

Figure 2-6 Torrefaction improves the chemical and physical properties of biomass [35]

• Combustion:

Although biomass torrefaction technology has been intensively studied by various researchers, it is still far from commercialization and industrialization. Most studies focus on the effect of process parameters on torrefaction and the properties of torrefied biomass [41]. Even the research related to torrefied biomass combustion, most studies are focused on the combustible properties of the fuel such as the ignition temperature, burnout temperature, burnout ratio, and burnout time. In particular, there are few studies on the emission of combustion pollutants.

The popular applications of torrefied biomass are combustion and co-combustion with coal for combined heat and power (CHP) generation. It is reported that the torrefied biomass has a higher reactivity than the lignite. Torrefaction has been reported to increase the ignition temperature and burnout temperature [42]. A report on the combustion characteristics of raw straw and torrefied straw in a fluidized bed burner stated that the torrefied biomass could rapidly increase the furnace temperature due to its high calorific value, low moisture content, and low atomic ratio [43]. Torrefied biomass has a higher ignition, burnout temperature, and activation energy; a lower burnout ratio and reactivity, and longer burnout time compare with raw biomass [44, 45].

Several studies have found that torrefied materials also have lower emissions of particulate matter and greenhouse gases (CO and CH_4) during combustion compared to biomass and lignite due to lower moisture content and longer combustion time [46]. In contrast, higher NO_x emission can be observed during the combustion of torrefied biomass, caused by an increase in fuel N in the torrefied fuel [47, 48]. Further analysis of pollutant emissions from torrefied biomass combustion is necessary.

2.4 Environmental impact of gas emission

Biomass combustion is a significant global source of gaseous and particulate matter emissions. As mentioned above, biomass energy is considered being the most potential renewable energy source to meet global energy requirements. This result in more biomass-combustion events in the future and probably impact global atmospheric chemistry, biogeochemical cycles and the human health [49]. Therefore, there are amount of research about the composition of biomass combustion emissions and the impact of these emissions on the atmosphere. The polluting emissions of biomass combustion are detailed below:

• Carbon dioxide (CO_2):

CO_2 is produced when the carbon in biomass is completely oxidized.

• Carbon monoxide (CO):

CO is the second most important compound following carbon dioxide in any combustion process of organic material. It is formed during the carbon oxidation stage of the fuel, and it is an indicator of the quality of combustion. Most CO is emitted during the smoldering stage. Only very low levels of CO are produced under complete combustion conditions [50].

• Nitrogen oxides (NOx):

NOx mainly comes from the nitrogen contained in the fuel. The pyrolysis of wood produces a few molecules of NH_3 and HCN, which are then oxidized to NO and NO_2. Studies have shown that most of these compounds are emitted in the form of NO and NO_2, and these two compounds are mainly released during the flaming phase of the fire. The emission of ammonia is very low and most of it

occurs during the smoldering phase, the emission ratio being 20 times higher than during the flaming phase [51].

• Chlorine and sulfur oxides compounds:

The chlorine and sulfur content in wood biomass is generally very low, which means that the emissions of reaction products of these elements are very low, and they are only present in trace amounts.

• Particulate matter (PM):

Particulate matter, also known as atmospheric aerosol particles or suspended particulate matter, are microscopic particles of solid or liquid matter suspended in the air. The term aerosol generally refers to a mixture of particles and air, as opposed to PM alone. PM can have natural or anthropogenic sources and are either primarily emitted or formed in the atmosphere from precursor gases. PM consists of complex mixtures of organic and inorganic compounds, exhibiting a wide spectrum of physical and chemical properties. It is both a major driver of climate change and a source of toxicity for health [52].

• Volatile organic compounds (VOCs):

VOCs are hydrocarbons that easily evaporate at room temperature. They are formed during the carbon oxidation stages and are emitted significantly by biomass combustion. As directly toxic to the environment and indirectly as ozone/smog precursors, VOCs are listed as major contributors to air pollution [53]. The formation of ozone and other photo oxidants from the conversion of VOCs may have a significant impact on the regional environment and the health of the population even living thousands of miles away [54].

• Polycyclic Aromatic Hydrocarbons (PAHs):

PAHs are a group of organic compounds that contain aromatic rings. They have been reported to be emitted in large amounts during biomass combustion [55]. The growing attention to PAHs is due to their associated health risks, as some individual compounds have been identified as mutagenic, genotoxic, and carcinogenic [56, 57]. Several studies have demonstrated that higher combustion temperatures in the modern boiler may lead to higher PAH emissions [58].

• Dioxins and dioxin-like compounds:

Dioxins and dioxin-like compounds are the generic terms for polychlorinated organic compounds. They are persistent organic pollutants (POPs) in the environment. Dioxins have different toxicity depending on the number and

position of the chlorine atoms. In general, dioxins are very hazardous to the human body because they accumulate in animal and human fats which can cause cancer, damage the immune system and interfere with the hormonal system [59]. Generally, biomass fuel usually is lean in chlorine which is one of the key factors for dioxins formation. However, anthropogenic biological wastes or other synthetic substances, as well as their additives and coatings (such as wood preservatives, paints, pesticides, etc.) are usually present in the biomass, making the emissions of dioxin higher than the emissions during pure combustion [60].

• **Tars:**

Refers to the heavy hydrocarbons which condense, they mainly come from the wood pyrolysis stage.

The majority of pollutants emitted by the combustion of biomass come from domestic heating, and not from industrial or collective heating. Despite the growth and development of domestic combustion systems on the market, their operation remains constrained by certain specific characteristics of biomass. The latter contains humidity, alkaline elements, and other constituents such as nitrogen (N) and sulfur (S) which are present in different proportions depending on the type of biomass used.

During combustion, the humidity contained in the biomass causes problems such as delayed ignition, increased fuel residence time in the combustion chamber, and reduced flame temperature [61]. These problems lead to incomplete combustion and therefore to increased emission levels of CO, NOx, VOCs, PAHs, and soot. Therefore, this chapter focus on these pollutant emissions.

2.4.1 Formation of carbon monoxide (CO)

As mentioned before, CO is formed during incomplete combustion, when the amount of air supplied is less than stoichiometric. During the combustion of biomass fuels, CO may be released directly as a volatile compound or form as an intermediate product in either heterogeneous reactions involving the char oxidation or homogeneous reactions in the gas phase. A distinction was made between the mechanisms involved in the heterogeneous phase and the homogeneous phase [62].

The heterogeneous reactions are written as:

$$\varphi\ C\ + O_2\ \rightarrow 2(\varphi - 1)CO + (2 - \varphi)CO_2 \qquad \text{Equation } 2 - 7$$

$$C + CO_2 \leftrightarrow 2CO \qquad \text{Equation } 2-8$$

$$C + H_2O \leftrightarrow CO + H_2 \qquad \text{Equation } 2-9$$

and the homogeneous reactions as:

$$CO + 0.5O_2 \rightarrow CO_2 \qquad \text{Equation } 2-10$$

$$CO + H_2O \leftrightarrow CO_2 + H_2 \qquad \text{Equation } 2-11$$

$$CO_2 \leftrightarrow CO + 0.5O_2 \qquad \text{Equation } 2-12$$

Where φ is the equivalence ratio.

Under air-fired conditions, the release of volatiles and oxidation of the char (Eq. 2-7) are the main drivers for CO formation. Since char oxidation occurs at higher temperatures than devolatilization, the char temperature must therefore be higher than the vaporization temperature to activate this reaction. The carbon monoxide then react with oxygen in homogeneous reactions (Eq. 2-10). However, under oxyfuel-fired condition, the gasification reactions (Eq. 2-8 and Eq. 2-9), the water-gas shift reaction (Eq. 2-11) and CO_2 dissociation (Eq. 2-12) may affect the formation of CO [63].

2.4.2 Formation of nitrogen oxides (NO_x)

Emissions of nitrogen oxides from combustion and high-temperature industrial processes continue to be of major environmental importance. When NO_x and volatile organic compounds react in the presence of sunlight in the atmosphere, they form photochemical smog, a significant form of air pollution. Nitric oxide and nitrogen dioxide are precursors of acid rain and participate in the production of photochemical smog, while nitrous oxide is a greenhouse gas [64]. Life cycle assessment studies indicate that a great part (40%) of the environmental impact of a modern automatic wood furnace may be associated with NO_x emissions [65].

There are three gas-phase reaction mechanisms for NO_x formation in combustion processes:

• Thermal NO_x mechanism:

Nitrogen in the air begins to react with O radicals and forms NO at temperatures above approximately 1300°C. The reactions are temperature,

pressure, and residence time-dependent. Decreasing any of these three reduces the NO_x. However, the exponential dependence on temperature makes reducing combustion temperature the key strategy to low NO_x combustion [66].

While thermal NO_x mechanisms can be significant for fossil fuel combustion applications, in biomass combustion, the temperature in the combustion chamber is typically below 1300°C, which makes this mechanism less efficient [67].

• Prompt NO_x mechanism:

Nitrogen in the air reacts with radicals such as C, CH, and CH_2 fragments derived from fuel. This results in the formation of fixed species of nitrogen which can oxidize to NO [64]. The fast NO_x mechanism is less temperature-dependent and much faster than the thermal NO_x mechanism. However, it is only significant under fuel-rich conditions and strongly depends on the CH mole fraction. In fuels that contain nitrogen, the incidence of prompt NO_x is comparatively small, and it is generally only of interest for the most exacting emission targets [68].

• Fuel NO_x mechanism:

NO_x formation in biomass combustion is dominated by the fuel-N mechanism. Nitrogen in the fuel is converted to NO and NO_2 through a series of elementary reaction steps called the fuel oxidation mechanism. The conversion of fuel-N starts with the pyrolysis of biomass material.

Large amounts of NO and N_2 can be found in the pyrolysis gases while a part of the fuel-N is converted to volatile-N (NH_3 and HCN). If enough O_2 is available, NH_3 and HCN were mainly converted to NO through different reaction pathways. However, under fuel-rich conditions, NO react with NH_3 and HCN, forming N_2. This reaction is used as a primary measure of NO_x reduction. By optimizing the ratio of excess primary air, temperature, and residence time, maximum conversion of NH_3 and HCN to N_2 can be achieved [69].

The other part of the fuel-N that remains in the char matrix is called char-N. Char-N is oxidized to NO and N_2O in the presence of oxygen through homogeneous or heterogeneous reactions [70].

The distribution of the fuel-N between the volatiles and the remaining char is roughly proportional to the volatile matter in the fuel and it is important because while the conversion of volatile-N can be reduced by air control, char-N conversion into NO_x emissions is more difficult to overcome [71].

There is a logarithmic dependence between the amount of NO_x formed and the mole fraction of N in the biomass. To reduce NO_x emissions, it is necessary to

take into account factors such as the air supply, the air staging, the design of the boiler, and even the combustion gases recirculation [72].

Due to the limitations of analyzer, this thesis does not measure and analyze NOx.

2.4.3 Formation of VOCs

Volatile Organic Compounds (VOCs) are a general term for organic compounds existing in the gas phase at normal temperature and pressure. VOCs include lower hydrocarbons, alcohols, aldehydes, ketones, etc.

A large variety of different VOCs is formed during the process of biomass pyrolysis and devolatilization. These VOCs have very different vapor pressures and molecular structures. If these VOCs cannot be burnt out during the subsequent combustion process, they exist on fine particles through condensation and/or adsorption [73].

VOCs are classified as major contributors to air pollution. They contribute both indirectly as ozone/smog precursors and directly as substances toxic to the environment. The effect of VOCs on the atmosphere depends on the nature of VOCs, their mole fraction, and emission sources. However, they have been identified as being responsible for stratospheric ozone depletion, tropospheric ozone formation, ground-level smog formation, climate change, sick building syndrome, decay of plants, the toxicity of the atmosphere, and carcinogenic effects in humans [74, 75].

Methane is one of the most important VOCs from biomass combustion. It contributes to both the emission of organic particles and global warming.

2.4.4 Formation of PAHs

PAHs are a group of organic compounds comprising two or more aromatic benzene rings. They have received much attention due to their toxicity to humans.

Some studies have found that PAHs were metabolized after entering the human body and converted into quinones, epoxides, and hydroxyl derivatives. These metabolites have been identified as mutagenic, genotoxic, and carcinogenic. Therefore, exposure to PAHs may lead to adverse health effects, including asthma, bronchitis, pulmonary tuberculosis, and even lung and laryngeal cancer [76].

In addition, PAHs emitted from the biomass combustion can be mixed with lignin-derived products (veratraldehyde and vanillic acid) and flavonoids to

produce enhanced PAH mixtures [77]. This enhanced mixture not only poses a serious hazard to human health but also extends the lifespan of PAHs in the atmosphere, enabling them to spread over long distances [78].

PAHs are produced by incomplete combustion or pyrolysis of organic fuels such as fossil fuels and biomass. The PAHs from biomass burning represented a high proportion of the total emissions. Therefore, although biomass fuel is a renewable carbon-neutral energy source, to promote its eco-friendly and healthy development, it is crucial to study the PAHs characteristics of biomass combustion emissions and their influencing factors [79].

The formation of PAHs is affected mainly by biomass properties and combustion conditions. In the theoretical biomass combustion process, the volatile in the biomass is completely oxidized to CO_2 and H_2O under high temperature and aerobic conditions, and the remaining char in the biomass is oxidized to form CO, CO_2, and ash in the presence of sufficient oxygen. However, in the actual biomass combustion process, some theoretical combustion steps occur simultaneously. For example, the drying and pyrolysis process occurs simultaneously with char combustion, thereby reducing the combustion temperature. The oxidation of volatiles and char occurs simultaneously, resulting in insufficient oxygen supply for both processes [78]. Insufficient temperature and oxygen lead to incomplete combustion of volatiles and char. These processes facilitate the production of PAHs.

In addition, the volatile react with char to produce gaseous products, including small hydrocarbon radicals and hydrocarbons. These gaseous products were converted to PAHs through incomplete combustion during devolatilization [80].

2.5 Soot particles formation and properties

Particulate matter (PM) is a microscopic particle of solid or liquid matter suspended in the air as mentioned above. Airborne PM is a pollutant of great importance which presents many challenges. Firstly, the presence of PM is more dangerous to human health than ground-level ozone or other common air pollutants such as carbon monoxide. Numerous scientific studies have explained particle exposure as the source of various health problems including heart disease and stroke, lung cancer, chronic lung disease, and respiratory infections [81, 82]. Besides, PM both absorbs and reflects solar radiation, influencing upon the albedo of clouds therefore affects climate [83, 84].

Biomass burning is a principal contributor of PM to the environment [85]. Generally, PM released from biomass combustion consists of organic carbon (VOCs, PAHs, and black carbon) and inorganic elements. VOCs and PAHs are the pollutants mentioned above, the black carbon could be an important factor in global warming since it absorbs visible solar radiation. Therefore, it is necessary to understand the PM emissions from biomass combustion in detail.

• PM Classification:

Although PM can be classified in many ways, aerodynamic diameter is one of the main criteria to describe its transportability in the atmosphere and inhaling ability through a respiratory organism [86].

-Coarse particles (PM10): The particles whose aerodynamic diameter is less than 10 μm. PM smaller than about 10 μm, can settle in the bronchi and lungs and cause health problems [87]. PM10 is approved by regulatory agencies to monitor particulate matter in the air and much of the earlier research has focused on it.

-Fine particles (PM2.5): The particles whose aerodynamic diameter is less than 2.5 μm. Due to its small diameter, PM2.5 not only damages airway cells to trigger an inflammatory response, but also enters the bloodstream, causing high blood pressure and blood vessel damage, and even spread to other organs, such as the heart, damaging its cellular structure and function. Sustained exposure to high levels of PM2.5 has also been linked to various diseases, such as diabetes and prenatal disorders [88, 89]. PM2.5 has replaced PM10 as the preferred indicator in most contemporary studies due to these significant health impacts.

-Ultra-fine particles (PM0.1): The particles whose aerodynamic diameter is less than 0.1 μm. These are often also referred to as nanoparticles because of their nanometer dimensions. Research on the effects of PM0.1 is still ongoing. Early results indicate that it may be more hazardous than PM2.5 due to its smaller size and larger surface to volume ratio, it can penetrate alveoli (the gas exchange area) and hence the circulatory system [90]. There is still more research needed to understand the apparent substantial negative effect of PM0.1 on human health.

PM can be also classified as primary particles which are the particles directly emitted into the atmosphere, and secondary particulate matter (SPM) which formed within the atmosphere from the condensation of trace gases [91]. Particulate matter in the ambient air is a mixture of directly emitted primary particles and secondary particles formed in the atmosphere.

- Primary particles: Coarse particles from primary particles originate mainly from mechanical processes such as construction activities, road dust, etc., whereas fine particles are particularly produced through Diesel engines and biomass combustion [92].

- Secondary particles: which are formed in the atmosphere through the conversion of gaseous precursors such as sulfur oxides (SO_2, SO_3) and nitrogen oxides (NO, NO_2) from energy, industry, and domestic fuel combustion, ammonia (NH_3) from diesel engines combustion, non-Methane Volatile Organic Compounds (NMVOC) from use of solvent, chemical industry and petrol chemistry [93, 94].

• PM of biomass combustion:

Biomass combustion is one of the major contributors to fine particulate matter emissions. In particular, small-scale combustion systems are accused of generating significant amounts of particles in Europe [95,96]. Investigations show that biomass combustion contributes more than 20% of carbonaceous PM in France during winter [97]. Therefore, it is necessary to identify the most important particulate sources in biomass combustion and to derive measures to reduce PM. There are three main sources of particulate matter from biomass combustion: soot particles, organic particles, and ash particles. Soot and organic particles are formed by incomplete combustion in the flame zone, while ash particles are non-combustible material. The following sections briefly describe the different types of primary particles.

• Soot particles:

Soot particles represent a complex mixture of amorphous elemental carbon (main component) and other organic matter. Soot consists mainly of carbon with a significant percentage of hydrogen [98]. Soot properties and morphology can be classified from nascent to mature soot by carbonation ratio (H/C ratio) [99]. A primary soot particle may have about 106 carbon atoms and 10% to 25% H atoms. Nascent soot particles contain a high H percentage, while the H percentage in mature soot is only almost 10%. The smallest nascent soot particles are only 1 nm in diameter, However, mature soot particles agglomerates built from primary particles with different size diameters can reach hundreds of nanometers in diameter [99].

Soot particles are formed mainly inside the flame in the fuel-rich area via complex mechanisms. The major steps leading to soot formation are nucleation,

coagulation, surface reactions, and agglomeration [100]. The schematic of soot formation was shown in Figure 2-7.

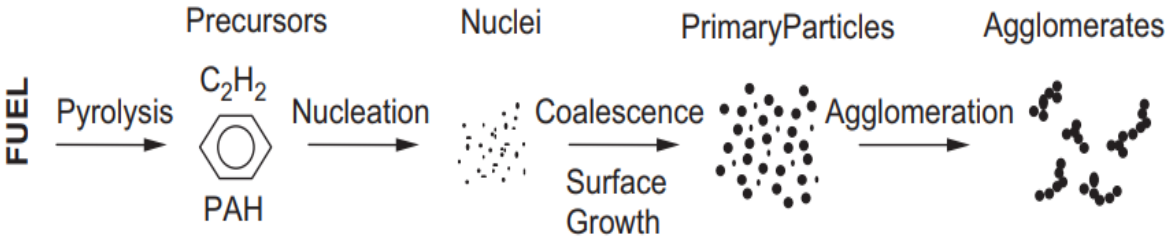

Figure 2-7 Schematic diagram of the steps involved in soot formation [103]

Firstly, during the process of biomass pyrolysis and devolatilization, some hydrocarbon fragments leave the fuel particles and crack into smaller pieces.

Then these fragments react with one another and surrounding gases to form aromatic rings which form polycyclic aromatic hydrocarbons (PAHs). Acetylene (C_2H_2) is one of the most abundant hydrocarbons in the incipient zone of a flame. The C_2H_2 molecule realizes the growth of the PAHs from the first aromatic ring to large molecules through the HACA mechanism [101]. The formation of PAHs with a high number of rings is the next step in the soot formation process.

The next step is the birth of a particle nucleus whose growth by adding acetylene or other gaseous molecules leads to the final formation of the soot particle. Generally, there are two pathways for soot formation. The first way is the aromatic hydrocarbons which directly produce soot by transforming into a structure similar to graphite at lower temperatures. Another way is aliphatic and aromatic hydrocarbons first fragment and then the fragments polymerize to form larger molecules, thus forming soot at higher temperatures [102].

Thereafter, the soot particle size grows larger through two processes. The first process is based on the condensation of PAHs onto the soot carbon matrix. The second process involves heterogeneous reactions between the soot carbonaceous matrix and the surrounding gaseous precursors. Through these two physical or chemical pathways, the newly formed soot particles (nanoparticles) are called nascent soot particles [103].

The particles produced by the nucleation step coalesce and then form aggregates through coagulation. These aggregates are quickly covered by the outer shell generated by material deposition from the gas phase. The coagulation

increases the particle size and decreases the particle number without changing the soot volume fraction. This process is accompanied by a gradual reduction of hydrogen and a rearrangement of the internal structure of the soot particles. The size and structure of the particles change as the soot grows. After coagulation and surface growth, the particle size can reach several nanometers [104].

The last process is the aggregation of the particles. The soot particles can undergo several surface reactions having as consequence aggregation. The mature soot is not coagulating anymore, but particles can merge. Thus, aggregation reactions allow the formation of soot aggregates with complex morphology and shape [105].

The soot particle formation process mainly depends on the fuel, the combustion conditions, and the type of flame. In industrial-scale biomass burners, the amount of soot in the emissions is usually negligible, whereas, in traditional small burners, soot can be a significant portion of fine PM emissions.

• Organic particles:

A large variety of different VOCs is formed during the process of biomass pyrolysis and devolatilization. These VOCs have very different vapor pressures and molecular structures. If these VOCs cannot be burnt out during the subsequent combustion process, they were emitted in the flue gas as organic particles. If the combustion is highly incomplete, heavy complex organic compounds are released from the flue gas.

Incomplete biomass combustion produces hundreds of VOCs. Methane is one of the most important VOCs from biomass combustion. It both contributes to the emission of organic particles and contributes to global warming. In flue gas conditions, the VOCs are mainly present on existing fine particles through condensation and/or adsorption [106].

• Ash particles:

Biomass fuels contain considerable amounts of inorganic elements responsible for the formation of ashes during combustion. These elements can be divided into different categories [107]:

- Non-volatile elements, such as calcium (Ca), magnesium (Mg), aluminum (Al), ferrous (Fe), etc.

- Easily volatile elements, such as sodium (Na), potassium (K), sulfur (S), and chlorine (Cl).

- Easily volatile heavy metals, such as zinc (Zn), cadmium (Cd), lead (Pb), etc.

The ash formed in biomass combustion can be divided into two main fractions, fly ash (PM found in the fumes) and bottom ash (remaining in the installation). Bottom ash mainly consists of non-volatile species but also contains the not released part of the easily volatile elements. Fly ash consists of ash entrained from the fuel bed with the combustion gases and is therefore mainly composed of refractory species. Their particle size can vary from a few nm to about 200 nm [108].

As shown in Figure 2-8, fly ash is mainly formed by two pathways [109]:

- the formation of fine ash particles (< 1 μm): during biomass combustion, volatile elements and compounds such as alkali metals, S, Cl, and heavy metals form inorganic vapors through homogeneous reactions in the gas phase. Then the inorganic vapor forms new particles through nucleation or condensation. Finally, fine ash particles with a size range of higher than 1 μm are formed by agglomeration processes.

- the formation of coarse ash particles (> 1 μm): a minor portion of the ash particles is entrained from the fuel bed with the flue gas and forms the coarse fly ash particles with a size range of more than 1 μm.

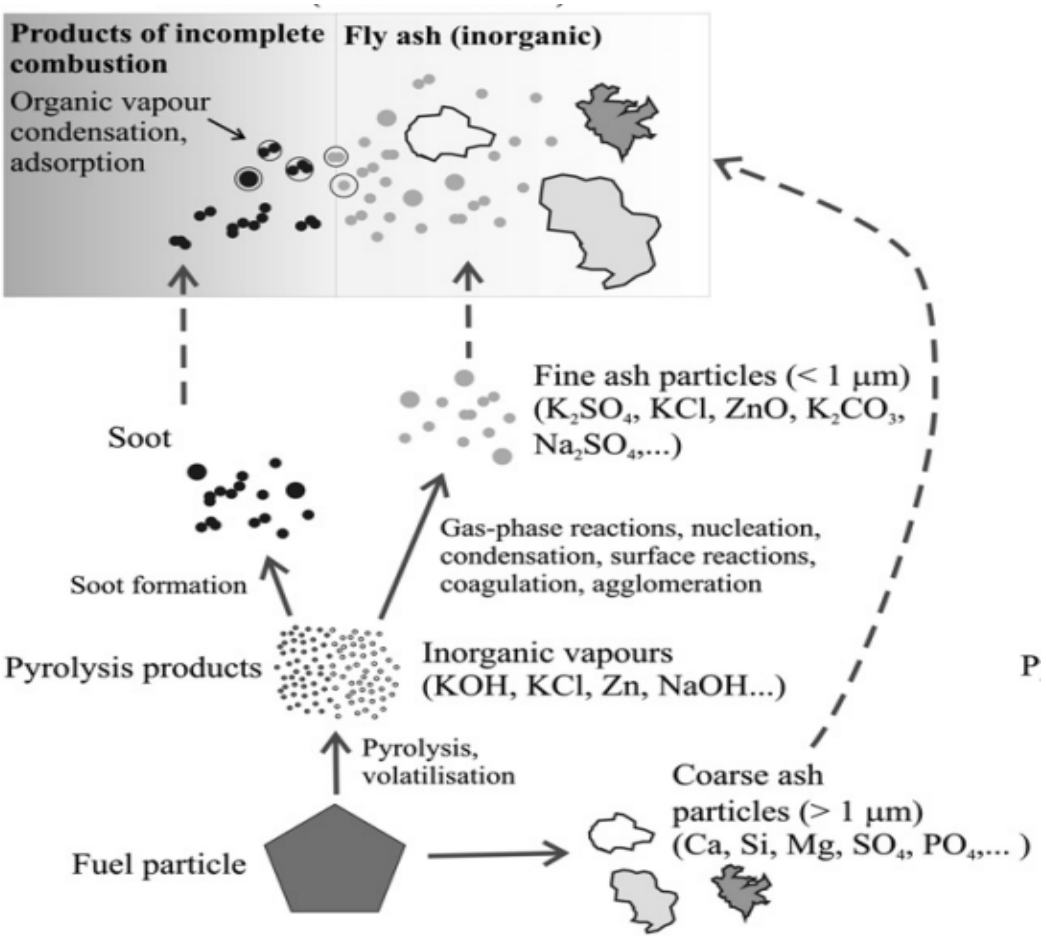

Figure 2-8 Particle formation process [109]

The behavior of ash forming species is significantly influenced by the fuel ash properties such as the chemical form, ash composition and the ash forming materials. In addition, Ash behavior is also related to combustion technology, combustion temperature, and combustion conditions [102].

2.6 Emission reduction methods

Methods to reduce pollutant emissions can generally be divided into two categories, primary measures to avoid the formation of such substances and auxiliary measures to remove pollutants from exhaust gases. Both methods can effectively reduce pollutant emissions in the exhaust gas, due to the special characteristics of small combustion installations - low and medium activity levels, two general approaches can be used.

Primary measures: in relation to small combustion installations, primary measures of emission reduction include technological activities for reducing original emissions from incomplete combustion. Therefore, it is necessary to

ensure the optimal content of air relative to the fuel, to maintain the proper combustion temperature for the fuel, to ensure that air turbulence is required for adequate air-fuel mixing, and to ensure the residence time so that the fuel is fully burned in the furnace.

Secondary measures: this involves setting up flue gas treatment systems at the outlet of the device. Specific devices must be developed depending on the nature of the pollutants to be treated:

- PM treatment systems: there are many types of systems such as settling chambers, cyclone separators, fabric filter and electrostatic precipitators. The selection of a PM treatment system mainly compares the technology used, the equipment size, installation location and cost, and the efficiency limit particle size fraction which is the smallest size of particles after filtration.

- CO and VOC treatment system: use of catalysts (often more effective for CO emissions than for VOC emissions). The catalytic converter is usually placed inside the flue gas channel beyond the main combustion chamber. When the flue gas passes through the catalytic combustor, some pollutants are oxidized.

- NO_x treatment systems: use of selective non-catalytic reduction (SNCR) and selective catalytic reduction (SCR).

Since secondary emission reduction measures which common to large-scale biomass boiler are still too expensive, they are not feasible to be applied in small-scale biomass boilers. Although the primary measures also increase the combustion equipment cost, they are viable for small-scale boilers compared with the secondary measures costs.

2.6.1 Air staging

Air staging is an important primary emission reduction measure and is now commonly used even in small-scale biomass combustion system [110]. The mixing between combustible gases and the air is often a limiting factor for burnout quality. Air staging combustion is applied with primary air injection in the fuel bed and consecutive secondary air injection in the combustion chamber. This allows creating a fuel-rich zone in the primary combustion zone where reduction conditions prevail due to lack of oxygen, and a secondary burnout zone where the air mixes well with the combustible gases formed by devolatilization and gasification in the fuel bed to complete the fuel combustion [111].

Essentially, air staging spatially separates the combustion of solid fuel into two or more streams to facilitate the formation of a reaction zone. It manifested in the spatial and temporal separation of devolatilization processes, coke oxidation processes and gas-phase oxidation [112].

The experimental study of small wood pellet boilers operating under air classification conditions has always been one of the hotspots in the study of energy technologies to reduce pollutant emissions. Such studies mainly include experiments under laboratory conditions, such studies mainly consist of experiments under laboratory conditions and consider various process parameters such as secondary air (SA) to primary air (PA) ratio, excess air, air preheating, and geometrical parameters such as grate design, SA injection design, SA injection location, etc. It was shown that air staging strategies can not only reduce NO_x emissions but also have the potential to reduce particulate matter and CO emissions [65].

• NO_x and CO:

The parameters influencing NO_x control in air staging can be further investigated with laboratory reactors. For example, Skreiberg et al. [113] concluded that there was an optimum combination of temperature, residence time, and PA ratio for each combustion appliance which minimized the NO_x emissions. However, the PA ratio was the key variable in reducing NO_x emission.

Saastamoinen et al. [114] showed that lower primary airflow rates can achieve lower NO emissions. The lower oxygen mole fraction causes NO to act as an oxidant for CO, CH_4, HCN, and NH_3 in the reduction zone, reducing the nitrogen in NO and NH_3 to molecular nitrogen.

Lamberg et al. [115] investigated the effect of air staging on gaseous emissions from a small biomass pellets boiler. It was found that while maintaining a constant total air-fuel ratio, CO emissions levels significantly decrease with a decrease in PA. On the contrary, a decrease in SA resulted in higher CO emissions.

Houshfar et al. [116] state that emissions of NO_x can be reduced by 50–80% through its use in combination with air staging strategies and other primary measures such as flue gas recirculation. The NO_x emission levels were sensitive to the PE ratio, and an optimum value was determined at about 0.9 at a total excess air ratio of 1.6.

Qiu et al. [117] investigated the CO and NO_x emissions of a 50 kW domestic biomass boiler. The results show that PA supply plays an important role in

combustion. The NO_x emissions increase with the PA ratio increase, but the CO mole fraction decrease when excess air ratio increases.

Liu et al. [68] investigated the effect of different PA/SA ratios and different SA inlet positions on NO_x emissions. The authors concluded that air staging can be effective and lead to substantial NO_x reduction, especially for biomass fuels containing relatively high fuel N. Furthermore, the height of the SA inlet above has a significant effect on both NO_x and CO emissions.

Caposciutti et al. [118] observed the CO and NO_x emissions at several SA/PA ratios and excess air combinations. The CO emissions were minimized with an air excess equal to 2 but at a considerably lower SA/PA mass flow ratio of 0.06. The minimum NOx emissions recorded at an air excess was equal to 7.7 and SA/PA ratios of 0.19 respectively.

Li et al. [119] studied the correlation between SA/PA ratio, PA to total air ratio, overall air excess, and NO_x emissions. The results showed that air staging can significantly reduce NO_x emissions. The lowest NO_x emissions were achieved when the SA/PA ratio, PA to total air ratio, and overall air excess were at 0.4, 0.71, and 2.04.

The above experiments demonstrate that air staging can be effectively used to reduce NO_x emissions from biomass combustion. The trade-off between NO_x and CO emissions should be carefully considered, since air staging may cause an increase in CO and unburnt hydrocarbons.

The optimum primary air ratio is independent of the fuel used for any given technology whereas the actual primary air ratio at which NO_x emissions are minimized is a characteristic of the technology/boiler design [120]. The PA/SA ratios help to control the combustion partition between the fixed fuel bed and the post-combustion region, sort of as a “fine-tuning” parameter for minimizing the pollutant production [116]. Experimental results for both staged and non-staged air combustion have shown that NO_x emission levels are not affected significantly by temperature for temperatures lower than 1000°C [120]. NO_x reduction requires residence time greater than 0.3-0.7 s, and the main combustion chamber in residential heating boilers is usually too small (short residence time) to effectively reduce NO_x [121].

• PM:

The impact of air staging on PM emissions has also been extensively studied. Nussbaumer reported that PM emissions can be reduced up to a factor of five

owing to the lower conversion rate of potassium (K) to volatiles at low primary excess air ratios. However, higher excess air levels may reduce combustion efficiency by reducing combustion temperature, leading to higher PM and CO emissions [65].

Wiinikka et al. [122] report that imperfect combustor design resulted in higher PM emissions. The secondary air injection angle and higher residence time influenced temperature in the post-combustion zone and associated total PM emissions.

Lamberg et al. [115] concluded that sufficient primary and secondary airflow reduces PM emissions by increasing the mixing rate in the post-combustion zone; therefore, the ideal ratio of primary to secondary air should be maintained to achieve complete combustion.

Carrol et al. [120] studied the effects of excess air ratio in the primary combustion chamber, the temperature in the primary combustion chamber, and overall excess air ratio, on NOx and PM emissions of five biomass fuels. It was concluded that by optimizing the PA ratio and keeping the temperature of the main combustion chamber around 900 °C, it is possible to minimize PM emissions while reducing NOx.

Khodaei et al. [111] investigated the effects of different air staging strategies on CO and PM emissions. A 50% CO reduction and 9 times less particle mass mole fraction than no staged combustion were achieved by deploying a uniform SA module in a higher position from the bed.

The experimental results demonstrate that by implementing an effective air staging strategy, it is possible to reduce the emission of gaseous pollutants while reducing the PM emissions.

It is clear that the effectiveness of air staging depends greatly on the geometry and process parameters of the observed combustion system, whereas the geometry parameters are determined by the design of the boiler, the process parameters are adjusted mainly for the specific properties of the fuel used, and are largely limited by the geometric parameters [112]. It concluded that establishing an optimal PA/SA ratio and an optimal global air excess is of great importance to achieve an effective reduction of emissions in staged air small-scale biomass combustion systems.

The aim of this study was to investigate the possibility of reducing CO, unburned hydrocarbons and PM emissions by air staging. The focus is on how

simple modifications to boiler installation and configuration can be used to control CO and unburnt hydrocarbons emissions and at the same time keep PM emissions low.

2.7 Parameters of sampling methods

Sampling and characterizing the products is an essential experimental method to study the thermochemical processes. High-temperature flue gas sampling is often applied in the research on fuel thermochemical conversion [123]. There are seven main parameters to clearly define a sampling method:

• The sampling temperature:

The sampling temperature plays a very important role. Low temperature may result in a decrease in the accuracy of the acquisition. These results can be explained by the condensation of certain elements collected in the adopter.

• The sampling time:

The sampling time also has a significant effect on the measurement results. The phenomena considered here are mainly related to the moment of sampling. Emissions of pollutants are mostly related to incomplete combustion, so emissions during the ignition and extinction phase may be higher. Shorter samples taken during steady state overestimate the performance of the device compared to samples during the full cycle.

• The sampling distance:

The distance between the outlet of the combustion system and the sampling point in the chimney is the sampling distance which affects the temperature of the flue gas, as the further away from the fireplace, the lower the temperature of the flue gas. This is similar to the effect of temperature on sampling results.

• The sampling speed:

Sampling speed has very little effect on the flue gas. However, for particle sampling, large-diameter particles may not enter the nozzle if the sample is collected at high speed. Conversely, if samples are collected at very low speeds, there is a risk of accumulation in the sampling probe.

• The dilution of the sample:

If samples are collected at high temperatures, they still undergo chemical reactions, and gas dilution is important to freeze these chemical reactions as quickly as possible.

• The orientation of the sampling nozzle:

The orientation of the nozzle may also impact the particle sampling. For example, countercurrent to the direction of the flue gas may cause problems with rapid particle accumulation, while at right angles to the direction of the flue gas may lose some particles, especially larger-sized particles.

• The physical characteristics of the sampling nozzle:

The physical characteristics of the sampling nozzle such as size, shape, and internal and external diameter impact the particle sampling by blocking particles larger than a certain size.

2.8 Chapter summary

This chapter provides a review and literature study on the process and technology of biomass combustion. First it introduced the different processes of biomass combustion. It describe the mechanism and products of each process in detail. It introduced the classification and characteristics of biomass boilers. The advantages and technical characteristics of biomass pellet boilers are introduced emphatically. Secondly, it introduced wood pellets and black pellets. In particular, the production process and advantages of torrefied black pellets are demonstrated. The formation mechanisms of gaseous and particulate pollutants that can be produced by biomass combustion were then analyzed in detail. Finally, some commonly used methods for reducing emissions and sampling were introduced. A review of the state of the art in biomass combustion shows that biomass combustion has great potential. However, the problem of simultaneous pollutant emissions poses a challenge. As a relatively new biomass fuel, black pellets have many advantages over wood pellets, but at the same time combustion experiments and pollutant comparisons under the same conditions are still lacking. This is the focus of this study.

Chapter 3

Experimental techniques

3.1 Introduction

This chapter describe the equipment used to implement the experiments carried out during this thesis.

It also show the combustion installation and the modifications necessary for different measurements (gas sampling and laser diagnostics).

A new test bench including the new KWB biomass boiler was developed. This boiler was connected to its environment to both ensure and control the incoming (air, pellets) but also to dissipate the heat and finally extract the fumes to the outside.

The boiler and its environment were then instrumented to measure various quantities related to its operation (temperatures, flow rates, hygrometry and pressure) but also to characterize the species present in the combustion chamber, the flue gases in the chimney, and particularly the soot.

3.2 Experimental bench of biomass combustion

3.2.1 Diagram of the bench

The experimental bench which was used in this thesis is composed of a biomass combustion boiler using wood pellets, a hydraulic installation allowing to dissipate off the thermal energy contained in the water, and a smoke circuit for extracting the emissions from the combustion of wood during operation of the boiler, an analyzer rack unit for measuring the gaseous emissions inside the combustion chamber and in the chimney as well as a laser diagnostic bench for measuring the Laser induced incandescence (LII) signal in the combustion chamber and in the chimney for soot volume fraction measurements. A specific interface has been developed using LabVIEW to monitor boiler operation in real-time and measure the various quantities detailed above. Figure 3-1 shows the schema of the experimental bench with its instrumentation. Each part was described in detail in the following sections.

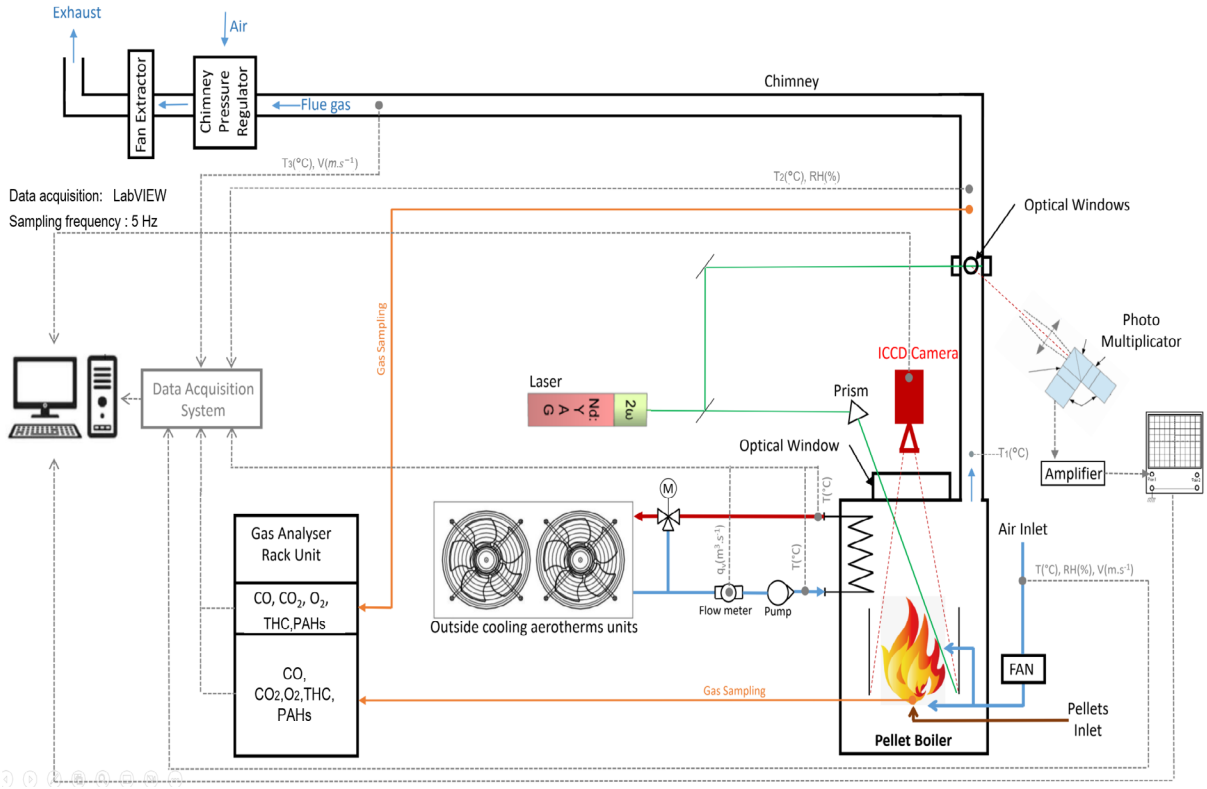

Figure 3-1 Schema of the experimental bench

3.2.2 The boiler

The boiler chosen for carrying out the experiments is a pellet boiler of the KWB brand model Easyfire 1. It is a domestic boiler with a nominal power of 10 kW. A picture of the boiler used is shown in Figure 3-2.

Thanks to the pellets supply system, the pellets are supplied automatically by a conveyor screw. The boiler has a volcano burner which allows a regular supply of pellets from below the flame.

The conveyor screw gently pushes the pellets up from below onto the burner plate. This ensures a stable fire bed and prevents additional dust from being kicked up.

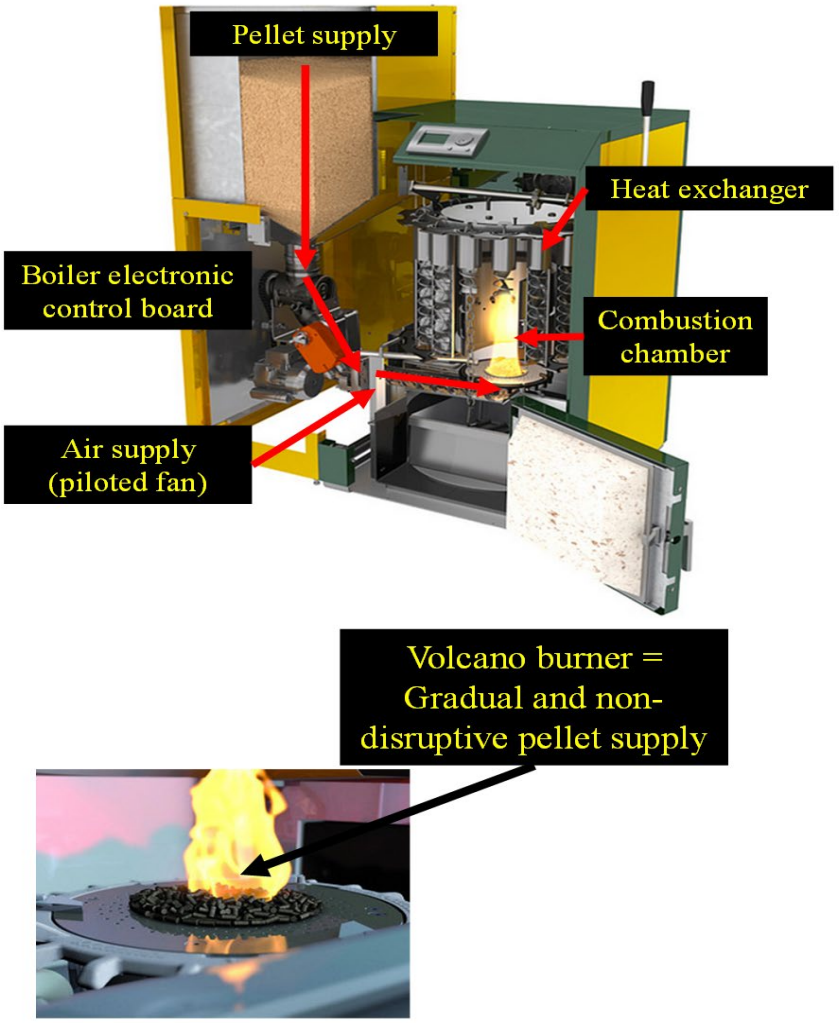

Figure 3-2 KWB Easyfire 1 boiler for testing

The pellets burn fully out in the combustion zone and then the ash was pushed off the edge of the burner plate by the pellets that are pushed onto the burner plate, which then lands in the ash box. The boiler is fitted with a hot air igniter located near the central base of the combustion chamber.

This boiler has a heat exchanger made up of tubes distributed all around the flame. After combustion, the fumes are directed to an internal heat exchanger located above the combustion chamber. In this exchanger, the heat transfer takes place with the water on the shell side.

A hydraulic circuit makes it possible to circulate the water in the burnt gas/water exchanger and transports the heat in an exchanger connected to an external air heater which dissipates the stored thermal energy, to carry out an energy balance of the entire installation.

As mentioned before, air staging is an important emission reduction and the experimental study of small wood pellet boilers operating under air classification conditions has always been one of the hotspots in the study of energy technologies to reduce pollutant emissions. Secondary (post-combustion) air is injected into the combustion chamber for emission reduction.

The boiler has coupled primary and secondary air injections in its factory configuration. The fan blows in a manifold that is connected to the 2 pipes simultaneously supplying the fireplace with primary and secondary air. The overall airflow can be controlled manually. However, this configuration does not allow the two air flows to be controlled separately (Figure 3-3). The intake air distribution between the 2 pipes is approximately 50% to 50%. A plug can be used to completely block the secondary air supply before the start of a single test (Figure 3-3).

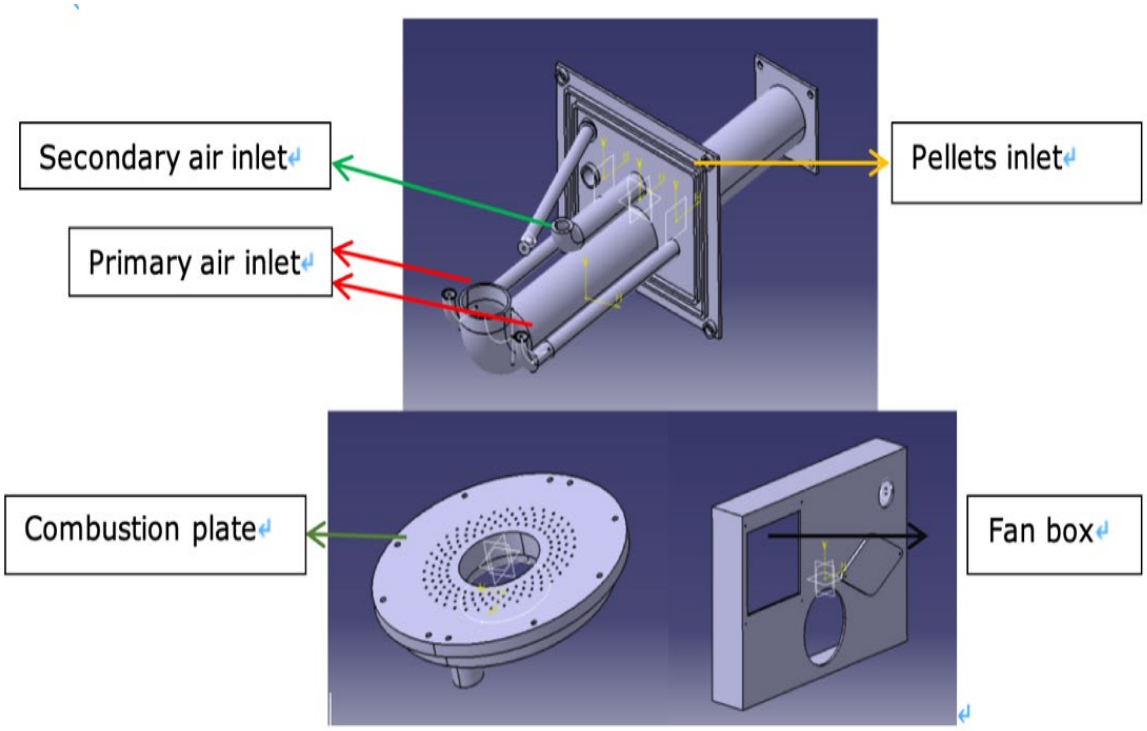

Figure 3-3 Configuration of air injection

The boiler was instrumented to measure many experimental parameters (flow rates, temperatures, humidity, pressure, gaseous species and soot). The hydraulic circuit was also instrumented to carry out an energy balance of the entire installation. The smoke extraction circuit was finally instrumented to measure the mass flow of smoke, the temperature as well as the emissions of gaseous pollutants,

and the volume fraction of soot. These were introduced in detail in the following sections.

According to the specification sheet of the boiler in accordance with EU Regulation, when using wood pellets, the PM emission is less than 30mg/m^3 (10% O_2), the CO is less than 380mg/m^3(10% O_2) and the NO_x is less than 200mg/m^3(10% O_2).

3.2.3 The hydraulic circuit

In order to use the boiler in a way similar to its continuous operation in a house, a complete hydraulic circuit (Figure 3-4 and Figure 3-5) was designed in a previous thesis and implemented to ensure the thermal dissipation from the boiler water circuit to the external air heater by combining flow/temperature measurements.

Figure 3-4 shows the schema of the hydraulic circuit.

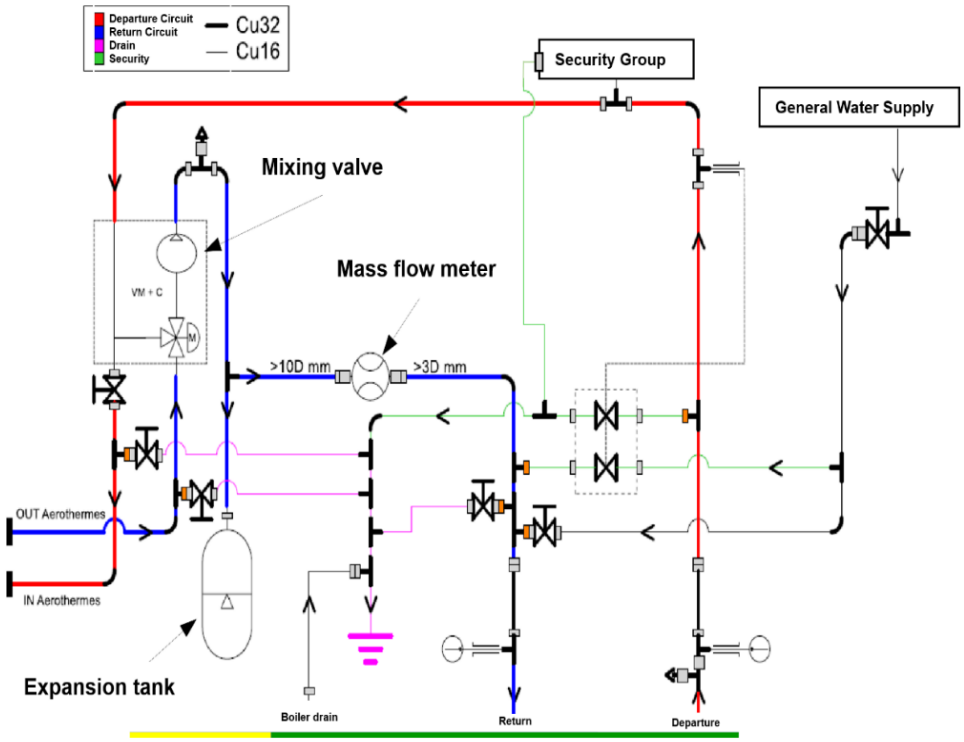

Figure 3-4 Hydraulic circuit

A start-up, shutdown, and maintenance procedures have been associated with this installation. The circuit temperature is protected by a 4-way thermostatic valve which introduces cold water into the circuit and rejects hot water if the circuit

temperature reaches 110°C. Several pressure safety devices have also been installed on the circuit to guarantee discharge of the circuit beyond 3 bars.

The Figure 3-5 shows 2 pictures of the system.

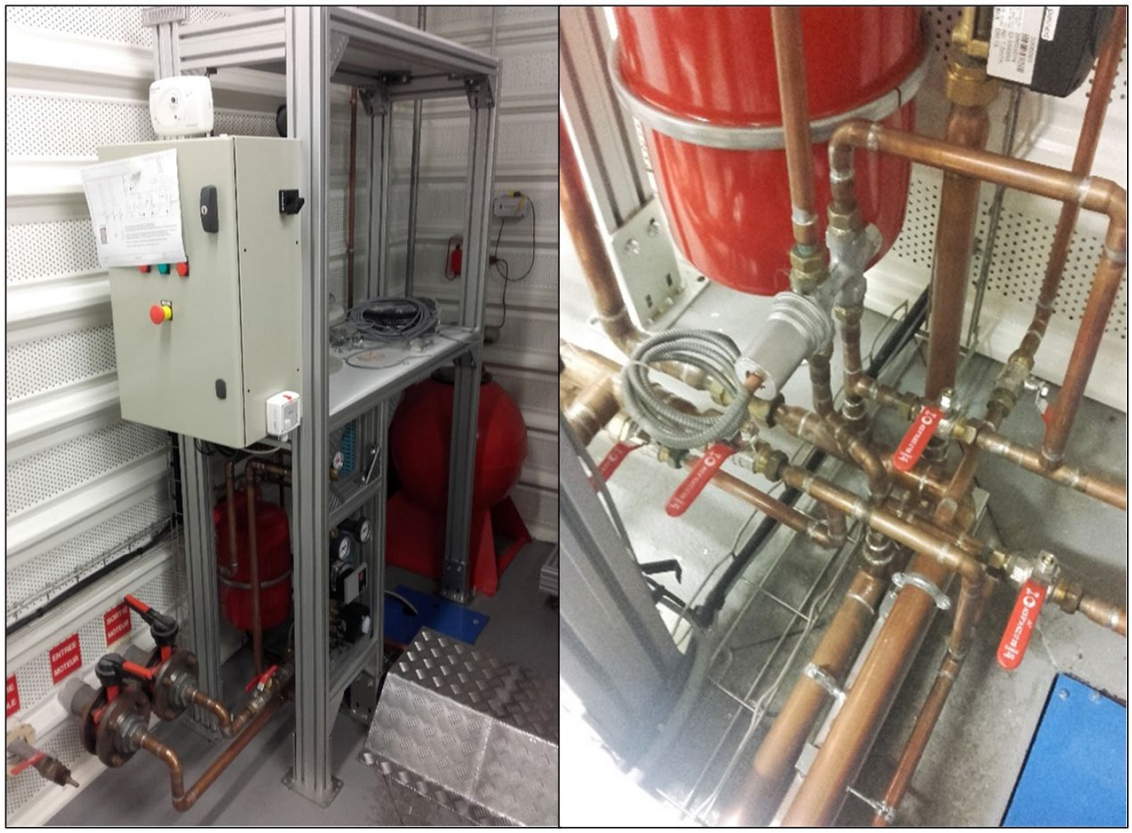

Figure 3-5 Hydraulic installation between the boiler and the air heaters

Finally, a CO alarm was also installed to shut down the installation and warn the experimenter if the admissible threshold in the cell is reached.

3.2.4 The sensors

As shown in the diagram in Figure 3-1, many sensors have been installed on the boiler and its environment to characterize its operation.

1) Sensors for inlet air

The air inlet was channeled through a PVC tube and 2 convergent-divergent to ensure the connection to the fan and the reduction of pressure drops at the entrance of the PVC tube (Figure 3-6). Using the humidity and temperature sensor KIMO TH 110 and the air velocity/airflow transmitter KIMO CTV 210 measures the temperature, humidity, and velocity of the air inlet into the combustion chamber, enabling the calculation of the inlet airflow rate in real-time.

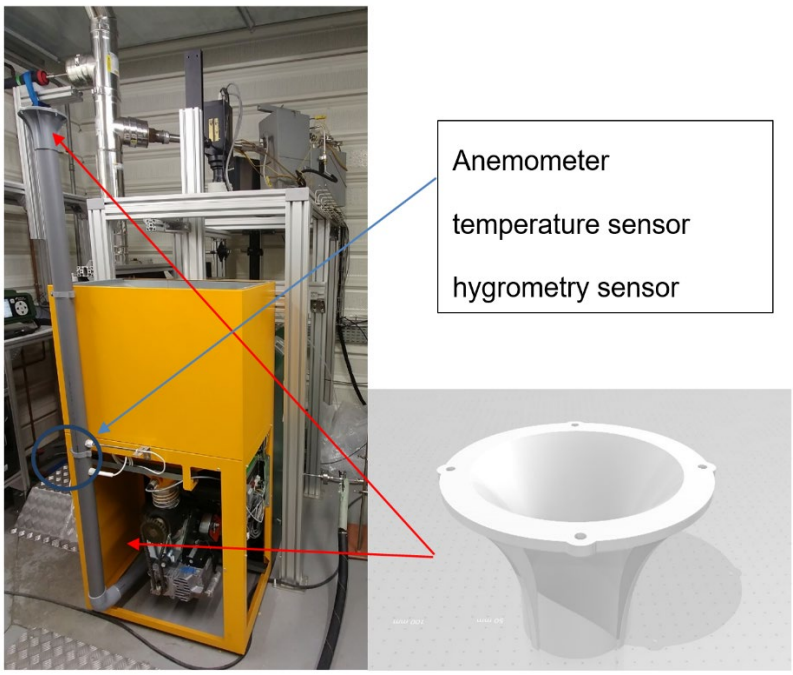

Figure 3-6 Air inlet tube of the boiler for instrumentation

2) Sensors for inlet and outlet water

Temperature measurements by thermocouple type T are also made at the inlet and outlet of the water exchanger (Figure 3-1) coupled with a water flow rate measurement by ultrasonic flowmeter Burkert Flow 8081 to calculate in real time the output power of the boiler.

3) Sensors for smoke

The temperature of the smoke entering the chimney was measured with a thermocouple type T located at the junction of the combustion chamber and the chimney. A KIMO Multifunction transmitter C310 for smoke speed measurement is carried out well downstream just before the draft regulator to place the anemometer in less hot fumes and a slightly reduced section, to both guarantee its temperature resistance and be able to take advantage of the full sensor scale. This Multifunction transmitter also measures the humidity of the smoke in the middle of the chimney and the temperature of the smoke at the point downstream of the chimney.

All the sensors and gas analyzers were connected to an acquisition unit to both supervise the operation of the boiler but also to record the various quantities every second to ensure post-treatment. The software interface was provided using LabVIEW software well suited to the development of a test bench. The flow rate of pellets is not measured, it is calculated from a carbon balance on the smoke

associated with the measurement of the gas flow rate in the chimney mentioned above.

3.3 Gas emissions measurements in the flame and chimney

3.3.1 Gas dilution in the flame

A validated commercial dilution probe of the EPM Environmental brand model 797 has been used for gas dilution in the flame, the operating principle of which is presented below.

The dilution is done by a Venturi effect at the level of a quartz nozzle which has a critical orifice allowing to ensure a constant dilution rate. This is determined at the start of each test by analyzing, through the probe, a standard gas with a known mole fraction. Tests and adaptations were also necessary to improve the filtration of effluents and the management of condensates upstream of the dilution probe (addition of a filtering casing with filters suitable for subsequent analyzes, of a condenser, and installation of heated coats). Figure 3-7 shows the operating principle of the EPM Environmental 797 probe.

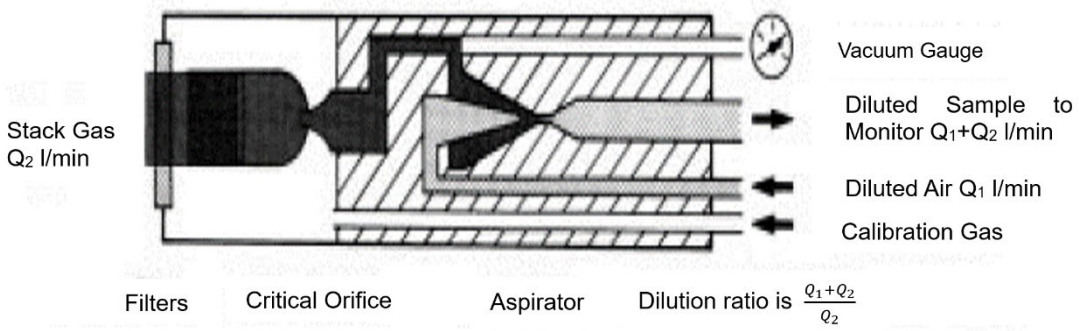

Figure 3-7 Operating principle of the EPM Environmental 797 probe

Tests on different dilution gases (nitrogen, air, and helium) have shown that nitrogen is the most suitable gas to guarantee the reliability of the results. Figure 3-8 shows the passage of the probe through the door wall and its positioning in the flame.

Figure 3-8 Passage of the probe through the door wall and its positioning in the flame

3.3.2 Measurement of combustion gases

The methods used can characterize in parallel the combustion gases in the chimney and in the flame.

1) Gaseous measurements in the chimney

CO, CO_2, oxygen (O_2), and total hydrocarbons (THC) are continuously measured by an Environment SA bay (ENVEA MIR9000 analyzer and ENVEA Graphite 52M). The analyzer bay is connected to the chimney via a heated and filtered transfer line. A filter and a water trap separate water and particulates respectively from gases before sending these to the detection room. Therefore, the analyzer measures the mole fraction of different gases on a dry basis.

2) Gaseous measurements in the flame

As mentioned before, a validated commercial dilution probe has been used for Gas dilution in the flame. Then CO, CO_2, O_2, THC are continuously measured by the Horiba PG350 multi-gas analyzer and Cosma Graphite 655 after filtration and gas treatment (heated line then cooler).

Figure 3-9 shows the instrumentations and analyzers for measuring combustion gases in the flame and in the chimney.

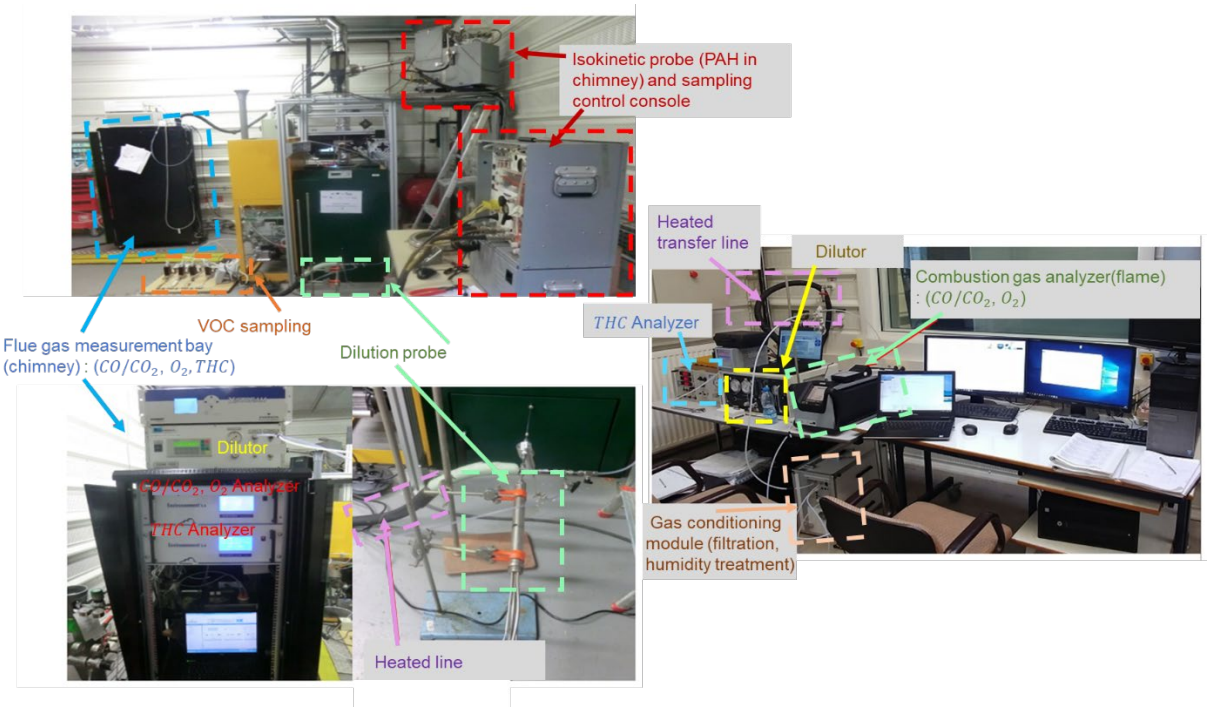

Figure 3-9 Instrumentation and analyzers for measuring combustion gases in the flame and in the chimney

3.3.3 PAHs measurements

For PAHs measurements in the chimney, these samples are taken over two hours to have a good representativeness with a correct isokinetics. The sampler (Figure 3-10) consists of a heated sampling probe fitted with an adjustable nozzle according to the smoke flow. The particles are trapped on a heated quartz fiber filter for the sampling of particulate PAHs, then the gases are cooled to condense the water vapor before passing through a trap containing XAD resin for trapping of gaseous PAHs. The filters are extracted by Soxhlet using dichloromethane. The extract is then analyzed by gas chromatography coupled with mass spectrometry (GC / MS) to assay the particulate PAHs. XAD resin undergoes the same treatment to dose the same compounds in the gaseous state. The PAHs trapped in the condensates are analyzed following a liquid/liquid extraction.

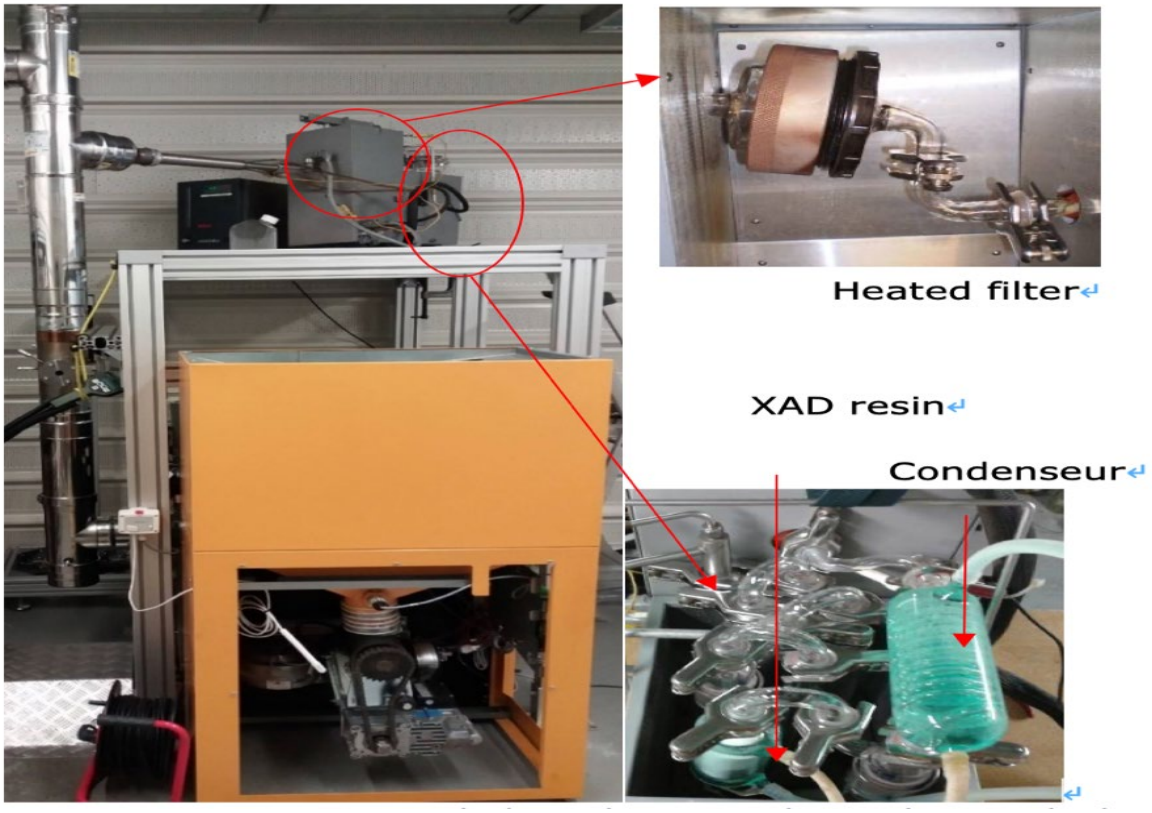

Figure 3-10 PAHs measurements with the isokinetic probe on the KWB boiler

For PAHs measurements in the flame, the measurements are carried out by trapping on a coalescing filter (particulate PAHs) and a cartridge containing XAD resin (gaseous PAHs), these samples are not taken isokinetically due to the limitation of the dilution, that involves an uncertainty on the mass fraction of PAHs but not on their composition

3.3.4 Measurement of Volatile Organic Compounds (VOCs)

The aldehydes and BTEX (Benzene, Toluene, Ethylbenzene, and Xylenes) in the flame and chimney are measured using absorbent cartridges. Cartridges impregnated with DNPH (Dinitrophenyl hydrazine) are used for aldehydes and Tenax cartridges for BTEX. The sample flow is controlled by mass flow meters. These samples are then extracted and analyzed in the laboratory.

In addition, the VOCs are taken and analyzed directly in the gaseous effluents using a portable GC / MS Fondis HAPSITE. It is equipped with a sampling pump, and a heated transfer line, and protected by a filter. VOCs are first trapped on a tube made up of three complementary adsorbents before being desorbed and

analyzed directly. The identification of the detected compounds is carried out by comparison of the experimental mass spectra with the theoretical mass spectra of the NIST library. The measurements are carried out alternately in the smoke and the flame.

3.3.5 Characteristics of measurements

The main characteristics (measurement range, precision, dynamics) of the different measurement parameters used on the test bench created for the KWB boiler have been set out in Table 3-1. The data acquisition device used (National Instrument CompactRio) has better measurement range, accuracy, and dynamic characteristics guaranteeing overall characteristics of the measurement chain limited to those of instruments or sensors.

Table 3-1 Main characteristics of different measurement parameters on the test

Measuring	Measuring Device	Extent of measurement	Precision	Dynamic
Temperature (water, smoke point 1)	Thermocouple type T	-40°C to 350°C	+/- 0.5°C	1 Hz
Pressure (air)	Kimo CP116	800 to 1100 mbar	1 mbar	0.1 Hz
Temperature (air)	Kimo TH110	0°C to 50°C	0.1 °C	0.06 Hz
Humidity (air)	Kimo TH110	5 to 95% HR	0.1%	0.25 Hz
Velocity (air)	Kimo CTV210	0 to 30 m/s	+/- 0.1 m/s	0.625 Hz
Flow rate (water)	Burker FT8081	0.1 to 50 L/min	+/- 0.05 L/min	1 kHz
Velocity (smoke)	KIMO C310 + sonde SVH-100	0.3 to 35 m/s	0.1 m/s	1 Hz
Humidity (smoke)	KIMO C310 + sonde SHDI-150	0 to 100% HR	0.1 % HR	1 Hz
Temperature (smoke point 2)	KIMO C310 + sonde SHDI-150	-40°C to +180°C	0.1 °C	1 Hz
O_2 (chimney)	ENVEA MIR9000	0 to 25%	2 % of Full Scale	1 Hz
CO (chimney)	ENVEA MIR9000	0 to 5000 ppm	2 % of Full Scale	1 Hz
CO_2 (chimney)	ENVEA MIR9000	0 to 20 %	2 % of Full Scale	1 Hz
THC(chimney)	ENVEA Graphite 52M	0 to 10000 ppm	1 % of Full Scale	1 Hz
Volume fraction (soot in the chimney)	Laser + PMTs	1 -100 ppb	1 ppb	0.02 Hz
O_2 (flame)	Horiba PG 350	0 to 25 %	0.1%	0.2 Hz
CO (flame)	Horiba PG 350	0 to 5000 ppm	1 ppm	0.2 Hz

CO_2 (flame)	Horiba PG 350	0 to 20 %	0.1%	0.2 Hz
THC (flame)	ENVEA SA Graphite 655 M	0 to 10000 ppm	5 ppm	0.2 Hz
Volume fraction (soot in flame)	Laser + ICCD	1-100 ppb	1 ppb	0.02 Hz
PAHs	Isokinetic sampling + GC / MS analysis	>0.003 ppb	+/- 17%	Chimney: 2 to 3h Flame: 45 min

3.4 LII emission measurements in the flame and chimney

The soot volume fractions were measured in the chimney and qualitatively detected in the flame using the Laser-Induced Incandescence (LII) optical technique. This technique makes it possible to obtain a measurement in real-time but requires the insertion of optical accesses on the boiler. Therefore, it was necessary to modify the boiler and the chimney to place portholes for the passage of the laser beam but also for the return of the response of the soot excitation through small optical windows

The laser diagnostic bench includes a YAG laser whose wavelength is doubled at 532 nm pulsed at 10 Hz with a time width of 6 ns. The photonic response measurement devices are different depending on the area measured: photomultipliers system for point measurement in the center of the chimney and ICCD camera for spatial mapping in the combustion chamber.

3.4.1 LII working principle

The potential of optical diagnostics has long been shown to be very effective in in-situ measurements. Laser-induced incandescence is one of the most commonly used soot volume fraction detection techniques since the 1980s. LII involves the use of high-power pulsed or continuous lasers to heat soot particles to temperatures high enough to emit blackbody radiation. An advantage of LII is that it is particularly sensitive to the detection of soot particles, as they absorb different excitation wavelengths, whose temperature can reach nearly 4000 K.

The first evidence of a laser-induced incandescence technique was an observation of different temporal emission profiles of laser-irradiated carbon black and alumina aerosol particles [124]. The LII emission signal was first observed as an interference in Raman measurements in a flame [125]. Further, it has been shown that the LII signal is proportional to the soot volume fraction [126]. Currently, the physical process behind the LII signal has been employed and tested,

and the technique is used to characterize particles emitted by various combustion systems: engines, laboratory flames, nanoparticles synthetization, etc. [127].

Laser-induced incandescence is a technique that relies on high-power lasers to heat soot particles to very high temperatures, typically in the range of 2500-4000 K, characterized by blackbody emission. When particles interact with laser radiation, they absorb light, temperature increases, and emit radiation according to Planck's law. During and after radiation absorption, other processes such as conduction, oxidation, annealing, sublimation, and thermionic emission may also occur [128].

Figure 3-11 illustrates the processes that influence the temperature and mass of a particle during LII-signal collection. Particles are first heated by absorption of laser radiation. The oxidation and annealing contribute also to the heating process but in a very small contribution. Afterward, particles are cooled down to environment temperature by conduction to the surrounding environment, sublimation, thermionic emission and radiative emission. LII signal originates from particle radiation emission [128].

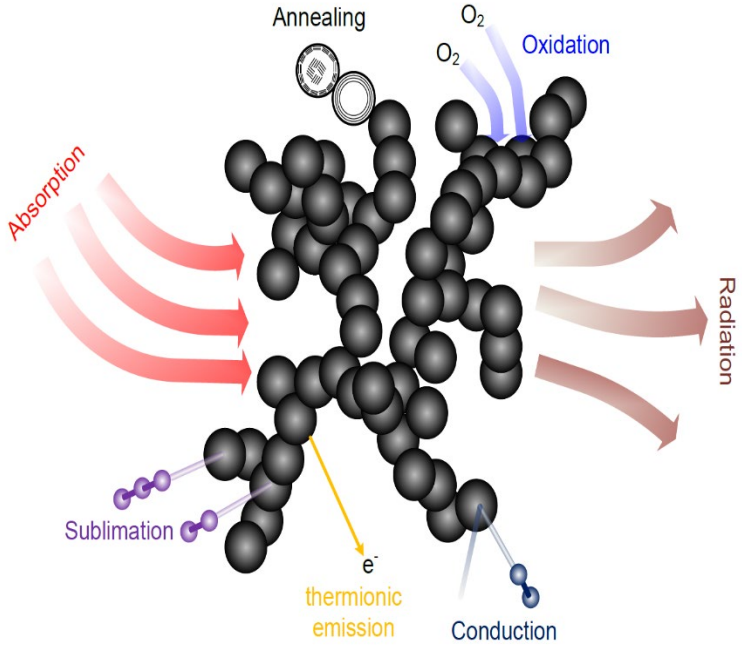

Figure 3-11 Illustration of processes influencing the collection of the LII signal [128]

The emitted radiation is recorded with a fast photo-detector (PMT) or a CCD camera at the start of the laser pulse or immediately after the laser pulse. Depending on the detection system, temporal or spatial LII signal can be measured.

Spatial LII signal is used to determine the soot volume fraction or the local temperature of the particles on a defined period during the laser pulse.

The temporal LII signal is approximated the particles size by measuring the decay time during the cooling process. In this case, more sophisticated procedures with LII model comparisons are required [129]. Indirect comparisons are possible if a simulation model of the LII time distribution is missing. However, other techniques such as laser extinction or gravimetric sampling are required for quantitative volume-fraction measurements using the LII technique.

In 2005, a new technique was proposed that could calibrate the soot volume fraction in a flame based on the absolute light intensity and blackbody temperature of the two-color LII (2C-LII) technique. In this study, the two-color LII (2C-LII) technique was used to measure the absolute soot volume fraction.

During irradiation and emission, soot particles may undergo processes that affect the intensity of the LII signal. All the processes that take place during and after the absorption of radiation by the soot particles are described in detail below adapted from the work of Michelsen et al.[128]:

1) Energy and mass balance equation

The energy balance equation of particles can be described as the power accumulated or loosed by soot particles in time. It is equal to the sum of different powers involved in different mechanisms suffered by particles in the process of energy transfer:

$$\frac{dU_{int}}{dt} = \dot{Q}_{abs} + \dot{Q}_{raq} + \dot{Q}_{cond} + \dot{Q}_{sub} + \dot{Q}_{oxi} + \dot{Q}_{ann} + \dot{Q}_{therm} \qquad \text{Equation } 3-1$$

Where U_{int} is the internal energy of the particle with t represents the time. All of these $\dot{Q}$ represent a power (W): $\dot{Q}_{abs}$ is due to the absorptive heating rate for a single primary particle, $\dot{Q}_{raq}$ is for the radiative cooling rate, $\dot{Q}_{cond}$ represents the conductive cooling rate, $\dot{Q}_{sub}$ is due to the evaporation cooling rate, $\dot{Q}_{oxi}$ is due to the oxidative heating rate, $\dot{Q}_{ann}$ represents the heating rate from annealing and $\dot{Q}_{therm}$ is due to the thermionic cooling rate. Soot particles present a specific heat capacity, which allows them to accumulate heat function of the time. The rate of change of particle internal energy can also be expressed as:

$$\frac{dU_{int}}{dt} = MC_s\frac{dT}{dt} = \rho_s C_s \frac{\pi d_p^3}{6}\frac{dT}{dt} \qquad \text{Equation } 3-2$$

Where M is the particle mass, ρ_s is the particle density, C_s is the particle specific heat, d_p is the primary-particle diameter, and T is the particle temperature.

The mass loss is expressed as:

$$\frac{dM}{dt} = \left(\frac{dM}{dt}\right)_{sub} + \left(\frac{dM}{dt}\right)_{ox} \qquad \text{Equation } 3-3$$

Where sub represent the sublimation and ox represent the oxidation.

It is related to the particle diameter as:

$$d_P = \left(\frac{6M}{\pi p_s}\right)^{1/3} \qquad \text{Equation } 3-4$$

2) Absorption of laser radiation

The absorbing ability of a body represents the ratio of the radiation flux absorbed by the body to the radiation flux incident on the body. According to Kirchhoff's law, the emissivity is equal to the absorption coefficient for the same couple of λ and T values, whereas λ is the wavelength and T is the temperature of the considered soot particle. The emissivity is given in the Rayleigh approximation by, where $\pi d_p \ll \lambda$:

$$\alpha(\lambda, T) = \frac{4\pi\, d_p E(m)}{\lambda} \qquad \text{Equation } 3-5$$

Where m is the complex index of refraction and $E(m)$ is the refractive index function for absorption. The absorption function $E(m)$ is dependent on wavelength λ. Soot absorption heating rate represents the power delivered by the laser pulse to the soot particles. This absorption of energy depends on the laser irradiance (W/m^2) and on the soot absorption cross section (function of $\alpha(\lambda, T)$ and the geometrical section of the spherical soot) as:

$$\dot{Q}_{abs} = \frac{\pi^2\, d_p^3 E(m)}{\lambda} I_l(t) \qquad \text{Equation } 3-6$$

Where $I_l(t)$ is the time-dependent irradiance of the incident beam.

Soot particles are very effective absorbers and emitters in the ultraviolet, visible, and infrared regions. Visible light efficiency is verified by the yellow

luminosity emitted by the sooting flame, while infrared emission could be captured by infra-red detectors.

3) Thermal radiation

Each body emits electromagnetic radiation in a broadband emission spectrum. According to the Plank function, the radiative-cooling rate can be calculated integrated over all wavelengths. The radiative-cooling rate can be described as below if there is no wavelength dependence to $E(m)$:

$$\dot{Q}_{rad} = -8\Gamma(5)\zeta(5)\frac{\pi^3 d_p^3 (k_B T)^5 E(m)}{h(hc)^3} \qquad \text{Equation } 3-6$$

Where $\Gamma(5)$ is the value of the gamma function of 5, $\zeta(5)$ is the value of the Riemann zeta function of 5, k_B is the Boltzmann constant, h is the Plank constant and c is the speed of light.

4) Heat conduction

Conductive cooling is considered to be the most important process of particle heat loss at atmospheric pressure. It represents the transfer of thermal energy between the soot particles and the surrounding gas due to the temperature difference. The conduction equation states that the conduction rate is proportional to the difference between the particle surface temperature and the surrounding temperature [130]:

$$\dot{Q}_{cond} = -\frac{2k_a \pi d_p^2}{d_p + GL}(T - T_0) \qquad \text{Equation } 3-8$$

Where k_a is the thermal conductivity of the bath gas, L is the mean free path, and G is a function of the heat capacity ratio:

$$G = \frac{2(9\gamma - 5)}{\alpha_T(\gamma + 1)} \qquad \text{Equation } 3-9$$

Where α_T is the thermal accommodation coefficient. This coefficient represents the heat fraction transferred by the surrounding gas from soot particles after collision and it depends on the gas nature and the soot surface. γ is the heat-capacity ratio equal to the molar heat capacity of air at constant pressure C_p divided by the molar heat capacity of air at constant volume C_v.

5) Sublimation

As soot particles approach temperatures around 4000 K, evaporative-heat loss becomes the most important cooling mechanism. The mass loss by sublimation of parts of the matter into various gaseous species leads to a rapid decrease of the LII signal. The evaporative-cooling rate is explained by the thermodynamics principles in the following manner:

$$\dot{Q}_{sub} = \frac{\Delta H_s}{M_s}\left(\frac{dM}{dt}\right)_{sub} \qquad \text{Equation } 3-10$$

Where ΔH_s is the enthalpy of formation of the sublimed carbon clusters, Ms is the average molecular weight of the sublimed carbon clusters, and $\frac{dM}{dt}$ is the mass loss rate attributable to sublimation:

$$\left(\frac{dM}{dt}\right)_{sub} = \frac{-\pi\, d_p^2 M_s \alpha_M p_V}{RT}\left(\frac{RT}{2\pi M_s}\right)^K \qquad \text{Equation } 3-11$$

Where α_M is the mass accommodation coefficient, p_V is the average saturation partial pressure of the sublimed carbon clusters, and K is a constant that is typically equal to 0.5.

6) Oxidation

The oxidative mechanisms can lead to particle mass loss and temperature increase. However, this process is much slower than laser heating and evaporation mass loss. Therefore, oxidation is less critical at high laser energy. The oxidative heating can be expressed as:

$$\dot{Q}_{ox} = \frac{\left(\Delta H_{ox} + \alpha_T C_p^{CO} T\right)}{M_c}\left(\frac{dM}{dt}\right)_{ox} \qquad \text{Equation } 3-12$$

Where ΔH_{ox} is the enthalpy of the CO formation, α_T is the thermal accommodation coefficient, C_p^{CO} is the heat capacity of CO, and M_c is the molecular weight of a carbon atom.

7) Annealing

The annealing process is expected to be exothermic and lead to an increase in particle temperature. It may affect other processes due to changes in particle physics. The heating rate of the annealing mechanism can be expressed as:

$$\dot{Q}_{ann} = \frac{-\Delta H_{ann} k_{ann} N_d}{N_A} \qquad \text{Equation } 3-13$$

Where ΔH_{ann} is the enthalpy of annealing, k_{ann} is the rate constant of annealing, N_d is the number of defect sites in the particle and N_A is the Avogadro constant.

8) Thermionic emission

Thermionic emission has a weak effect on the particle cooling rate, this process can be expressed as:

$$\dot{Q}_{therm} = -\frac{4\phi m_e (\pi d_p k_B T)^2}{h^3} \exp\left(\frac{-\phi}{k_B T}\right) \qquad \text{Equation } 3-14$$

Where ϕ is the work function, and m_e is the electron mass.

9) LII emission of Np particles of spherical primary particle of soot

The LII signal from soot is the thermal emission induced by laser excitation.

Basically, the LII signal is based on the black body radiation according to the Planck law according to:

$$E_{bb}(T,\lambda) = \int_{\lambda_1}^{\lambda_2} \frac{2\pi hc^2}{\lambda^5} \frac{1}{\exp\left(\frac{hc}{\lambda k_B T}\right) - 1} d\lambda \, dS \qquad \text{Equation } 3-15$$

Where E_{bb} is the emittance (W) of an elementary surface dS (m^{-2}) emitted over 2π steradian (in "half the space"). The emittance is defined over a spectral range $d\lambda$. The black body is an ideal energy absorber and emitter and is used as a standard to compare the absorption/emission of real bodies. For real bodies, the emissity $\varepsilon(T,\lambda)$, being undimensionless and less than one, must be taken into account. So the emittance of real bodies E_{rb} is:

$$E_{rb}(T,\lambda) = \int_{\lambda_1}^{\lambda_2} \varepsilon(T,\lambda) \frac{2\pi hc^2}{\lambda^5} \frac{1}{\exp\left(\frac{hc}{\lambda k_B T}\right) - 1} d\lambda \, dS \qquad \text{Equation } 3-16$$

The Kirchhoff's law establishes the relationship between the abilities of emitted and absorbed electromagnetic energy by any physical body. It can therefore be approximated that the heated soot particles are in thermodynamic

equilibrium with the encountered radiation. So the absorption coefficient $\alpha(\lambda, T)$ and the emission coefficient (or emissivity) $\varepsilon(\lambda, T)$ are equal for the same couple of T, λ.

Thus, according to equation 3-5, the emissivity could be taking into account to define the equation 3-17 for a defined volume V, which contains N_p (m^{-3}) soot particles (spherical particles in the Rayleigh approximation, here with the same diameter, with a surface of πd_p^2). The following equation gives the LII signal emitted by N_p soot particles:

$$S_{LII}(T,\lambda) = \int_{\lambda_1}^{\lambda_2} N_p \cdot \frac{4\pi\, d_p E_m(\lambda)}{\lambda} \cdot \pi d_p^2 \cdot \frac{2\pi hc^2}{\lambda^5} \frac{1}{\exp\left(\frac{hc}{\lambda k_B T}\right) - 1} d\lambda \quad \text{Equation } 3-17$$

Considering the soot volume fraction f_v defined as $f_v = N_p \frac{\pi\, {d_p}^3}{6}$, the LII signal (in $W.m^{-3}$) emitted at 4π steradian (in "all the space") can be expressed as:

$$S_{LII}(T,\lambda) = \int_{\lambda_1}^{\lambda_2} \frac{48\pi^2 hc^2 E_m(\lambda)}{\lambda^6} \frac{1}{\exp\left(\frac{hc}{\lambda k_B T}\right) - 1} d\lambda f_v \quad \text{Equation } 3-18$$

Equation 3-18 represents the general equation (taking into account f_v) of the LII signal for N_p spherical soot particles emitting thermal radiation at temperature T according to their optical properties $E_m(\lambda)$ in the investigated wavelength domain.

The emission spectral range $\Delta\lambda$, centered on λ, is very narrow (due to the use of bandwidth filters, see paragraph 3.3.6 after). So, the expression of the total LII signal emitted at 4π steradian (in $W.m^{-3}$) could be expressed as:

$$S_{LII}(T,\lambda) = \frac{48\pi^2 hc^2 E_m(\lambda)}{\lambda^6} \cdot \frac{1}{\exp\left(\frac{hc}{\lambda k_B T}\right) - 1} \cdot \Delta\lambda \cdot f_v \quad \text{Equation } 3-19$$

According to these parameters:

- The detection system, having its own solid angle Ω and detection efficiency β (see paragraph 3.3.7 after),

- $E_m(\lambda)$ was defined as for mature soot inside the chimney (i.e 0.35),

- The temperature T of soot during the LII process (see paragraph 3.3.8 after),

- The volume of measurement V_m which could be defined according to the shape of the laser beam (see paragraph 3.3.9 after),

one can define the detected LII signal (in volt thanks to PMT detection coupled to an oscilloscope) by the detection chain according to equation 3-20:

$$S_{LII,detected}\ (T,\lambda) = \frac{12\pi\, hc^2 E_m(\lambda)}{\lambda^6} \cdot \frac{1}{\exp\left(\frac{hc}{\lambda k_B T}\right) - 1} \cdot V_m \cdot \Omega \cdot \beta \cdot \Delta\lambda \cdot f_v \quad \text{Equation } 3-20$$

One can note the unit of Ω in steradian and β in Volt/W.

So the soot volume fraction f_v could be calculated.

3.4.2 Excitation sources

The excitation source is a Quantel Q-smart 450 laser with 1064 nm fundamental, 6 ns pulse width and 10 Hz repetition rate. The device is equipped with a frequency doubling (2ω) module so it can generate 532 nm wavelength. The energy of the laser beam is adjusted using an energy attenuator module which contains a half-wave plate and a Glan prism. The 532 nm wavelength was used for the LII technique in this thesis.

3.4.3 Detection system

1) Photomultiplier tube (PMT)

The temporal profile of the LII signal is recorded by photomultiplier tubes. The PMT contains a photocathode, dynodes and an anode. All materials are constructed in vacuum glass enclosures. Due to the photoelectric effect, an incident photon of few eV reaches the photocathode of the PMT and emits an electron from the surface. The electron is accelerated by the electric field and then multiplied by the emitting surfaces. The output is an electrical signal proportional to the number of incident photons. The working principle of a photomultiplier tube is shown in Figure 3-12. PMTs are extremely sensitive to light and in our case have short rise time around 0.6 ns. It allows us to detect photons with very low incident flux, thanks to an amplification system.

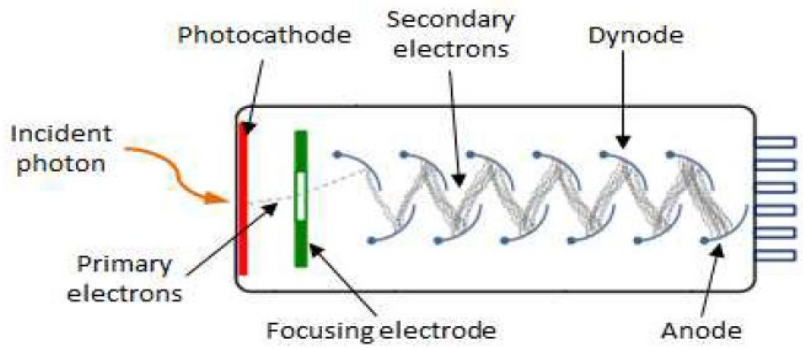

Figure 3-12 Working principle of a photomultiplier tube[131]

2) Intensifier charged-coupled device (ICCD) camera

ICCD camera is mainly composed of two parts: a CCD detector and an intensifier. Figure 3-13 shows the scheme of working principle of an ICCD camera.

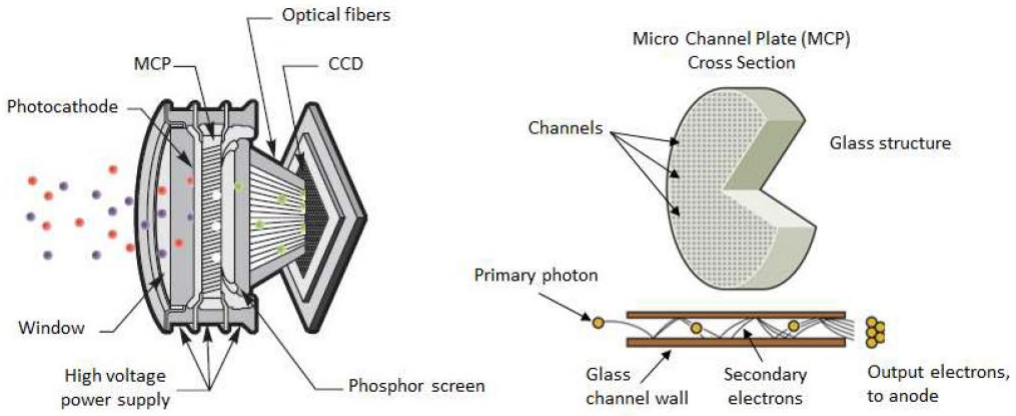

Figure 3-13 Scheme of working principle of an ICCD camera[131]

The intensifier consists of a photocathode, a microchannel plate (MCP), and a phosphor screen. The photocathode converts incident photons entering the intensifier into photoelectrons, which are then accelerated by an electric field toward the MCP (a mosaic of plates made of semiconducting glass containing very thin channels). Electrons entering the MCP are accelerated in these tubes and collide with the glass channel walls, multiplying them. Afterward, the phosphor screen converts the electrons back into photons. The formed image is transmitted via an optical fiber to the focal plane of the CCD. The final image is detected by a CCD array, digitized, and transmitted to a computer.

3.4.4 Configuration of 1-color LII measurement in the chimney

Figure 3-14 shows the LII configuration in the chimney. The laser beam is introduced into the chimney through a transparent window to heat the soot particles between 2500K and 4000K.

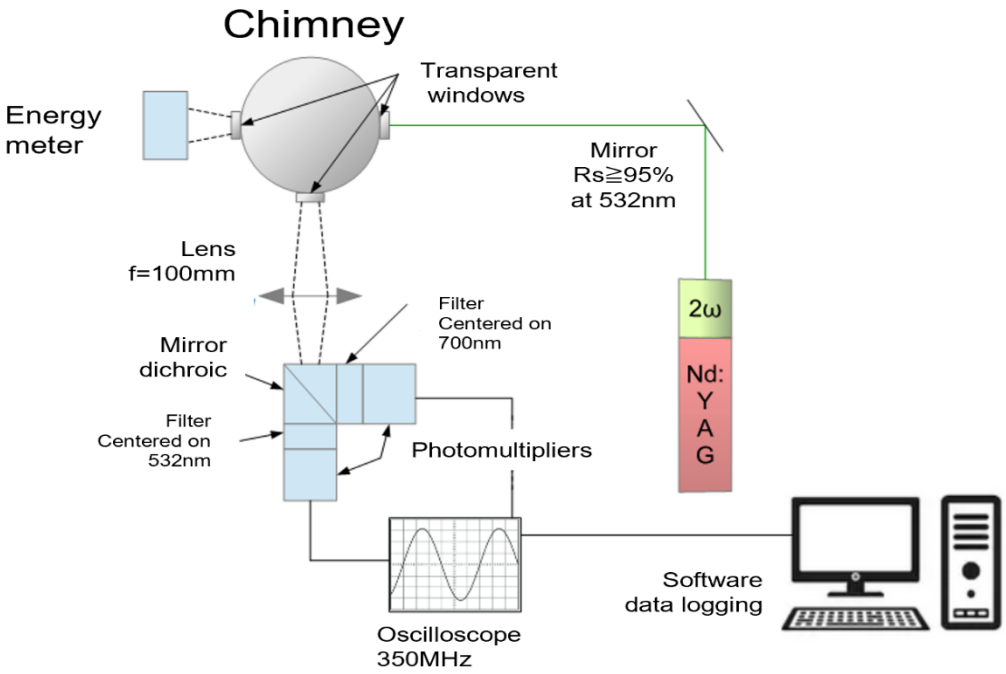

Figure 3-14 LII configuration in the chimney

The response of the particles is recovered and focused using lenses towards 2 photomultipliers. The signal is then directed using a 45° dichroic mirror (Hamamatsu A10034-90 interchangeable dichroic block) to two detection chains each composed of a Hamamatsu bandpass filter A10033-01 / 06 (respectively centered at 532 nm and 700 nm) and a Hamamatsu PMT H10721-20 photomultiplier + amplifier/converter C11184 (rise time of 0.57 ns and spectral response between 230 and 920 nm) powered by a Hamamatsu C10709 voltage source. The oscilloscope is used to receive the voltage signal of the photomultiplier and transmit the signal to the data logging software.

Figure 3-15 shows the assembly made on the chimney.

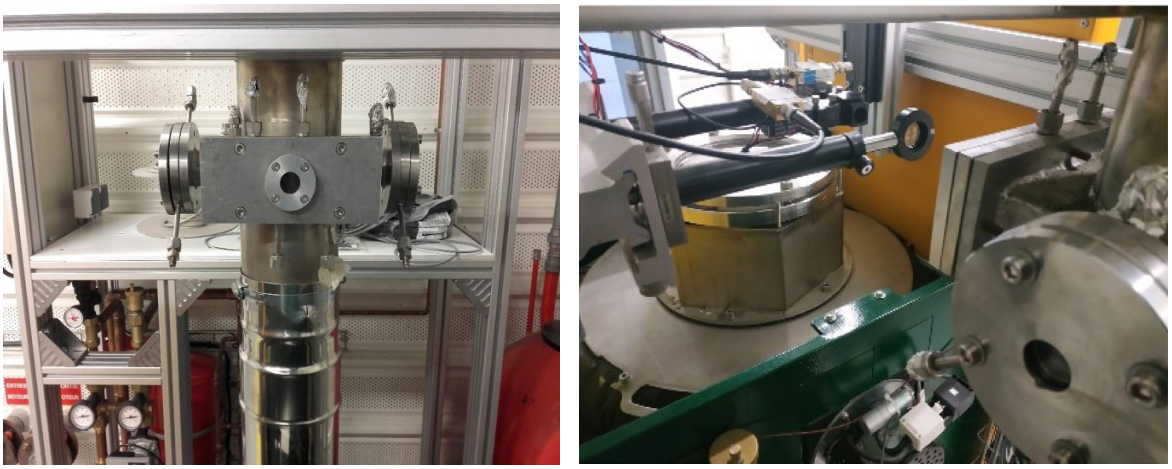

Figure 3-15 LII assembly performed in the chimney

Here, the channel 532 nm does not serve for LII detection. It is used to observe the scattering of the 532 nm laser light inside the chimney and to ensure good alignment of the detection system. So, only the channel 700 nm is used for 1color LII detection.

3.4.5 Configuration of LII measurement in the flame

The boiler was chosen for its symmetrical configuration (flame in the center of the exchanger) and to facilitate optical access. The manufacturer also responded to our request to modify the configuration of the gas-water exchanger to leave us the possibility of placing different windows without interactions with the tubes of the exchanger. Figure 3-16 shows the potential horizontal access areas through the exchanger. The accesses require piercing the exchanger right through with sealed welding from the outside but didn't cause an additional interaction with the tubes in which the fumes circulate.

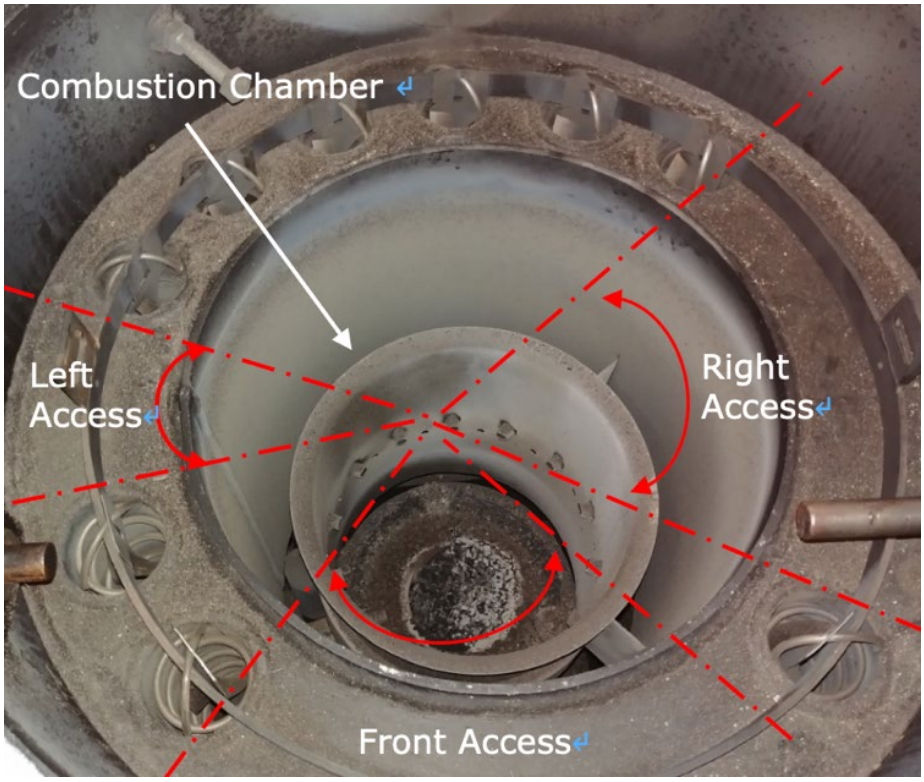

Figure 3-16 Potential horizontal optical access through the exchanger

Finally, the configuration shown in Figure 3-17 was chosen for LII measurements in the flame. The laser beam is introduced vertically into the combustion chamber through a transparent window located above the boiler. The ICCD camera receives the LII signal and transmits the signal to the special image processing software Winview. This configuration has been called backward-LII. The response obtained is on the trajectory of the laser in 3 dimensions, a geometric reconstruction is necessary between the image of the ICCD camera and the spatial distribution of the LII response.

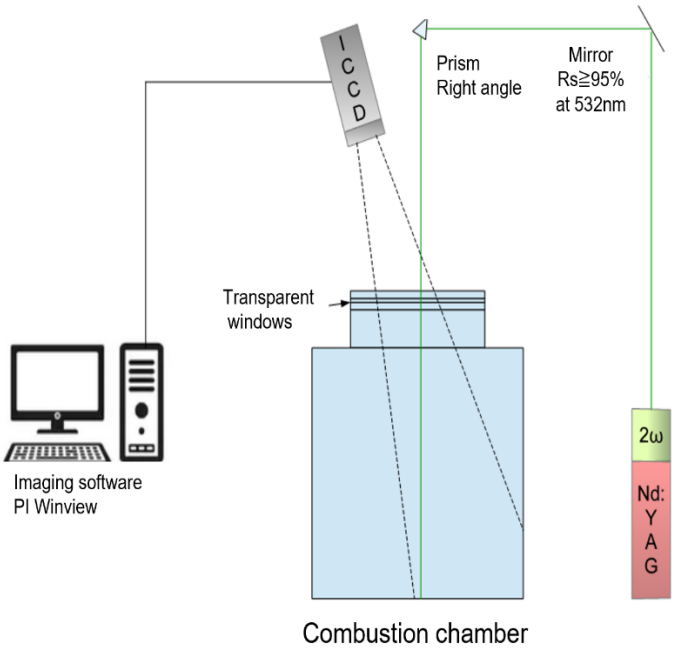

Figure 3-17 LII configuration in the flame

To receive the LII response from the combustion chamber, it was necessary to make a large optical window, ensuring that the geometric modification of the boiler for this optical access does not affect its performance. Several test campaigns were carried out, and one of them has verified that there is non-disturbance with the large optical window, compared to tests without this window. Figure 3-18 shows the design and implementation of optical access in the combustion chamber.

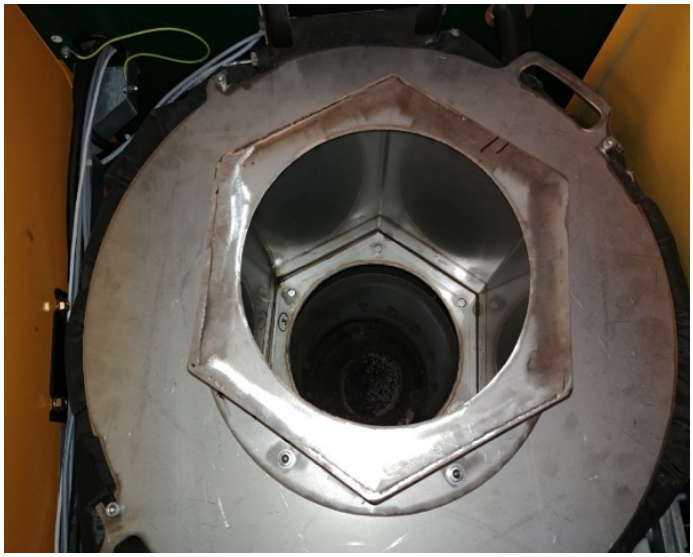

Figure 3-18 Design and implementation of optical access in the combustion chamber

This configuration also allows to visualize the combustion in real-time with a qualitative assessment of the soot content of the flames (Figure 3-19). The optical window, of the SILUX (Quartz) type, has an optical diameter when clamped of 225mm. It resists a temperature of 800 °C continuously and transparent from 250nm to 3µm.

Figure 3-19 Flame visualization in real-time

The pulsed intensified ICCD camera is associated with a high-pass (> 750 nm) bandpass filter and a 532 nm notsch filter to remove the laser scattering as well as a lens for focusing on LII emissions. The camera is of the PI MAX2 type,

intensified by a Hbf filmless Gen III intensifier. Its quantum efficiency is optimized between 280 and 700 nm and its detector is composed of 512 x 512 pixels with 19 µm sides (field of vision of 12.4 x 12.4 mm^2). It is cooled using Peltier elements and a fan.

3.4.6 Configuration of two-color LII measurement in the chimney

Figure 3-20 shows the configuration of two colors LII technique in the chimney. The laser beam is shaped as a "top-hat", meaning that the fluence is constant over all the section of the laser beam and is introduced and rejected into the chimney through 2 transparent windows.

A lens with a focal length of 20 cm and a pinhole (circular diaphragm of 5 mm, homemade in a Teflon disc) as shown in Figure 3-20. The lens is 40 cm from both the pinhole and the center of the chimney. The particle LII response is collected using a detection system with 2 photomultiplier tubes (the same as for configuration of 1-color, paragraph 3.3.4). The following describes the details of the detection system.

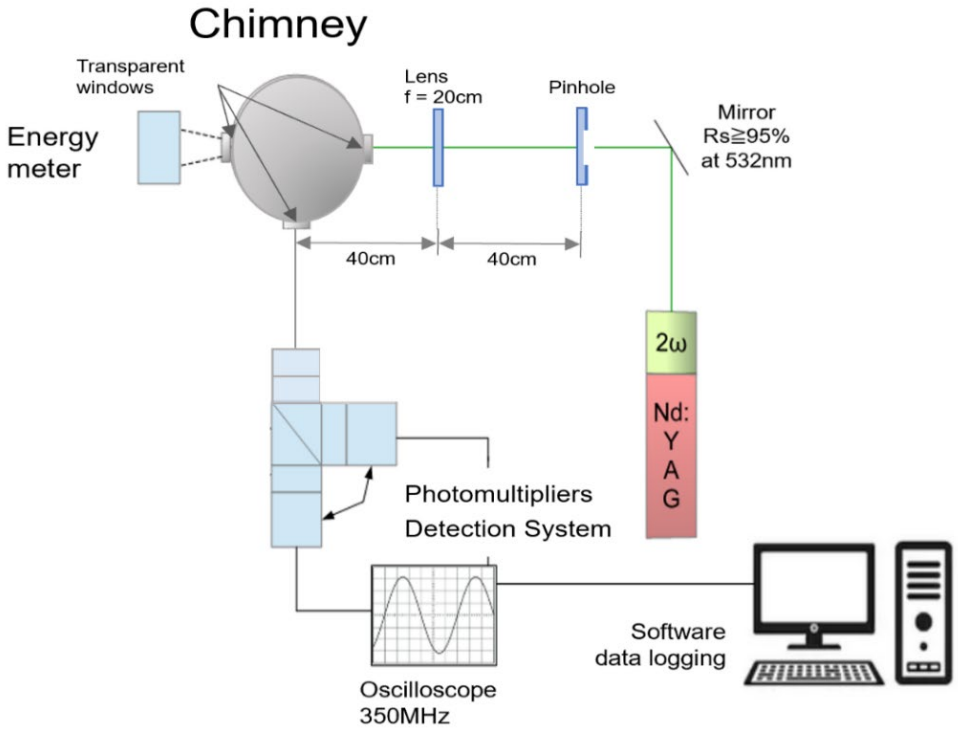

Figure 3-20 Configuration of two colors LII in the chimney

The detection system is described in detail here after:

The detection system contains a beam expander, two 532 nm notch filter which can remove the laser beam interference, a beam splitter dividing the detection beam into two equal parts, two bandpass filter blocks centered at 750 and 850 nm with 10 nm FWHMs placed in front of two identical photomultiplier tubes with an amplifier to record the LII signal. Figure 3-21 shows the configuration of the detection system.

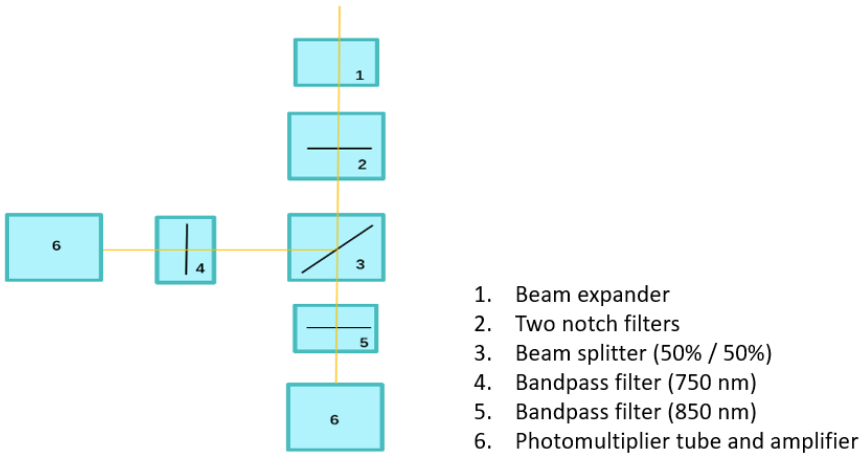

Figure 3-21 Configuration of the detection system

The different parts are numbered and described below:

N°1: Beam expander (HAMAMATSU A10031)

This beam expander widens the diameter of a collimated beam of light to 2.5 times its original size or reduces the diameter to 1/2.5 times its original size. It has a C-mount thread for connecting to another device. Figure 3-22 shows the incident light conditions of this beam expander.

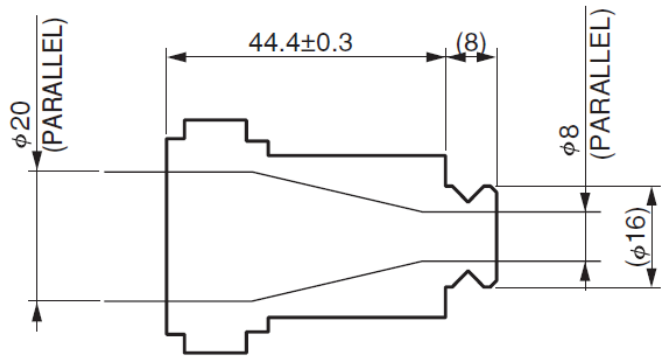

Figure 3-22 Detection light conditions

N°2: Two notch filters (THORLABS NF533-17) (Figure 3-23)

533nm Notch filter, Bandwidth = 17nm

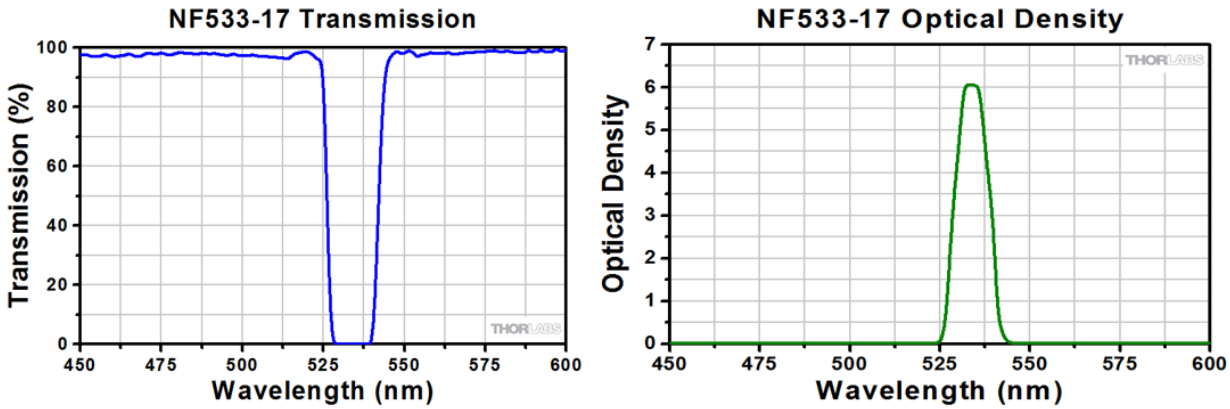

Figure 3-23 Spectral characteristics of 532 nm filter

N°3: Beam splitter (50% / 50%)

The incident light is transmitted/reflected in the investigated spectral range with ratio of 0.5.

N°4: Bandpass filter FB750-10 (Figure 3-24)

CWL = 750, FWHM = 10

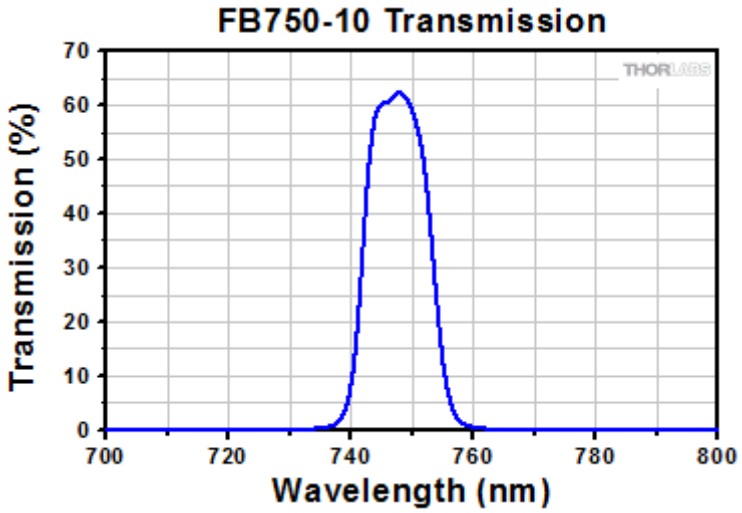

Figure 3-24 Spectral characteristics of 750 nm filter

N°5: Bandpass filter FB850-10 (Figure 3-25)

CWL = 850, FWHM = 10

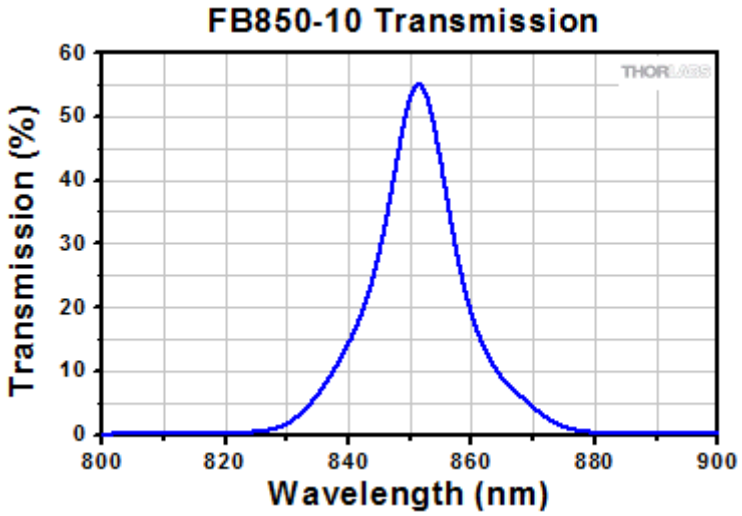

Figure 3-25 Spectral characteristics of 850 nm filter

N°6. Photomultiplier tube (HAMAMATSU H10721 series) coupled to an amplifier/converter (HAMAMATSU C11184)

The H10721 series are photosensor modules containing a metal package PMT and a high-voltage power supply circuit. This PMT delivers high gain, wide dynamic range, and high-speed response.

The output signal from a photomultiplier tube can be directly input to the amplifier and it provides a voltage output signal with a 50 Ω load at a fixed conversion factor of 1.25 mV/μA. The frequency of this amplifier at a bandwidth equal to -3 dB is DC to 300MHz which makes it fast enough to detect LII signals.

Pictures and spectral characteristics are shown after (Figure 3-26 and Figure 3-27).

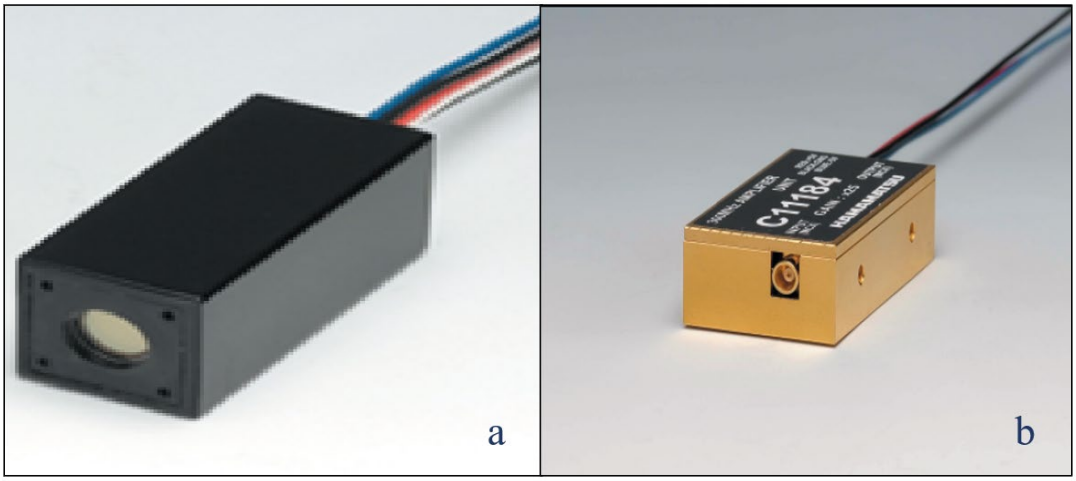

Figure 3-26 (a) Photomultiplier tube HAMAMATSU H10721-20 and (b) HAMAMATSU C11184 converter/amplifier

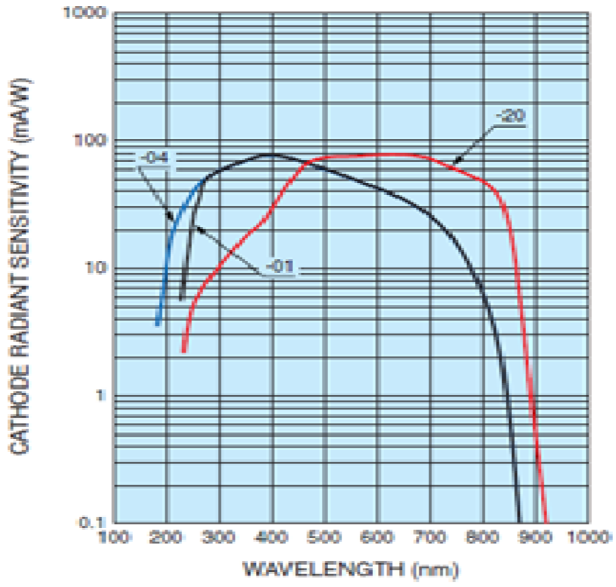

Figure 3-27 Sensitivity of the photomultiplier tube HAMAMATSU H10721-20 versus wavelength

3.4.7 Calibration of the 2C-LII detection system

To measure "absolute" soot volume fraction using the 2C-LII method, the entire LII system must be calibrated using another method. The calibration methods of LII data mainly include indirect methods or direct methods. The indirect method can use other particle sources with known volume fractions as a reference [132]. It is also possible to combine different measurement techniques such as laser extinction [9, 10], gravimetric sampling [135], or transmission electron microscopy or cavity ring-down spectroscopy [136]. The aerosol properties used to calibrate the measured soot volume fraction tend to vary with process conditions or time, resulting in inaccurate measurement results. So indirect measurement methods are considered introducing significant uncertainty. In addition, the implementation of indirect measurement methods is cumbersome and complex due to the need to work with other measurement techniques.

The direct calibration approach is also called the two-color approach. This method generally uses a light source with known radiation or irradiance to obtain the relative sensitivity of the measuring instrument. The temperature of soot particles heated with laser pulses can be obtained using two-color thermometry. The absolute soot volume fraction can be determined from the LII signal strength with known instrument sensitivity and soot particle temperature [137]. The light sources that are commonly used for the two-color method include tungsten lamps, halogen lamps and integrating spheres.

As previously introduced, an integrating sphere calibration was used to obtain the sensitivity of the experimental setup and then calculate the absolute soot volume fraction using the LII signal measured by the PMT device and the soot temperature is obtained by the two-color temperature method.

The calculation method is shown below. In order to measure the soot volume fraction f_v using the detected LII signal (equation 3-20), the detection chain must be calibrated, meaning that to determine the factor: Ω (solid angle) x β (detection efficiency).

For this reason, the signals at 750 and 850 nm recorded with our detection system are compared with the luminance of a calibrated source of black body photons. An integration sphere from SphereOptics was used. This sphere consists of a lamp located inside of a cavity, which is covered by white Lambertian substrate (BaSO4). It emitted a black body type radiation in the range of 360 nm

to 1000 nm with an adjustable temperature between 2000 and 3300 K by adjusting the voltage and current of the external power supply module. An optical fiber connected with the sphere directs the light to a calibrated spectrograph, which provides luminance L° spectra as reference. This optical configuration is represented in the Figure 3-28.

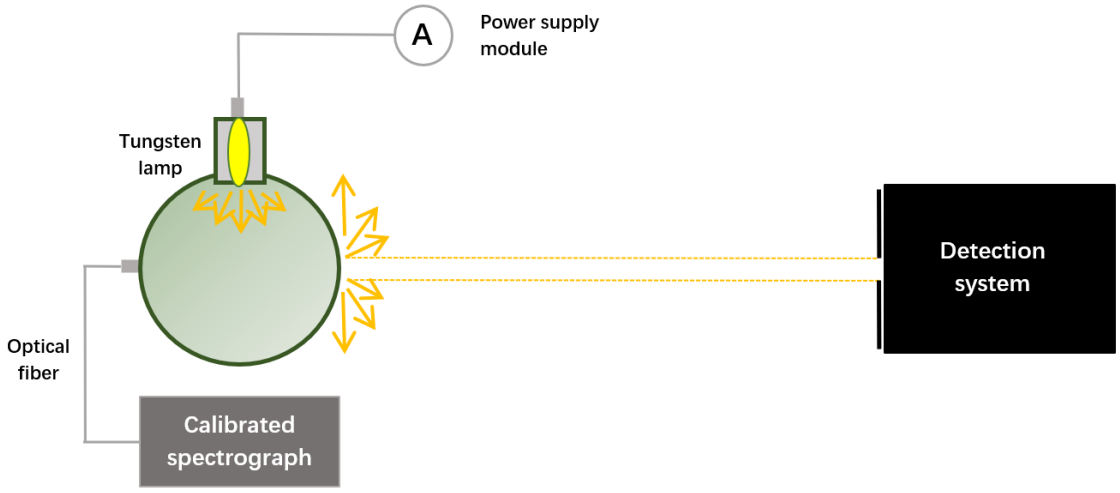

Figure 3-28 Set-up used to determine the optical response of the measurement system

The parameters of the detection system (position of the collimator, gain of the PMT) are the same as for LII measurements.

Here after, the PMT signal (in volt) is proportional to the luminance L° ($W.m^{-2}.sr^{-1}$ per wavelength), the surface of the sphere orifice $S_{sphere\ orifice}$ (m^2) and the spectral bandwidth $\Delta\lambda$ (m) as the equation:

$$S_{PMT\ (\lambda)} = L^{\circ} . S_{sphere\ orifice} . \Delta\lambda . \Omega . \beta \qquad \text{Equation } 3-21$$

Here after, the Figure 3-29 (a and b) show respectively the response of the detection system for the 2 detection wavelengths 750 and 850 nm versus the power emitted by the orifice of the sphere (meaning the product of the luminance given by the calibrated spectrometer of the sphere by the sphere orifice surface and by the wavelength bandwidth) for different power supply of the tungsten lamp (meaning different color temperatures of black body photons).

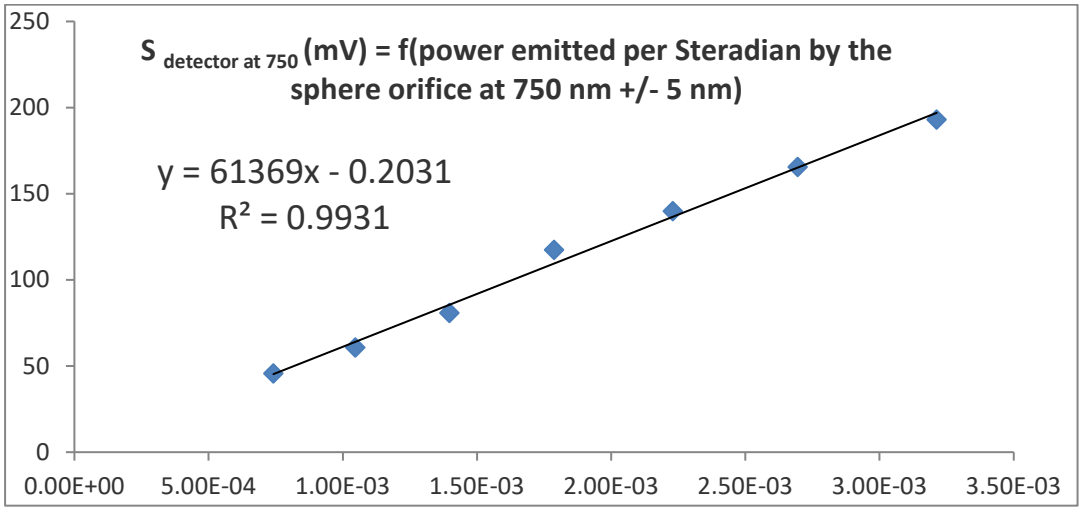

(a)

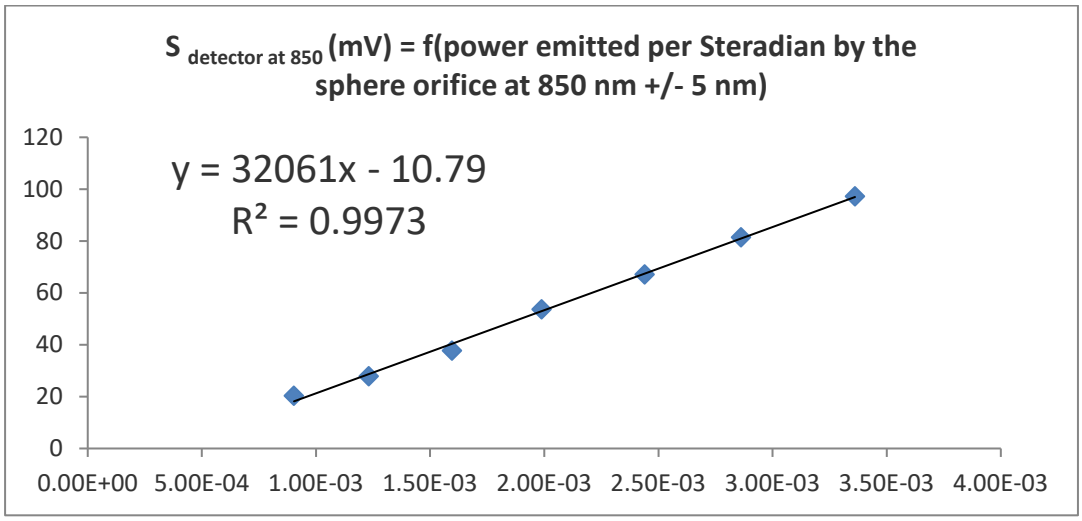

(b)

Figure 3-29 Calibration curve of the detection system for (a) 750 nm and (b) 850 nm

For a fixed gain of the PMT (adjusted at 0.5 Volt), the slope of both linear regression are equal to the factor "Ω (solid angle).β (detection efficiency)".

For 750 nm, Ω.β = 61369 in mV.Sr/W

For 850 nm, Ω.β = 32061 in mV.Sr/W

3.4.8 LII temperature measurement

In order to measure the soot volume fraction, one needs to measure the soot temperature T during the LII process. The temperature at time t which corresponds to the LII peak intensity was measured thanks to the 2 fast PMT measurements.

According to equation 3-18 and assuming $\exp\left(\frac{hc}{\lambda k_B T}\right) \gg 1$ in the spectral range and temperature conditions, the soot temperature could be measured instantaneously using the following equation:

$$T = C_2 \times \left(\frac{1}{\lambda_{850}} - \frac{1}{\lambda_{750}}\right) \cdot \left[\ln\left(\frac{S_{LII}(\lambda_{750}, t)}{S_{LII}(\lambda_{850}, t)} \cdot \frac{\beta_{850}}{\beta_{750}} \cdot \frac{{\lambda_{750}}^6}{{\lambda_{850}}^6} \cdot \frac{\Delta\lambda_{850}}{\Delta\lambda_{750}} \cdot \frac{E(m, 850)}{E(m, 750)}\right)\right]^{-1} \quad \text{Equation } 3-22$$

In the investigated spectral range of LII emission (the 2 wavelengths is mentioned as 750 and 850 nm), the refractive index function E(m, λ) is assumed to be constant. The 2 spectral bandwidths $\Delta\lambda$ at 750 and 850 nm are equal. The ratio of the 2 terms β are referred to the previous values of Ω.β (Ω_{750} and Ω_{850} being the same independent of the wavelength).

3.4.9 LII volume of measurement Vm

The laser beam is shaped as a “top-hat” with a diameter of 5 mm (see paragraph 3.3.6). The diameter of the circular detection orifice of the chimney is 20 mm. So, the volume of measurement could be calculated and is large enough to get enough LII signal in our case.

3.5 Scanning Mobility Particle Sizer measurements

An electric mobility diameter analyzer "Scanning Mobility Particle Sizer" (SMPS) device was used to measure the particle size distribution. The SMPS measuring devices are made up of different elements, the role and principle of use of which are described below.

3.5.1 Principle

The mobility diameter analyzer (SMPS, TSI brand) is an instrument composed of an electrical mobility analyzer (DMA) coupled to a CPC particle counter. The DMA selects aerosols according to their mobility diameter. Using a diameter scanning device, each particle class is sent to the counter which measures the number of particles per unit volume associated with each class. The measurement and classification are done in a range between 10 nm and 1 μm. The principle of this device is based on the electric mobility of particles in a [138].

Figure 3-30 SMPS measuring devices

3.5.2 TSI 3088 Neutralizer

TSI 3088 Neutralizer is an essential part of the Scanning Mobility Particle Sizer. Neutralizing aerosol particles reduces electrostatic losses from particles in pipes or other surfaces. Neutralization is also important for collecting reliable particle size data when using electrical mobility-based fractionation instruments.

3.5.3 TSI 3080 Electrostatic Classifier

The Model 3080 Electrostatic Classifier is the main component for generating or sizing aerosols. Given a polydisperse input aerosol, the instrument output can be a stream of monodisperse aerosol of known particle size. The family of Electrostatic Classifiers size-classifies highly monodisperse, submicrometer aerosols in the range from 2 to 1000 nanometers in particle diameter. The Electrostatic Classifier is most often used as an integral part of a monodisperse-aerosol generation system or a submicrometer-particle sizing system.

3.5.4 NanoScan SMPS TSI 3910

The NanoScan SMPS Model 3910 measures nanoparticle size distributions from 10 to 420 nm in one minute. Its internal CPC uses isopropyl alcohol as a

working fluid, so the NanoScan is suitable for use in a variety of sensitive environments.

3.5.5 The Ultrafine Condensation Particle Counter TSI 3776

The Ultrafine Condensation Particle Counter 3776 (UCPC) is a type of condensation particle counter (CPC) which was designed primarily for researchers interested in airborne particles smaller than 20 nm. It is a continuous-flow instrument that detects particles down to 2.5 nm. It uses a special sheath-air flow design that improves response to changes in particle mole fraction and increases counting efficiency for ultrafine particles.

3.6 Chapter summary

This chapter described the equipment used to carry out the experiments performed in this study. It is very important to invest time in the adaptation of research equipment. A great deal of time was spent on the design and construction of experimental set-ups, including the design of light-transmitting combustion chamber and chimney, secondary air intake lines that can be switched ON and OFF and equipment for simultaneous measurements of pollutants into the chimney and the flame (gaseous/condensed pollutants by chemical analysis and soot by LII). It is because of these adjustments that accurate emissions analysis is possible.

Chapter 4

Characterization of emissions produced by wood pellets combustion

Chapter 4 Characterization of emissions produced by wood pellets combustion

4.1 Introduction

In this chapter, all the results obtained from the natural wood pellets combustion were presented and analyzed. The parameters of the wood pellets used in the experiments were first analyzed and presented. The measurement results of gaseous emissions were then presented. The variation of gaseous emissions such as O_2, CO_2, CO, THC and PAHs under nominal conditions, different primary airflow rate, and with or without secondary air supply was analyzed. The measurement results of particulate emissions by using the LII method and SMPS method was showed. For LII, the difference in measurement results under several different LII configurations were introduced. The aerosol diameter measurement results are shown for SMPS.

4.2 Fuel analysis and boiler power

In this section, the experimental tests were carried out with a single type of wood pellets. Wood pellets are developed for small and medium-power biomass boilers, usually used for domestic heating. The physicochemical properties (PCI, particle size, humidity, density, ash content, etc.) and the classification of this type of biomass are regulated by European standard EN 14961-1 [128].

- The characteristics of the wood pellets

The pellets used to meet the criteria imposed by the DIN Plus certification which defines the quality of wood pellets. The characteristics given by the supplier are shown in Table 4-1.

Table 4-1 Characteristics of the wood pellets

Characteristics		Wood pellets
Diameter	mm	6
Length	mm	3.15 to 40
Density	kg/m^3	650
LHV	kWh/kg	5.1
Moisture	%	8
Composition		100% Wood

- The chemical composition of the wood pellets

The chemical composition of this fuel and its formula were obtained by an elemental analysis carried out by the Centre Commun de Mesures (CCM) of the University of Littoral-Côte d'Opale at Dunkerque. This made it possible to write the following combustion reaction using the air excess e_{air}:

$$C_{40.58}H_{55.24}O_{22.68} + 3.88H_2O + 205(1 + e_{air})(0.21O_2 + 0.79N_2) \rightarrow 40.58CO_2 + (27.62 + 3.88)H_2O + 43.05e_{air}O_2 + 161.95(1 + e_{air})N_2$$

Equation 4-1

with the ratio of excess air adjust through the intake line described above.

- The mass flow rate of wood pellets and the boiler power.

In this experiment, no instrumentation directly measures wood pellets mass flow. Pellets mass flow rate is calculated from experimental data and combustion reaction equations. Then the calculated mass flow of particles allow the calculation of the boiler power. The following is the equations used to calculate the boiler power.

The air excess e_{air} and mass flow rate of wood pellets $\dot{m}_{pellets}$ can be calculated by the combustion reaction formula from the ratio of the mole fractions of O_2 and CO_2:

$$e_{air} = \frac{40.58X_{O2}}{43.05X_{CO2}} \qquad \text{Equation } 4-2$$

Where X_{O2} is the mole fraction of O_2, X_{CO2} is the mole fraction of CO_2.

$$\dot{m}_{pellets} = \frac{\dot{m}_{air}M_{pellet}}{205(1+e_{air})M_{air}} \qquad \text{Equation } 4-3$$

Where $\dot{m}_{air}$ is the mass flow rate of inlet air, M_{pellet} is the mole mass of wood pellets and M_{air} is the mole mass of air.

The uncertainty of pellet mass flow rate depends on the uncertainties of the gaseous analyzers (2% of the full scale) and of the air mass flow rate (calculated from the air velocity with an error of +/- 0.1 m/s for the sensor) (cf. Table 3-1).

Then the Lower Heating Value of wood pellets allows to calculate the input thermal power of the boiler.

$$Q_{input} = \dot{m}_{pellets} \times LHV \qquad \text{Equation } 4-4$$

The output thermal power of the boiler, which is the energy obtained by the water in the heat exchanger, is calculated using the following equation:

$$Q_{output} = \dot{m}_{water} \times C_{water} \times (T_{out} - T_{in}) \qquad \text{Equation } 4-5$$

Where $\dot{m}_{water}$ is the mass flow rate of water in the heat exchanger, C_{water} is the specific heat of water, T_{in} is the inlet water temperature and T_{out} is outlet water temperature.

The following table shows the input and output power of the boiler in different five tests.

Table 4-2 Input and output power of the boiler

	Input power kW (combustion)	Output power kW (to the water)
Test 1	16.8	10.2
Test 2	17.4	11.4
Test 3	15.5	10.4
Test 4	16.5	9.2
Test 5	17.1	11.3

4.3 Gaseous pollutant emissions measurement

To study the gaseous pollutant emissions in the boiler and the chimney, several experiments were done and the gaseous emissions from the boiler were recorded. Gas emissions (mole fractions) during the ignition, steady state and extinguishing phases on nominal boiler operation were analyzed. After that, the change in gaseous emissions with and without secondary air supply was compared. Finally, the influence of the change of the primary air flow rate on the gaseous emissions of the boiler is analyzed.

4.3.1 Analysis of nominal boiler operation

In this part, the nominal performance of the boiler is investigated. European standards are well-defined regarding the testing of residential solid fuel appliances (EN 12809:2002, EN 13240:2001, EN 13229:2001, EN 14785:2006). They require the use of predefined and well-controlled combustion cycles. However, in this work, the European standardized cycle was not followed. This is because the behavior of the appliance between well-controlled use and actual use differs considerably, especially in appliances operated from wood, where the combustion process occurs throughout the main stages (drying, pyrolysis/gasification, combustion) exhibit great variability.

The operation described below corresponds to full power operation with both the primary air and secondary air supply, The first step is to analyze the pollutant

emissions of the boiler in the ignition phase, the steady state phase and the extinguishing phase. Then measure the temperature at the furnace outlet (point 1) when the boiler is thermally stable and take samples from the chimney to measure the pollutant mole fraction.

For the first statistical analysis carried out in this series of experiments, tests were carried out on different days under the same operating conditions. Each test represents an average value for one day. We selected test days with complete data and no interruptions or changes in the incoming air flow to ensure data comparability. The flue gas samples were taken to measure the gas mole fraction in the chimney. Figure 4-1 shows the average values of O_2 and CO_2 mole fractions at different stages in different tests. All the tests show lower O_2 percentage and higher CO_2 percentage in steady-state phase. This is a logical result since the steady state conditions burn more fuels than the ignition and extinguishing phases, so fuel combustion consumes more O_2 and produces more CO_2.

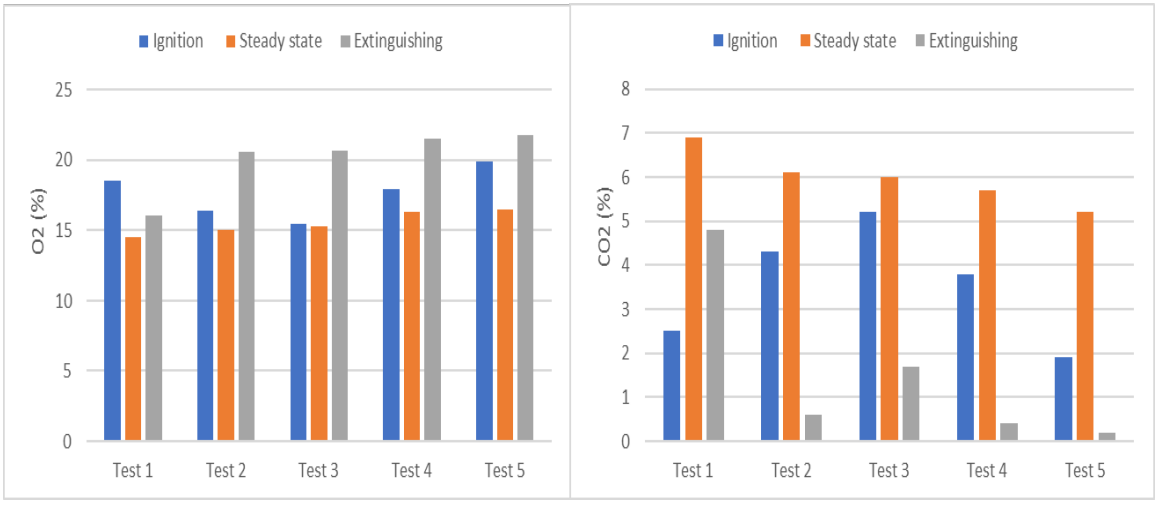

(A) **(B)**

Figure 4-1 Average values of O2 (A) and CO2 (B) mole fractions at different stages in different tests

Figure 4-2 shows the average values of carbon monoxide (CO) and total hydrocarbon (THC) mole fraction at different stages in different tests. For THC, it can be observed that the ignition and extinguishing phases have higher mole fraction. The THC mole fraction in these two phases is several times or even dozens of times more than in the steady state phase. This can be explained by the fact that during the ignition and extinction phases, insufficient combustion leads to the direct emission of more unoxidized hydrocarbons into the chimney.

There is not a similar trend for CO. This can be explained by the complexity of CO formation, which can be produced under both lean and eutrophic combustion, as previously mentioned. During the combustion of biomass fuels, CO may be released directly as a volatile compound or form an intermediate product in either heterogeneous reactions involving char oxidation or homogeneous reactions in the gas phase.

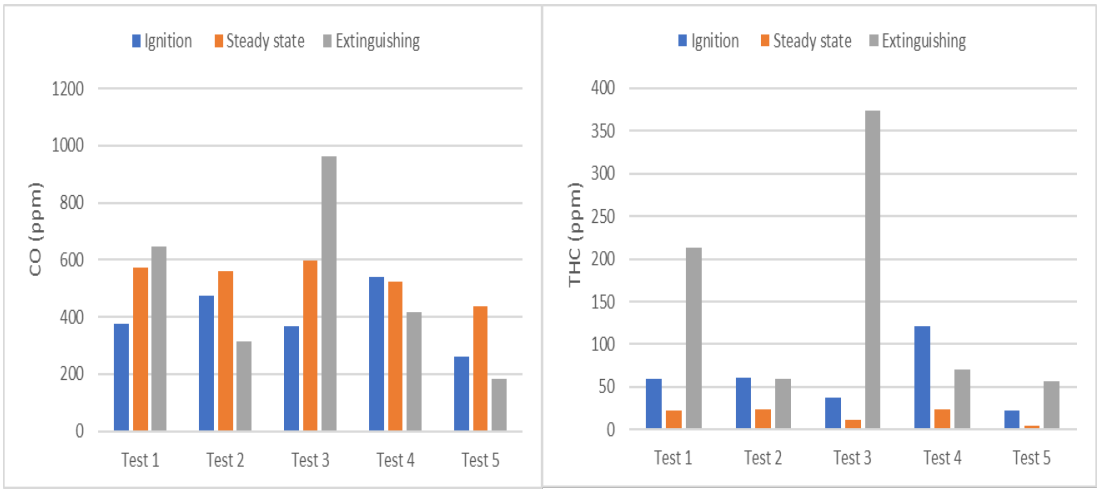

(A) **(B)**

Figure 4-2 Average values of CO (A) and THC (B) mole fraction at different stages in different tests

The measurements in the following figures (temperature, gaseous pollutant emissions) are started after the boiler has reached a steady state. and are made during 5 hours (cf. Appendix 3), to ensure the good repeatability of the operation of the system.

Figure 4-3 (A) shows the average temperatures for the tests at the furnace outlet (point 1). The data obtained were statistically analyzed by calculating the means and the standard deviations, the standard deviations are represented by the error bars. We noticed that although the temperatures obtained from each test differ, the maximum difference between them is as much as 6 °C, but the standard deviation of each test is less than 2 °C. Therefore, the system can be considered thermally stable after reaching a steady state. However, fluctuations in temperature can be seen in the test results from different days.

Figure 4-3 (B) shows the means and standard deviations of flue gas mole fraction for the tests (CO and THC corrected to 10% O_2, O_2refbeing here 10 % due to the more recent standard) in the chimney. The correction was carried out using the following equation:

$$C_{corrected} = C_{measured} \frac{(21 - O_2 ref)}{(21 - O_2 measured)} \qquad \text{Equation } 4-6$$

As observed in Figure 4-3B, the standard deviations for CO and THC are large. It has reached 23% and 50% of the mean value. While the standard deviation of O_2 and CO_2 is relatively small, only 3.8% and 11.4% of the mean value.

In the rest of the manuscript, the results of the CO and THC mole fraction were directly corrected at 10% O_2 (the mole fraction results for O_2 were not presented). As mentioned previously, the results are represented at 10% O_2 to be able to compare with many other authors who use this value of O_2ref.

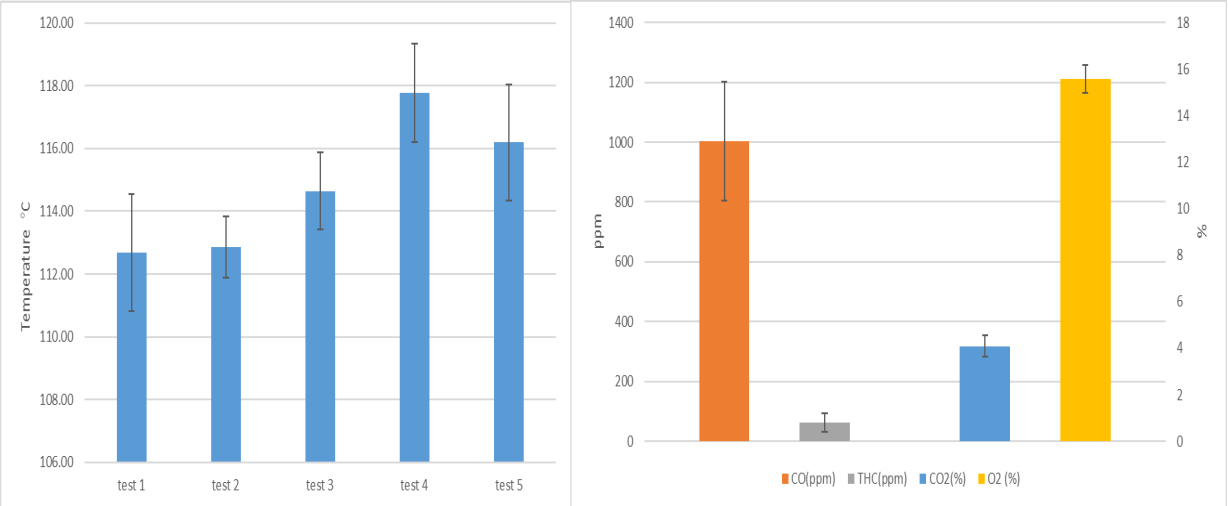

(A) **(B)**

Figure 4-3 (A) the average temperatures for the 5 tests at the furnace outlet (point 1) and (B) the average flue gas mole fraction for the 5 tests (CO, THC corrected to 10% O2)

To compare with other authors, the results must be correlated with the energy provided by the fuel. Here the mole fraction values are converted into emission factors, which can make the analysis easier.

Equation 4-7 is used to convert pollutant concentrations to emission factors E_i:

$$E_i = C_i \times \frac{V_s}{LHV} \qquad \text{Equation } 4-7$$

Where C_i is the pollutant concentration (mg/m^3)

V_s is the specific volume (m^3/kg)

LHV is the lower calorific value of fuel (MJ/kg)

Figure 4-4 shows the emission factor averages of CO and THC for the 5 tests.

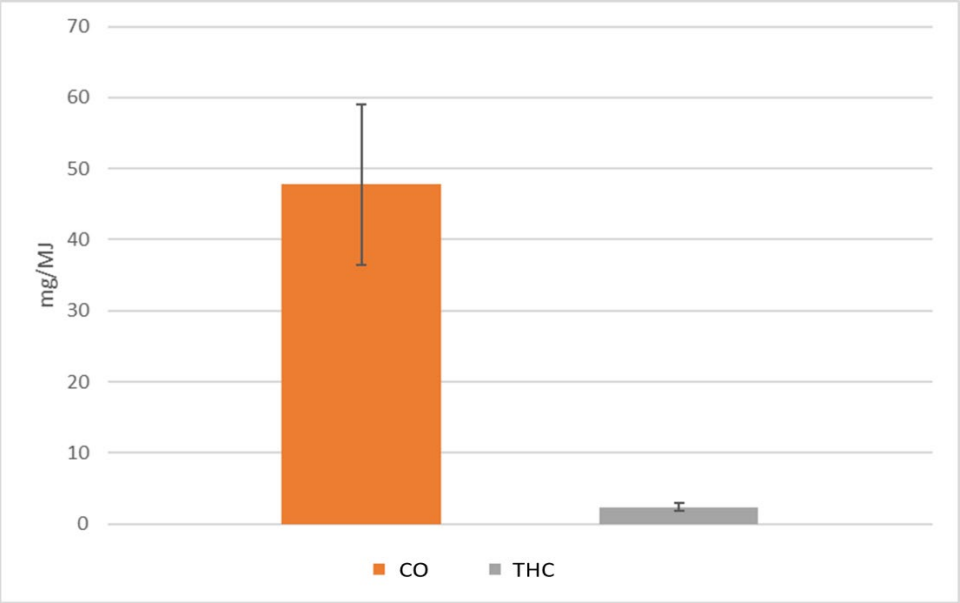

Figure 4-4 Average of emission factors over 5 tests for CO and THC

4.3.2 Influence of secondary air on gaseous emissions

In this subsection, the effect of secondary air on gaseous emissions from wood pellet combustion was investigated. Air staging strategies are methods used by many boilers to reduce pollutant emissions.

As mentioned in section 3.1.2, the primary inlet and secondary inlet pipes of the boiler share a total inlet pipe (cf. Figure 3-3). A fan blows into a manifold connected to 2 pipes, providing both primary and secondary air to the fireplace. The amount of intake air distributed between the 2 pipes is approximately 50% to 50%. The overall airflow can be controlled manually. However, this configuration does not allow to separate the control of the two airflows, but a plug can be used to completely block the secondary air supply before a single test begins.

To compare the effect of secondary air intake on gaseous pollutants, the results with secondary air are compared with the results without secondary air. The total inlet pipe is fully open so that the boiler reaches maximum air supply. After the boiler reached a steady state, gaseous pollutant mole fraction in the flame and the chimney were simultaneously sampled for at least 20 minutes. The results presented in Figure 4-5 are the average of the measurements.

It should be noted that due to the existence of the secondary air manifold, the maximum inlet air flow of the boiler is different when the second intake pipe is open or closed. The maximum air inlet in the open state of the secondary air is about 11 g/s according to the distribution of 50% to 50%, the primary air supply and the secondary air supply are each 5.5 g/s while in the secondary air pipe closed state the primary air supply is equal to the maximum air supply which is about 7.5 g/s.

In figure 4-5, the mole fraction of gaseous pollutants in the flame with and without secondary air supply was compared. The mole fraction of CO and THC are much higher when the secondary air is provided. In fact, with secondary air supply, the mole fraction of CO increased by about 25 times, the mole fraction of THC increased by about 14 times.

The following factors may have contributed to the observation: Emissions of CO, THC, PAHs and soot are a result of incomplete combustion. Since the secondary air injector is above the flame, the pollutant mole fraction in the flame is mainly affected by the primary air supply. The amount of primary airflow rate is known to affect the temperature in the flame. In the condition without secondary air supply, the primary air supply is higher. The increase of primary airflow rate increase the temperature in the flame leading to more complete combustion thus the mole fraction of CO and THC decreases.

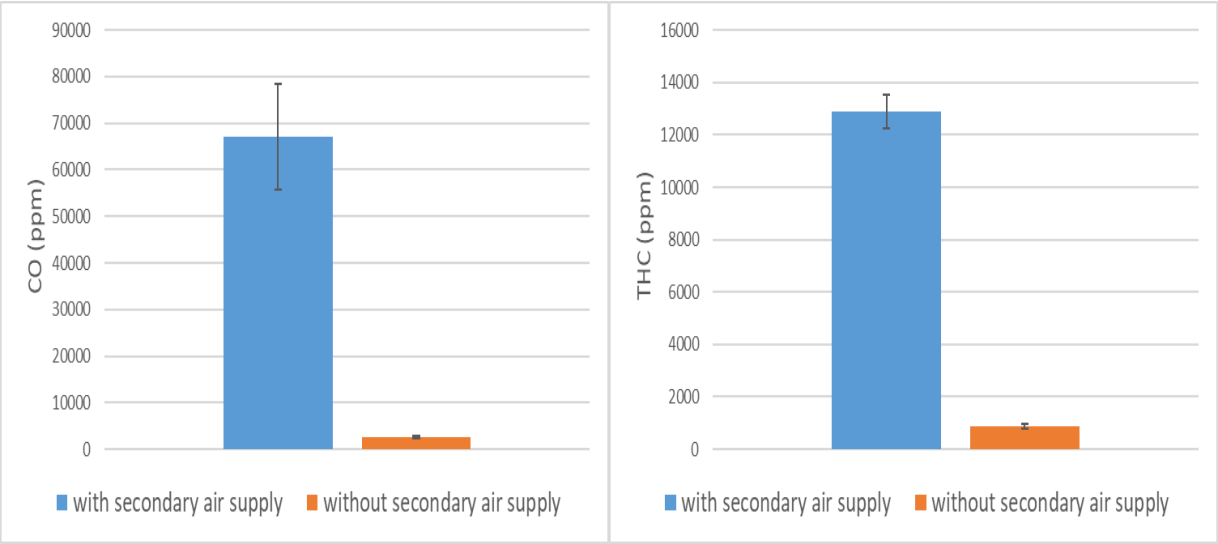

Figure 4-5 Average values of the mole fraction CO and THC in the flame

In Figure 4-6, the mole fraction of CO and THC in the chimney with and without secondary air supply was compared. It was found that the mole fraction of CO and THC were still higher with the secondary air supply than which without the secondary air supply.

In fact, with secondary air supply, the mole fraction of CO increased by about 59%, and the mole fraction of THC increased by about 138% compared to the situation without secondary air supply. Although the final mole fraction of CO and THC does not increase by a dozen or twenty times as in the flame, the presence of secondary air still increases the emission of CO and THC.

The reason for this result may be that the secondary air inlet pipe was directly connected to the main air inlet pipe, without adding a device to heat the secondary air. These results in the direct injection of cold secondary air into the combustion chamber, lowering the temperature of the furnace, and resulting in increased emissions of CO and THC. The mole fraction of CO and THC in the chimney were not as great as in the flame probably because of the dilution effect of the secondary air.

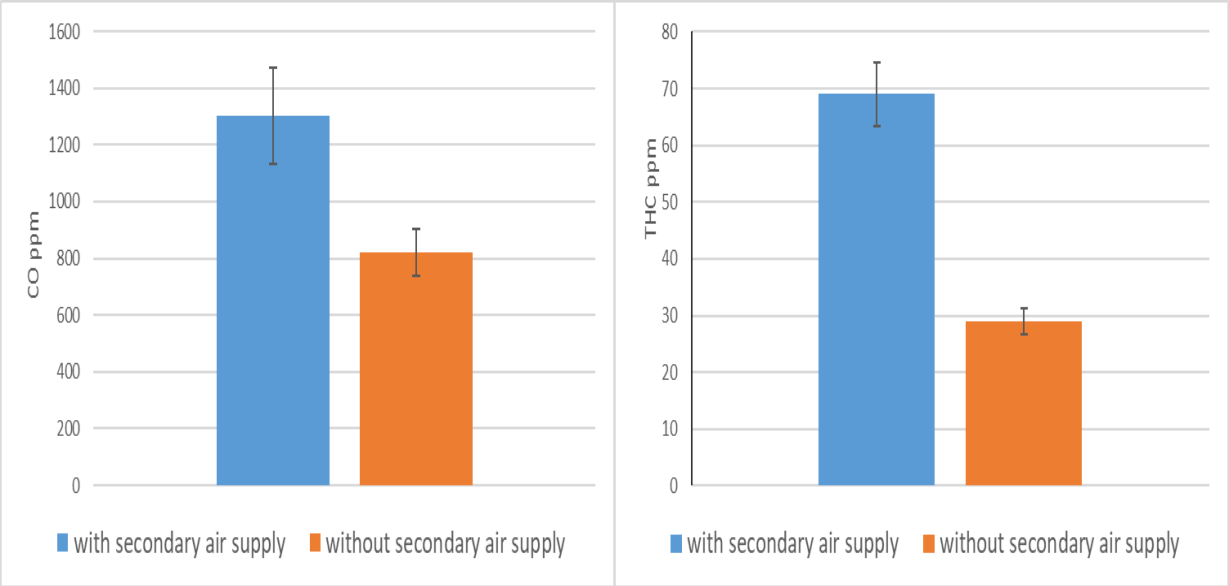

Figure 4-6 Average values of the mole fraction CO and THC in the chimney corrected to 10% O2

4.3.3 Influence of primary airflows rate on gaseous emissions

In this subsection, the effect of primary airflow rate on the emission of gaseous pollutants from wood pellet combustion was investigated.

As mentioned earlier, the inlet of the boiler consists of a PVC pipe and a converging-diverging pipe. There is an adjustable cover plate at the entrance of the PVC pipe of the total inlet boiler, which can adjust the covering cross-sectional area, to realize the manual adjustment of the inlet airflow.

The mole fractions of CO and THC are measured at different primary air flow rates. Simultaneously sample in the flame and in the chimney for at least 20 minutes after the boiler reaches steady state. The mole fraction of CO and THC in the chimney is the average values corrected to 10% O_2.

The evolution of gaseous emissions (CO and THC) in the flame as a function of the primary airflow rate is presented in figure 4-7 and figure 4-8. figure 4-7 is in the condition of both primary and secondary supply (distribution of 50% to 50%). It was found that mole fraction of all gaseous emissions decreased when the primary air supply was increased. It can be seen from the graph that the decreasing trend of each gas is similar. When the primary airflow rate is increased from the minimum of 2.9 g/s to the maximum of 5.7 g/s, the airflow rate increases by 95.7%, while the mole fraction of CO decreased by 28.9%, and the THC decreased by 75.8%.

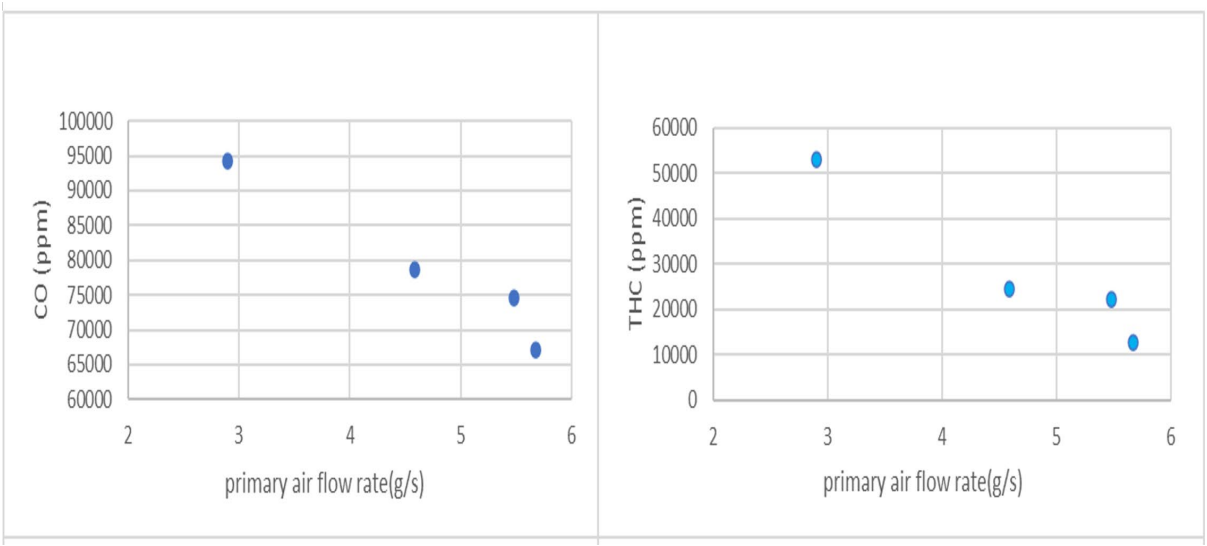

Figure 4-7 Evolution of the gaseous emissions (CO and THC) in the flame as a function of the primary airflow rate in the condition of both primary (50 % of total inlet air) and secondary (50 % of total inlet air) air supply

Figure 4-8 shows the evolution of gaseous emissions (CO and THC) in the flame as a function of the primary airflow rate in the condition of without secondary supply. Similar to the previous results, it was found that the mole fraction of CO and THC tended to decrease when the primary air supply increased. When the primary airflow rate is increased from the minimum of 6.3g/s to the maximum of 8.2g/s, the airflow rate increases by 30%, while the mole fraction of CO decreased by 73.3%, and the THC decreased by 78%.

Combining the data from the two figures leads to the following inferences. For CO, THC, increasing the primary airflow rate reduce their mole fraction in the flame, similar results are obtained in conditions with or without secondary air supply. This may be because the increase in primary air supply contributes to more complete combustion and thus reduces the mole fraction of pollutants in the flame.

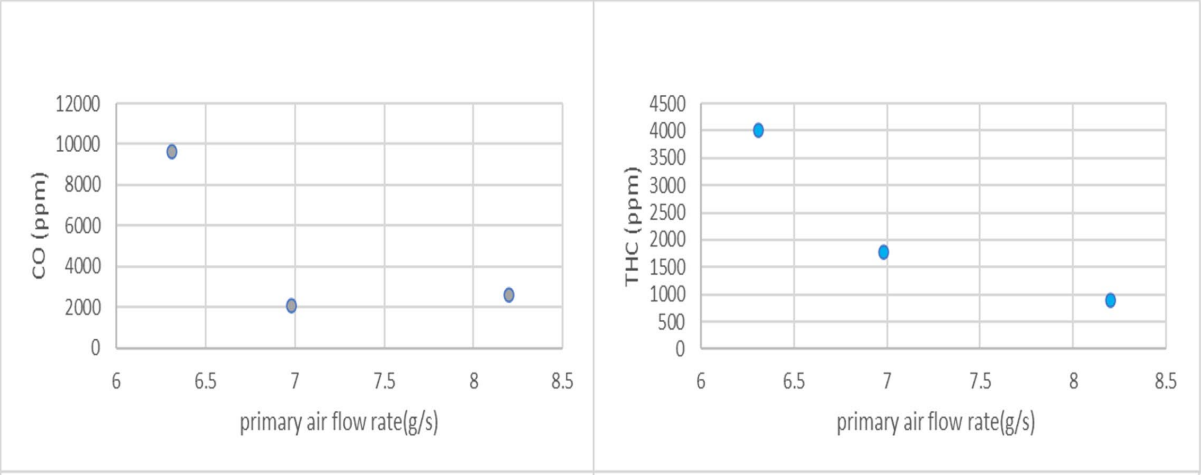

Figure 4-8 Evolution of gaseous emissions (CO and THC) in the flame as a function of the primary airflow rate in the condition without secondary air supply (primary air = 100 % of total inlet air)

After observing the evolution of the gaseous emissions mole fraction in the flame with the primary airflow rate, the gaseous emissions mole fraction in the chimney was analyzed (figure 4-9). These results are from different test days, and each value is an average of at least 20 minutes of measurements. It was found that this is not as clear as the data in the flames. For CO, the mole fraction increases first and then decreases with the increase of the primary air flow rate. The lowest point of CO mole fraction occurs at the lowest point of the primary airflow rate. When the primary airflow rate is equal to 5.3g/s, the CO mole fraction is 528ppm. The second lowest CO mole fraction occurs when the primary mole fraction airflow rate is equal to 7.5g/s which is almost the maximum value of the primary airflow rate in the measurement. The two highest points of CO mole fraction appear when the primary airflow rate is equal to 6.3g/s and 7g/s, and the CO mole fraction at these two points are 1022ppm and 1045ppm. The highest CO mole fraction value is almost twice as high as the lowest. For THC, it was also observed similar results. The two lowest points of THC mole fraction are that the primary airflow rate is equal to 5.3g/s and 7.4/s, and the THC mole fraction are 28.8ppm and 28.9ppm respectively. The highest THC mole fraction is when the primary airflow rate is equal to 6.9g/s, the THC mole fraction at this time is about 60ppm. The trend of THC is not as obvious as that of CO, its mole fraction distribution is more dispersed, but the highest mole fraction value is also twice the lowest mole fraction value. These results may be can explain by the high dilution due to the air.

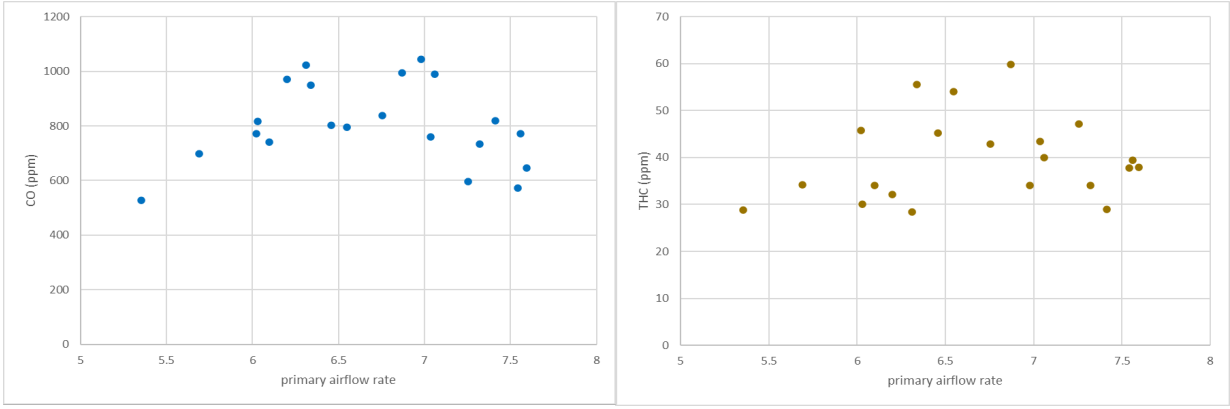

Figure 4-9 Evolution of gaseous emissions (CO, THC) in the chimney as a function of the primary airflow rate in the condition without secondary air supply (primary air = 100 % of total inlet air). Mole fraction being corrected to 10% O_2

4.3.4 Polycyclic Aromatic Hydrocarbons (PAHs)

The profiles of the total PAHs mass fraction in the chimney and the flame, are presented in Figure 4-10 and Figure 4-11. The average PAHs mass fraction under the condition with or without secondary air supply were compared.

It was found that the main PAHs in the chimney are naphthalene, acenaphthylene, and phenanthrene from Figure 4-10.

Removing secondary air seems to have a negative impact since the total PAH mass fraction is multiplied by a factor of 2.6. These behaviors could be explained by the fact that the contribution of secondary air to the boiler has the role of re-burning pollutants including PAHs. The elimination of the secondary air supply therefore logically induces an increase in their contents.

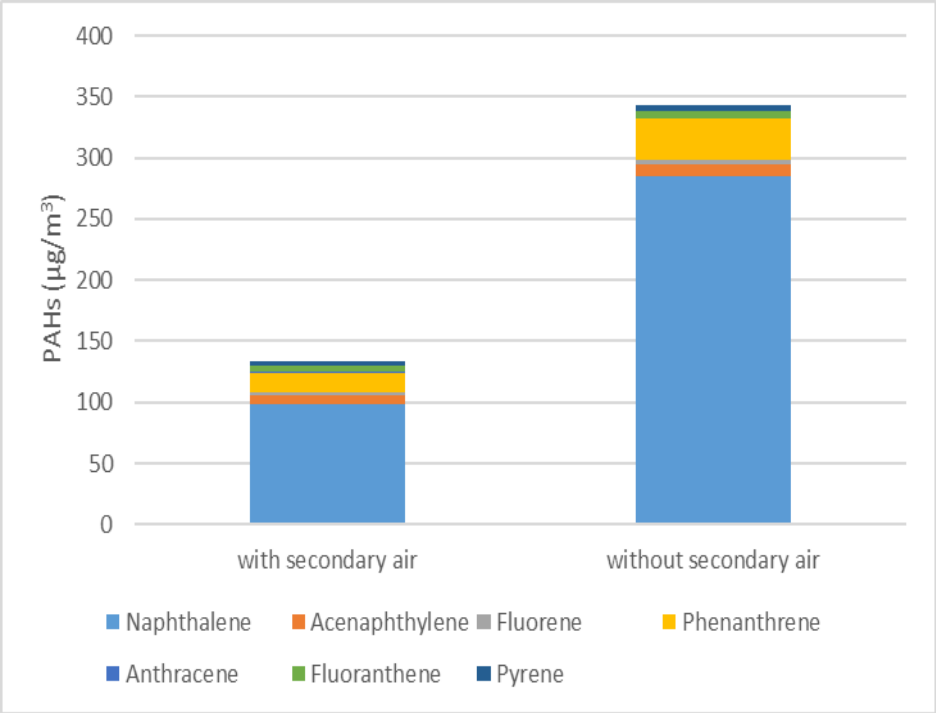

Figure 4-10 Total mass fractions of PAHs in the chimney

Figure 4-11 shows the total mass fractions of PAHs in the flame. The measurements carried out in the flame reveal much higher PAHs mole fractions than in the chimney.

In contrast to the results in the chimney, removal of the secondary air supply resulted in an approximately 85% reduction in the PAH mass fraction in the flame.

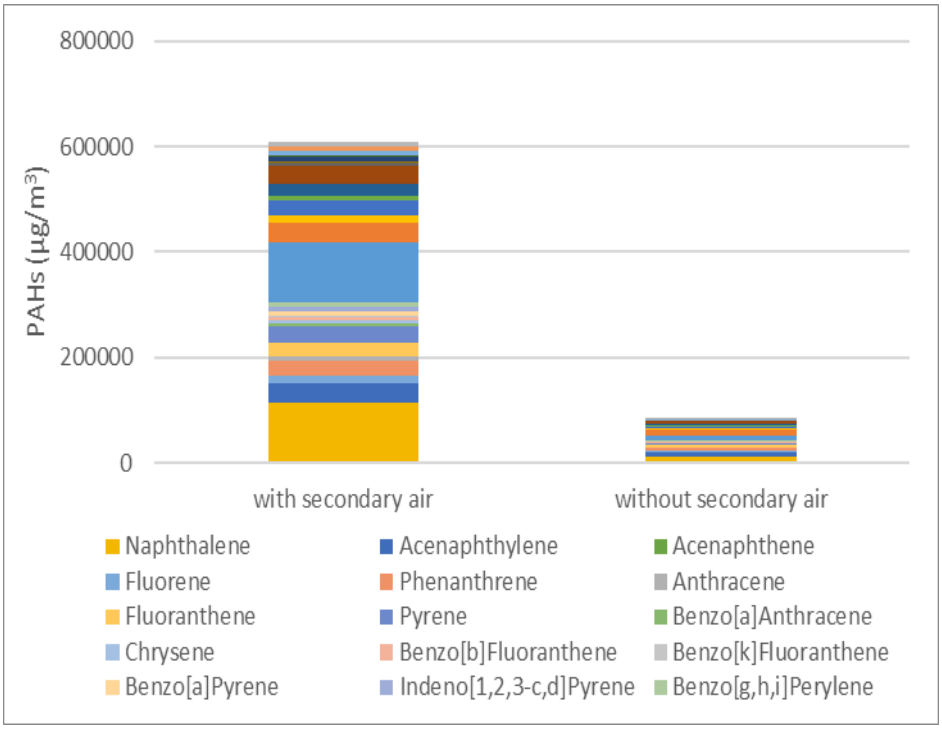

Figure 4-11 Total mass fraction of PAHs and in the flame

This opposite result may be due to the following reasons. Since the secondary air supply plays a role in re-burning a part of PHAs, the mass fraction of PAHs in the chimney must decrease with the secondary air supply. However, when measuring the mass fraction in the flame, it is not affected by the secondary air. Due to the ratio of primary-secondary air 50% to 50%, when there is secondary air supply, the absolute primary air flowrate is lower, so the PAHs in the flame is higher under the condition of high equivalence ratio.

4.4 Particulate emissions measurement

One of the objectives of the measurements carried out by LII is to determine the influence of the air flow on the soot. The intensity of the LII signal (at one color) being representative of the soot volume fraction. The next sections analyze the measurement results of LII under different conditions.

4.4.1 One color LII measurement in the chimney

As introduced in Chapter 3, a relatively simple LII configuration was chosen to measure soot volume fraction in the chimney. Only one photomultiplier is used

to measure the LII signal in this method, so only a qualitative analysis of the soot in the chimney can be made.

Two conditions were tested for the measurements: with and without secondary air. All the tests were carried out with a constant energy of 200 mJ / pulse at 532 nm. The laser excitation conditions are considered to be on the plateau of the LII fluence curve.

The table 4-3 summarizes the different tests carried out:

Table 4-3 Test conditions of LII measurement in the chimney

Condition	Total airflow rate (g/s)	Primary airflow rate (g/s)
with secondary air	11.4	5.7
	9.2	4.6
	5.8	2.9
without secondary air	8.1	8.1
	7.3	7.3
	6.2	6.2

Measurements are obtained through a LabView program. This makes it possible to make a sliding average of the signal measured on 512 laser shots and returns a LII trace per minute.

Figure 4-12 shows examples of LII traces obtained at a total air flow rate equal to 11.35 g/s and the gain of the PMT is 0.42. The LII traces have two significant parameters: the maximum value (LII peak) representative of the volume fraction of soot, and the duration of decrease (decay time) representative of the diameter of the particle.

By comparing the LII peak value and the decay time under the same gain, the soot volume fraction and particle diameter under two different air flow rate can be qualitatively compared.

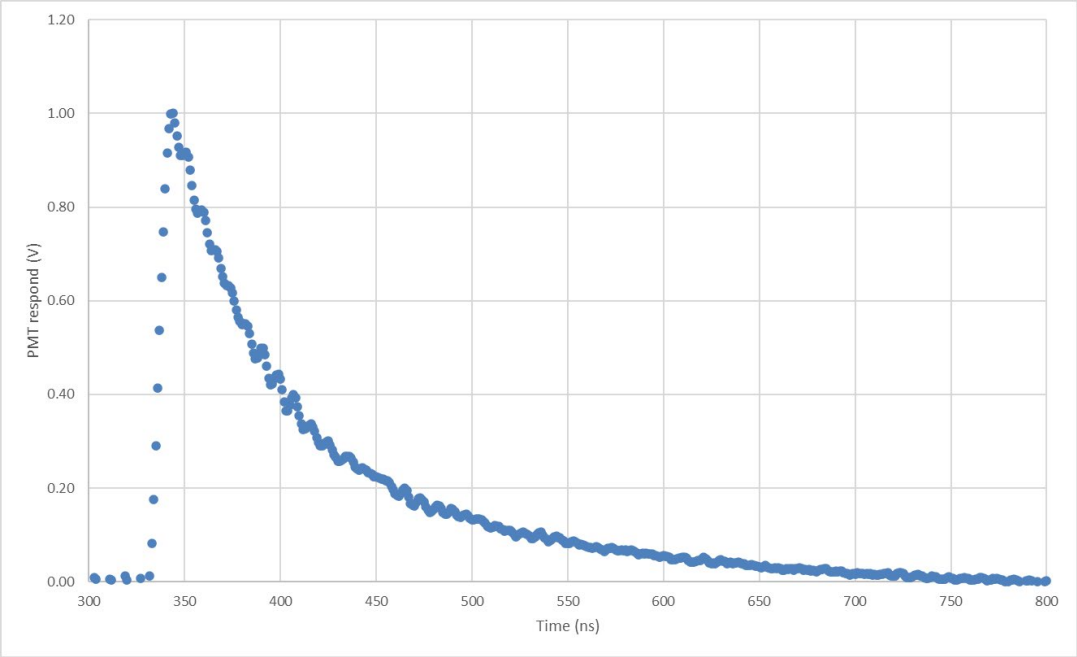

Figure 4-12 Example of one-color LII trace (primary air + secondary air configuration)

Table 4-4 LII decay time for the different conditions

Condition	Total airflow rate (g/s)	Primary airflow rate (g/s)	Decay time (ns)
with secondary air	11.4	5.7	500
	9.2	4.6	532
	5.8	2.9	458
without secondary air	8.1	8.1	338
	7.3	7.3	331
	6.2	6.2	378

Table 4-4 shows the mean values of the LII decay time (with a reference of $1/e^2$ of the LII peak with e the Euler constant, which corresponds to a decrease of the peak signal of 87%) for different airflow rate with and without secondary air supply.

With secondary air, no clear tendency can be highlighted. The primary flow rate is always smaller than for the case without secondary. And the decay time is longer, meaning the production of bigger soot particle in this condition. So the secondary air flow rate does not play the role of post-combustion to reduce the particle diameter. The higher primary air flow rate makes the particles produced by combustion smaller (meaning a global equivalence ratio C/O lower).

For the signals to be usable, it is necessary to carry out amplification via a photomultiplier (PMT). A calibration of PMT is necessary to obtain LII signal value. Figure 4-13 shows the value of the PMT signal as a function of the setpoint and makes it possible to obtain the correction to be applied to the measured values.

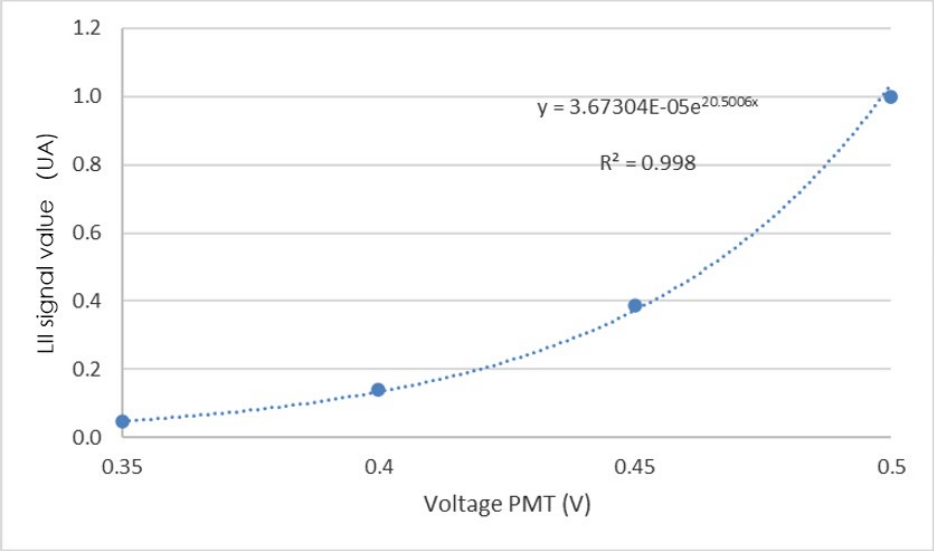

Figure 4-13 Determining the correction factor for raw values

The following correction formula is then obtained (normalization for a PMT setpoint of 0.5 V):

$$\text{Corrected Value} = \frac{\text{Original Value}}{3.67304 \times 10^{-5} \times e^{20.5006 \times \text{PMT}}} \qquad \text{Equation } 4-8$$

Figure 4-14 shows the temporal evolution of the LII peaks during the test with only primary air. The different colors of the line represent the different airflow rates. It can be seen that even under the same test conditions, the fluctuation of LII signal peaks measured at different times of a given experiment is very large. The LII peak value is the most unstable when the minimum airflow rate is equal to 6.2 g/s, which indicates that the volume fraction of soot fluctuates more under the condition of the lowest airflow rate. The two sets of data with higher air flow rate showed higher stability.

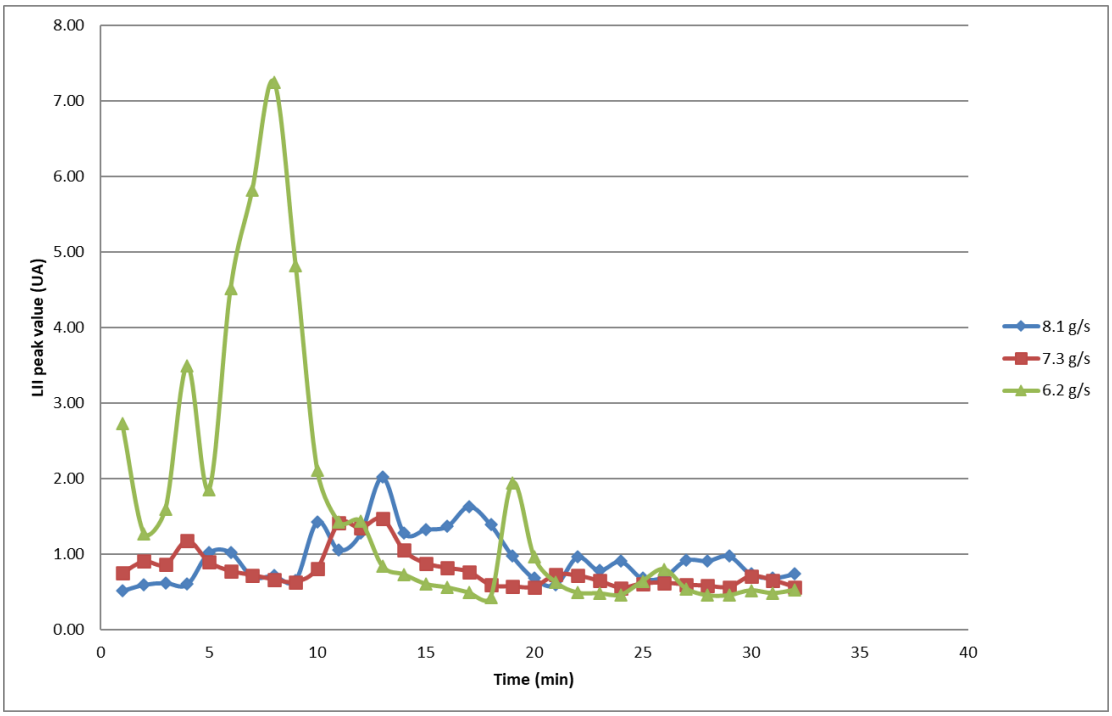

Figure 4-14 Temporal evolution of the LII peaks with only primary air

Figure 4-15 shows the evolution of the average value of the LII peaks as a function of the total airflow rate. The value retained for the signal LII was the average of the maximum values obtained during the measurement period. Values in blue were measured with both primary and secondary air supply, and red was measured without a secondary air supply. It was found that with the increase in the amount of airflow rate, only the data without a secondary air supply seems to be on an upward trend, while the data with both primary and secondary air supply first increased and then decreased.

The temperature inside the boiler was not measured in this thesis. For the case without secondary air, it has been assumed that when the total air flow rate is increased, the temperature inside the boiler is higher and the combustion produces more soot. The temperature inside the boiler decreases when the total air flow is reduced, resulting in pyrolysis rather than combustion reactions and producing less soot.

Due to insufficient measurement data, this trend cannot be confirmed by qualitative analysis, so the changes in soot volume fraction under different conditions were compared in quantitative analyses with two-color LII method.

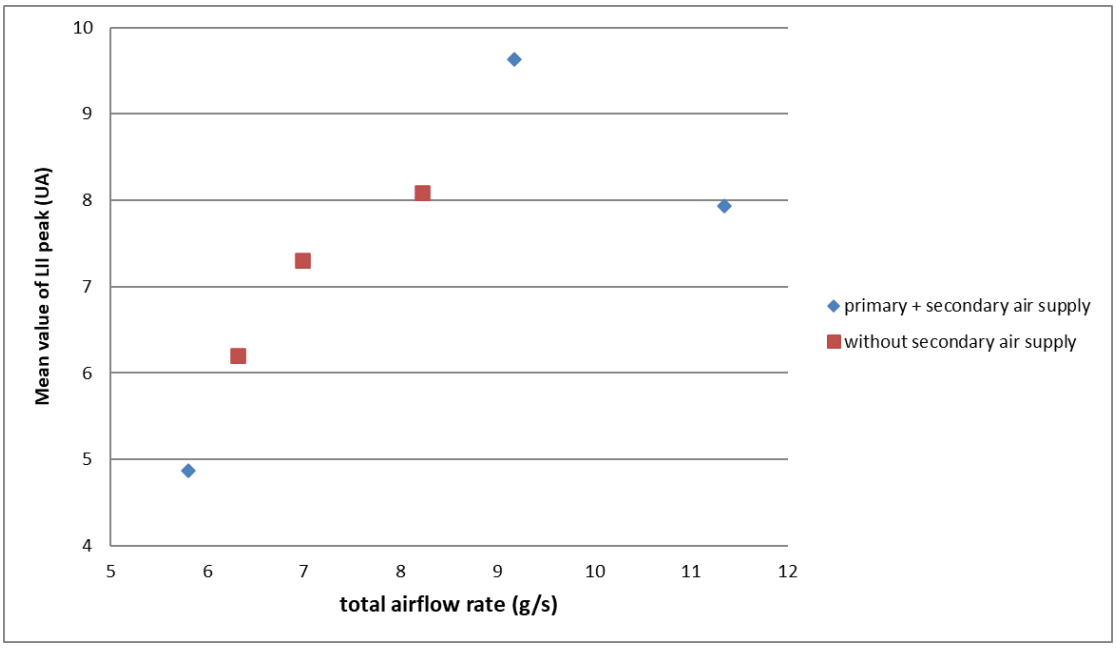

Figure 4-15 Evolution of the averages of the LII peaks as a function of the total airflow rate

4.4.2 LII measurement in the flame

As introduced in Chapter 3, the experimental setup was designed for direct observation of the LII signal in the combustion chamber with an ICCD came.

- **Experimental parameters**

The excitation conditions remain the same (200 mJ/pulse fixed at the laser output at 532nm). The excitation area in the furnace is chosen to maximize the

detected signal. The excitation area is not concentrated on the furnace due to the inhomogeneity and instability of the flame caused by the air inlet and fuel supply.

Figure 4-16 shows the configuration of the backward-LII. The beam reaches a fixed position that is not central to the burner plate but is perpendicular to the burner plate. Detection is undertaken by an ICCD camera fixed at a certain angle. The camera is equipped with a 700 nm high-pass filter (the quantum efficiency of the camera starts to drop from 800 nm) and an objective. The focal length and the aperture of the lens diaphragm are fixed to once again maximize the signal.

The incandescence signal is imaged by the camera. The intensifier amplifies (from 1 to 240, here set at 100) the photons received during its opening. Then the photons are transmitted to the CDD detector of 512x512 pixels.

With the camera pulser connected to the Q-Switch Out output of the laser, the opening of the CCD camera door is synchronized to the laser pulse to collect the LII signal. The setting of this opening is chosen to maximize the received signal while avoiding the pulse itself and the diffusion phenomena. An opening delay (gate delay) of 190 ns which corresponds to the QSwitch output delay added to the transmission delay of the electrical signal, to the duration of the laser pulse itself, and an estimate of the duration of the diffusion effects) and an opening time (or exposure) of 200ns.

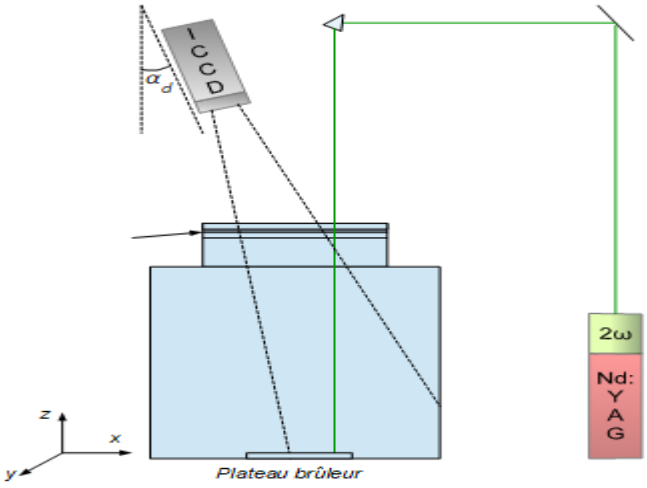

Figure 4-16 Backward LII assembly (choice and set of geometric parameters)

- **Experimental protocol**

The experimental protocol is the following. To homogenize the information with that received in the LII measurements in the chimney configuration, the image data accumulation is 512 frames at 10 Hz, i.e. approximately one minute. Indeed, the instability and inhomogeneity of the flame impose a long integration time. Also, the duration of the measurements may vary.

All tests were performed with primary and secondary air supply, the total air flow rates constituted the main experimental variables. The data obtained are 512x512 matrices (Figure 4-17) which are reduced to a "region of interest" drawn around the incandescence trace (Figure 4-18).

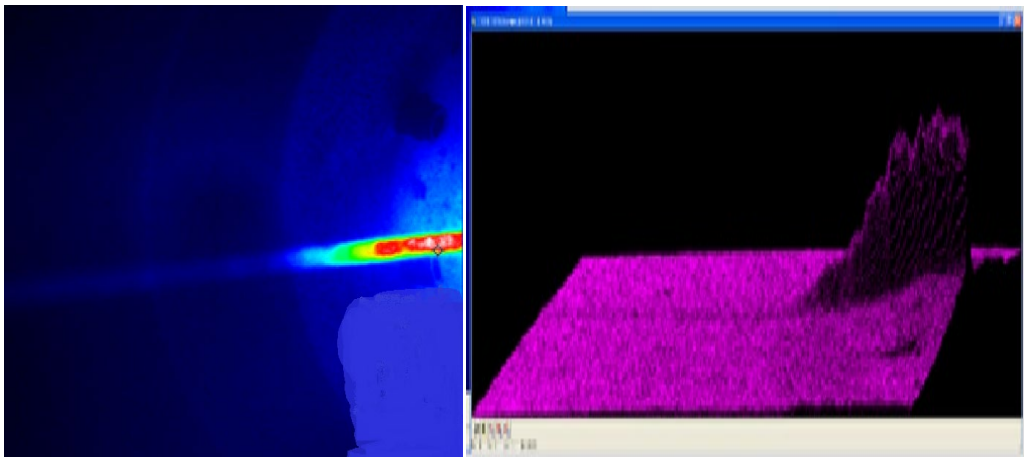

(A) **(B)**

Figure 4-17 (A) LII trace and (B) its graphic representation in 3D

To find the profile, the signal is summed transversely in this region. The compiled results are therefore the transverse profiles on the selected region of interest (Figure 4-18).

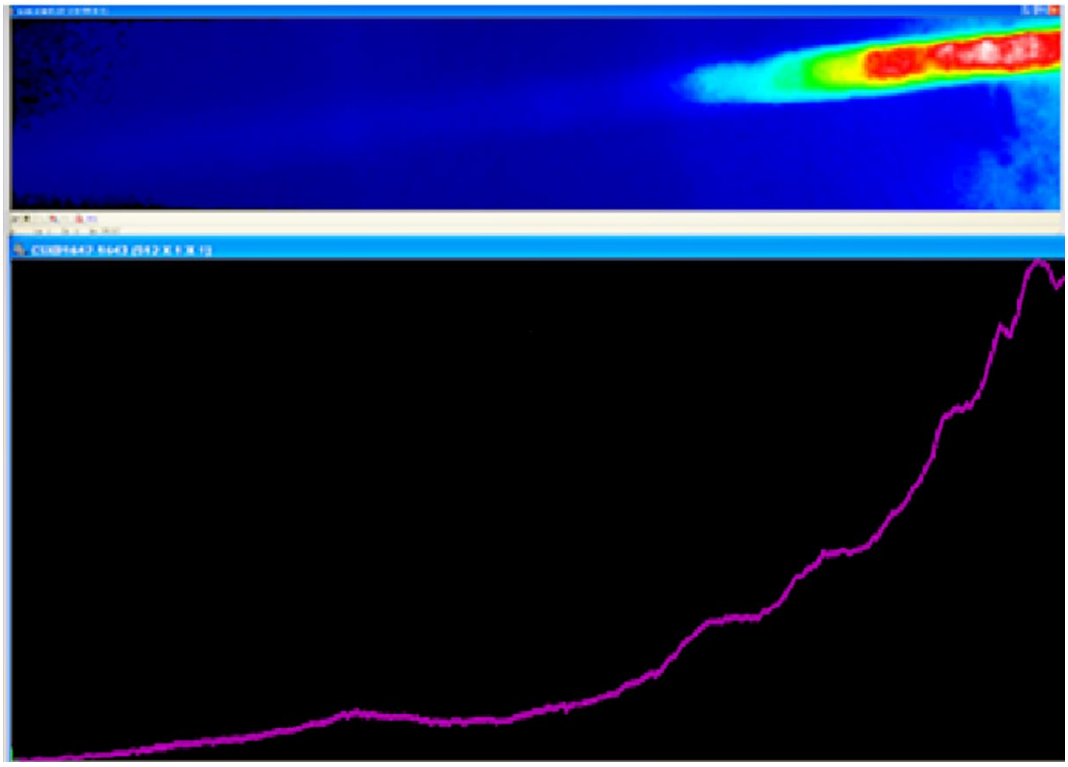

Figure 4-18 Region of interest with LII signal (at the top) and transverse profile of the LII signal (pink color) (at the bottom)

From this experimental protocol, only a qualitative analysis is possible. The signals can be averaged to observe the influence trends of the air injection variation. There is a tendency for the signal to increase with the increase in the incoming airflow. It was also found the strongest LII signal near the burner plate, and the LII signal decreased with increasing distance from the burner plate.

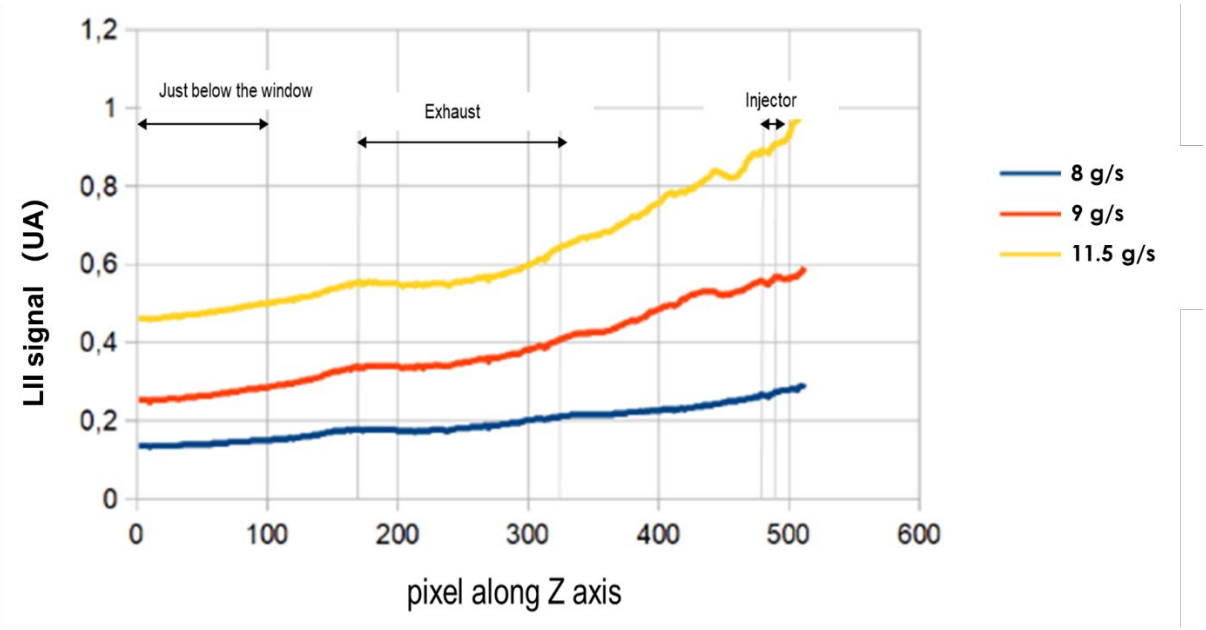

Figure 4-19 Means of the transverse profiles of the measurements according to air injection conditions

At the injector point of secondary air, no strong decrease of LII signal is clearly observable. The increase of LII signal with an increase of total air flow rate could be due to an increase of flame temperature giving more soot.

As there is no evidence of important post-combustion of soot by secondary air, it was plan to measure in the future the temperature by a thermocouple inside the boiler. The best solution is to map the temperature inside the boiler.

For future work, it would be interesting to analyze the LII signals obtained in a combustion chamber in the "without secondary air" configuration, to confirm the marked decrease of the LII signal in the chimney. Finally, it would be necessary to increase the measurement time per flow step and integrate the pellet feed cycle as a factor marking the variations in laser induced incandescence peaks.

4.4.3 Absolute soot volume fraction LII measurement

The one-color laser measurement method described above can only qualitatively compare the soot volume fraction, but cannot do quantitative analysis. To measure the absolute soot volume fraction using the LII method, the "2-colour

LII" configuration described in section 3.3.6 was developed and the formula derivation process and results obtained were presented.

- **The equation of soot volume fraction**

Laser-induced incandescence is a technique that relies on high-power lasers to heat soot particles to very high temperatures characterized by blackbody emission. According to Equation 3-20, the soot volume fraction can be obtained:

$$f_v = \frac{S_{LII}}{\Omega \times \beta} \times \left[\exp\left(\frac{hc}{\lambda k_B T}\right) - 1\right] \times \frac{\lambda^6}{12\pi hc^2 E(m)\Delta\lambda \times V_m} \quad \#\text{Equation } 4-9$$

Here V_m can be achieved with $V_m = l_{window} \times \frac{\pi \Phi_{laser}^2}{4}$. The l_{window} equals to 20 mm. The diameter of laser Φ_{laser} of the 532nm excitation laser beam with a top-hat profile is 5mm.

$E(m)$ is the function of the soot refractive index. The function of the soot refractive index is not constant with the wavelength range and strongly dependent on the maturity of the soot particles [4, 5]. In our work, a mean value of $E(m)$ equal to 0.35 for mature soot is used for both the 750 nm and 850 nm[131].

In Chapter 3, it was found the equation 3-22 for calculating the soot temperature and got the Ω (solid angle) and β (detection efficiency) for two sets of different wavelengths through the calibration method.

- **Soot temperature**

To explain how calculate the temperature of the soot using the two-color temperature method, here is a brief review of the experimental setup that used for the measurement of the LII signal. A configuration similar to one-color LII was used to measure the qualitative soot volume fraction, but the difference is that the LII signal was simultaneously measured in two different wavelengths using two bandpass filter blocks centered at 750nm and 850nm, and two identical photomultipliers (figure 4-20).

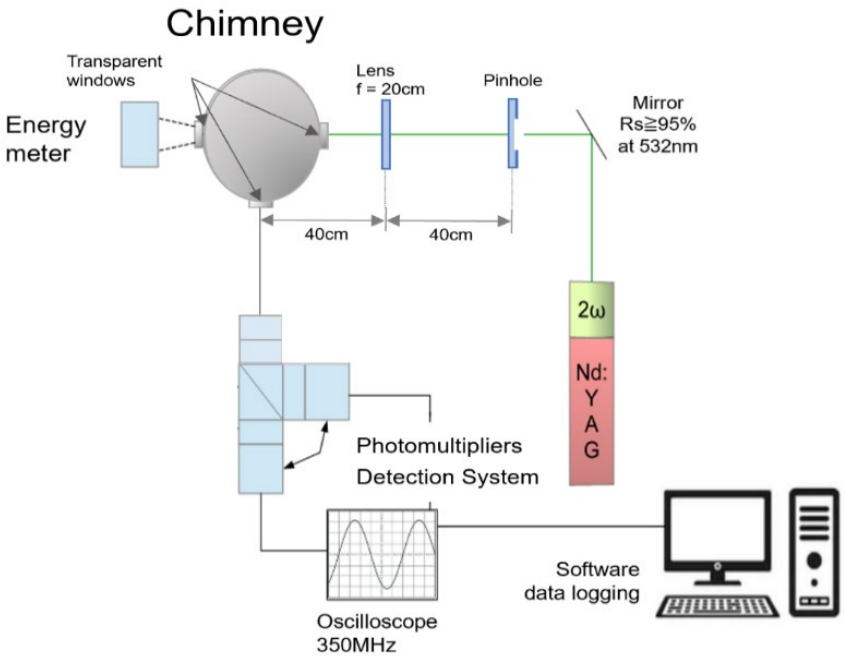

Figure 4-20 Configuration of two colors LII in the chimney

Using equations 3-22 and two LII signals of different wavelengths to deduce a formula for calculating the soot temperature (here the variation of the E(m) function is not taken into account):

$$T = \frac{-\frac{hc}{k_B}\left(\frac{1}{\lambda_1} - \frac{1}{\lambda_2}\right)}{\ln\left(\frac{S_{LII}(\lambda_1)}{S_{LII}(\lambda_2)}\frac{{\lambda_1}^6}{{\lambda_2}^6} \times \frac{(\Omega \times \beta)_{\lambda_2}}{(\Omega \times \beta)_{\lambda_1}}\right)} \qquad \text{Equation } 4-10$$

Figure 4-21 shows the decay of the LII signal during the 30 minutes test under the condition of wood pellets burning with maximum primary airflow. It was found that the decay time is really reproducible. This shows that the particle diameters are stable during this test.

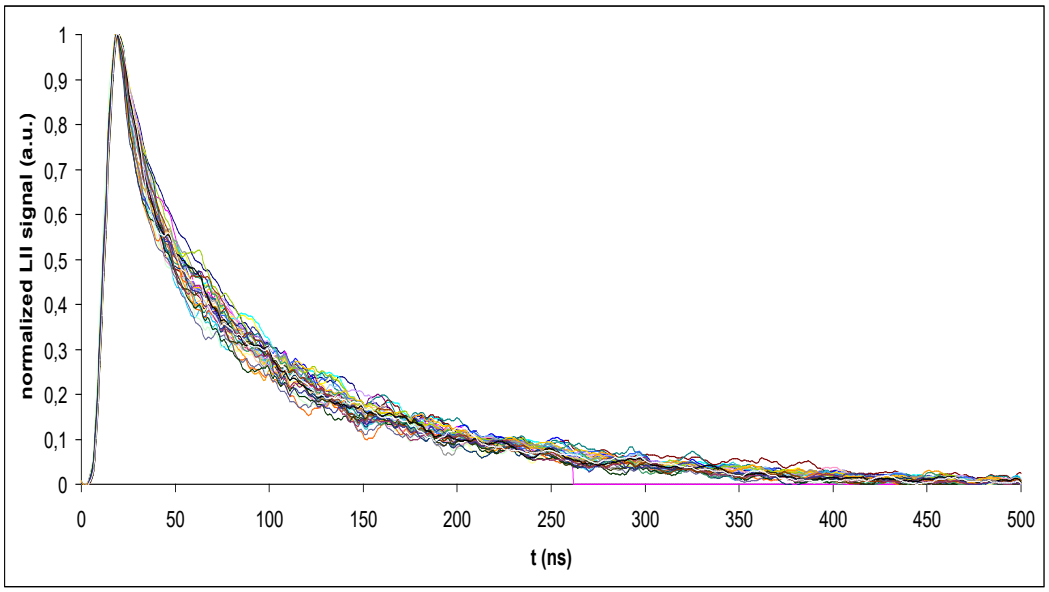

Figure 4-21 LII decays for wood pellet. 30 traces over 30 minutes (each trace being recorded during one minute)

Figure 4-22 shows the evolution of the soot temperature over 90 minutes, and each point in the figure is the average temperature of the soot temperature over one minute. It was found that the temperature of the soot varies with time without regularity. Most of the time the soot temperature is between 1150 K-1350 K, only a few points exceed 1350K, and the highest is 1536K. The relative temperature variation ($\Delta T/\overline{T}$) is around 30%. But in fact, for each point in this figure, the soot volume fraction is calculated.

The sublimation temperature is around 4000 K at atmospheric pressure. From Figure 4-22 we can see that in our example the peak temperature is around 1300 K. Therefore sublimation is not activated during laser heating.

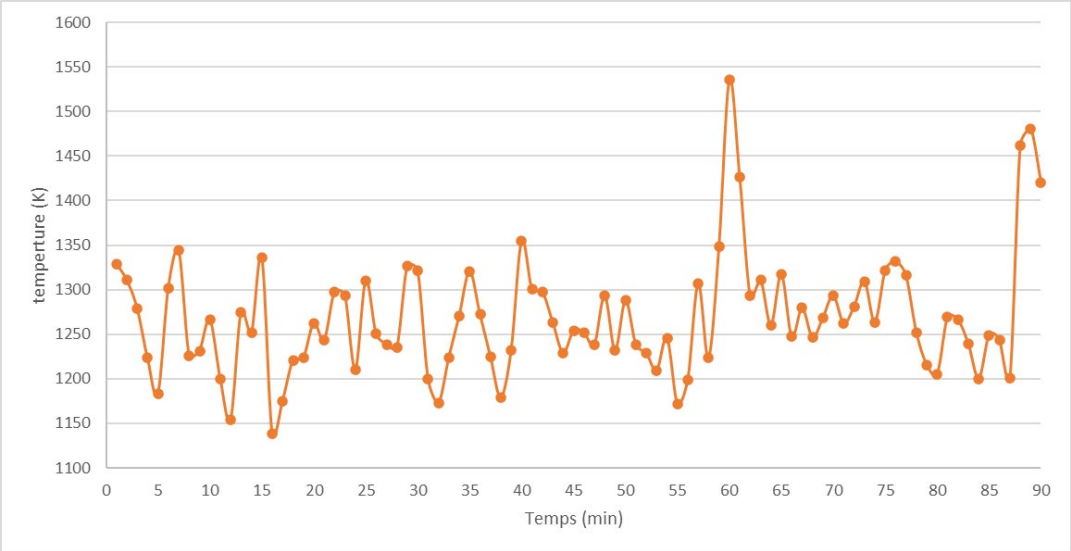

Figure 4-22 Evolution of soot temperature over 90 minutes

- **The soot volume fraction of wood pellets combustion**

The absolute soot volume fraction can be calculated using equation 4-9 and equation 4-10, the collection solid angle Ω and transmission efficiency β obtained earlier.

Figure 4-23 shows the evolution of soot volume fraction in the chimney as a function of the primary airflow rate in the condition without secondary air supply. The volume fraction of soot decreases significantly with the increase of the primary airflow rate. The soot volume fraction at the minimum airflow rate (4.7 g/s) is 10,000 times the soot volume fraction at the maximum airflow rate (7.5 g/s). Even if the primary airflow rate is reduced from 7.5 g/s to 7 g/s, the soot volume fraction increases significantly. This can be explained by the fact that the lower primary airflow rate reduces the flame temperature and thus significantly increases the soot emissions.

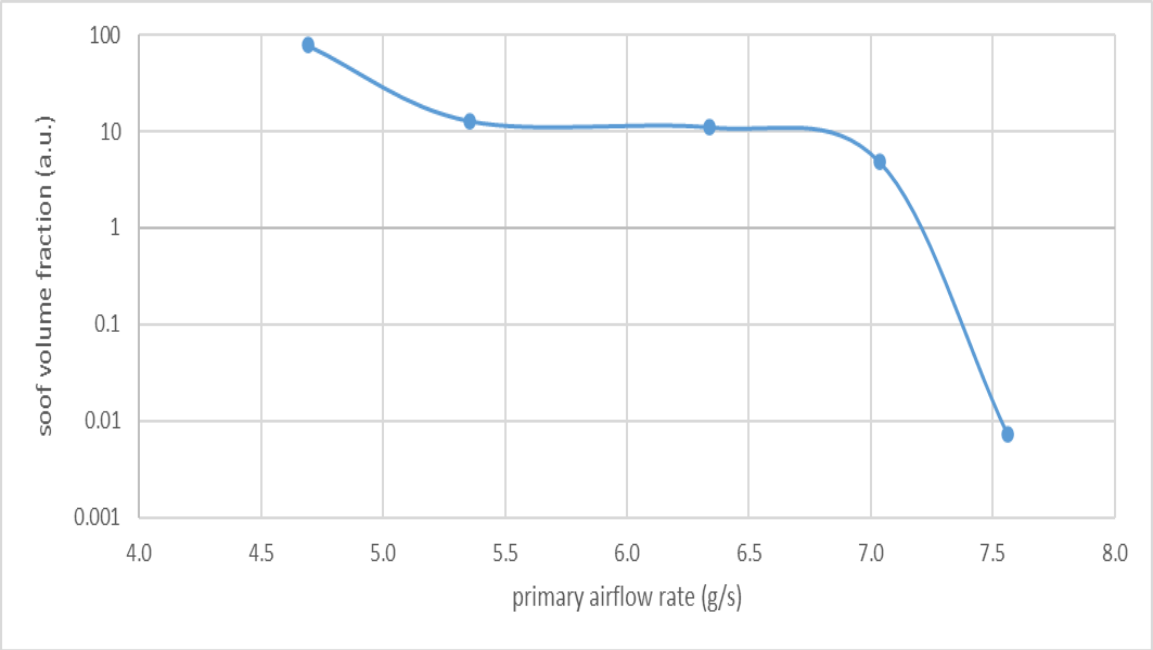

Figure 4-23 Evolution of soot volume fraction as a function of the primary airflow rate (corrected to 10% O_2)

The soot volume fraction was measured continuously for 90 minutes with maximum primary airflow and no secondary air supply, and the experiment was repeated on different days. Figure 4-24 shows two different test results. It was found that the soot volume fraction was still unstable at the maximum airflow rate. No matter the soot volume fraction of test 1 or test 2 showed a strong variation and no rules at all. For the test 1, the maximum value of the soot volume fraction is 729ppb, the minimum value is only 48ppb, and the maximum value is 15 times of the minimum value. For test 2, the maximum value of the soot volume fraction is 1287ppb, the minimum value is 55, and the maximum value is 23 times the minimum value. This instability in the soot volume fraction may be related to the turbulence of the flame which is observed in the boiler (cf. Figure 3-19)

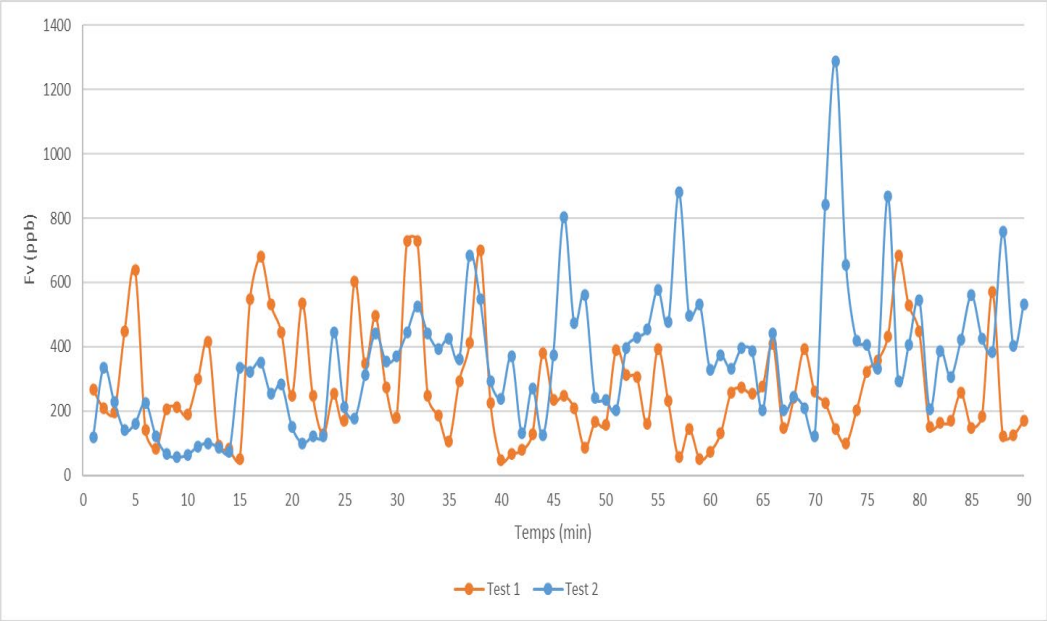

Figure 4-24 Evolution of soot volume fraction within 90 minutes at the maximum air flow rate (corrected to 10% O_2)

Figure 4-25 shows the soot emission factors measured on different tests under the condition of maximum airflow rate and no secondary air. It was found that the values measured on the four different test days are different. However, the data of the four measurements are within a certain range and there is no particularly large gap, which shows that the average value obtained by multiple measurements can describe the approximate range of the boiler soot volume fraction. The error bars representing the standard deviation are large. This again demonstrates the instability of the measured soot volume fraction.

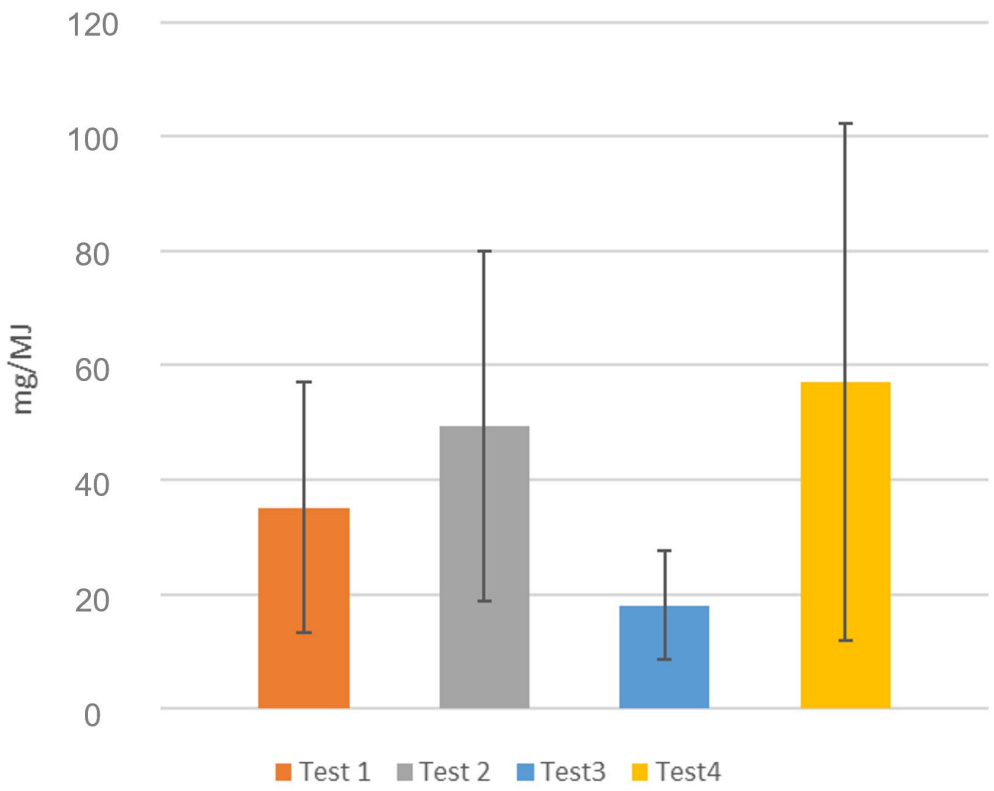

Figure 4-25 Soot emission factors of wood pellets (corrected to 10% O_2)

Table 4-5 shows the comparisons with emission factors for wood pellets from other studies. We found that the results were similar but varied across studies. This demonstrates the high variability of measurements, as observed in this study.

Table 4-5 Summary of emission factors found in the literature for wood pellet

Pellets boiler	KWB(this thesis)	Boman	Ozgen	Win	Lamberg
Power(kW)	20	5	25	22	25
CO(mg/MJ)	48	130	350	15	79
Particulates(mg/MJ)	35	16	61	0.5	20

4.4.4 Measurement of soot diameter distribution by SMPS method

Figure 4-26 compares the particle size distribution with and without secondary air supply. The test is carried out under the condition of maximum air flow rate. The results showed that while the shape of the particle distribution did not change, both the total concentration of particles and the diameter of the most

numerous particles changed. Under the two air supply conditions, the shape of the particle distribution is approximately normal distribution. However, compared with the graph without the secondary air supply, the diameter of the maximum number of particles under the secondary air supply condition has changed from 60 nm to about 80 nm. This is consistent with the results obtained by one color LII analysis of decay time.

The total number of particles can be obtained by integrating the distribution over all diameters. This is represented in figure 4-26 by the area under each curve. Under the condition of secondary air supply, the total number of particulate matters is smaller than that without secondary air supply.

It is known that for operating conditions in boilers, the particles most present in the flue gases are ashes and they have diameters between 50-90 nm [144]. If the majority of the particles were soot, an increase in their number would result in an increase in their size due to the agglomeration process. The particles present in the smoke from this installation seem to be mainly ash.

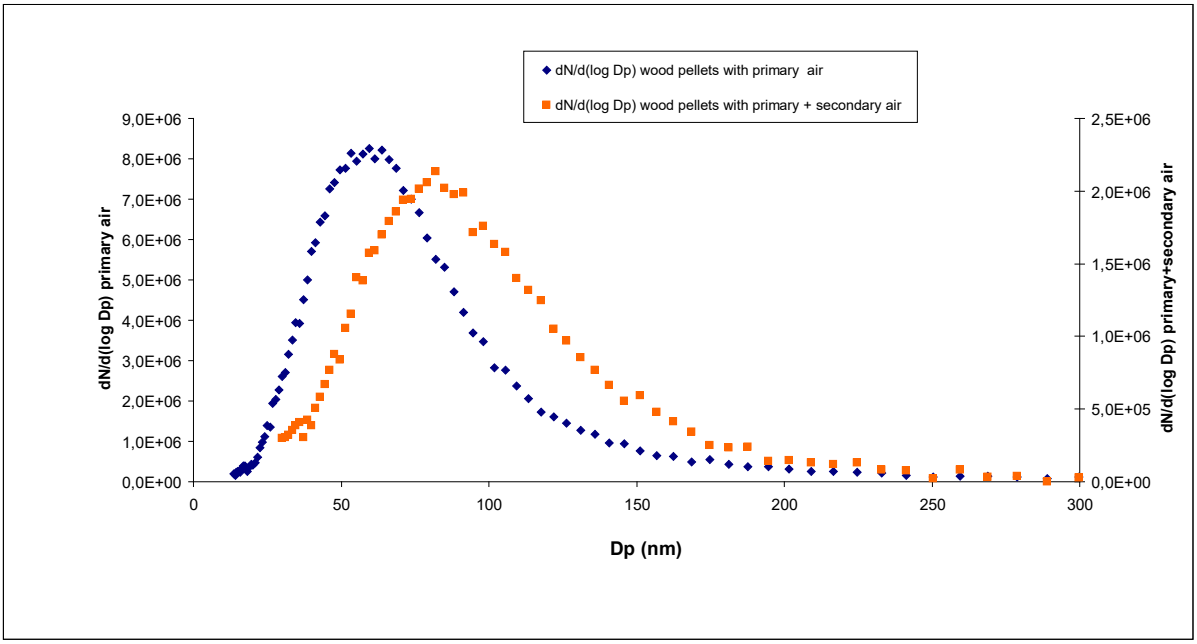

Figure 4-26 Particle diameter distribution curves for the different secondary air supply conditions

Figure 4-27 shows the particle size distribution in the range of 10-420 nm. Both curves are normal distribution. The biggest particle size is about 60 nm in the

condition with only primary air supply but increases to about 80 nm with secondary air supply. The area enclosed by the curve and the X-axis can represent the total number of particles. By comparing the areas of the two curves, it can be seen that the total number of particles is more under the condition of with only primary air supply. The reason for this result may be due to the dilution effect of the secondary air. As mentioned before, the injected secondary air is too cold to achieve post combustion. This inference can also be confirmed by the larger particle diameter under the secondary air condition. Particle diameters should be smaller if the secondary air causes post combustion.

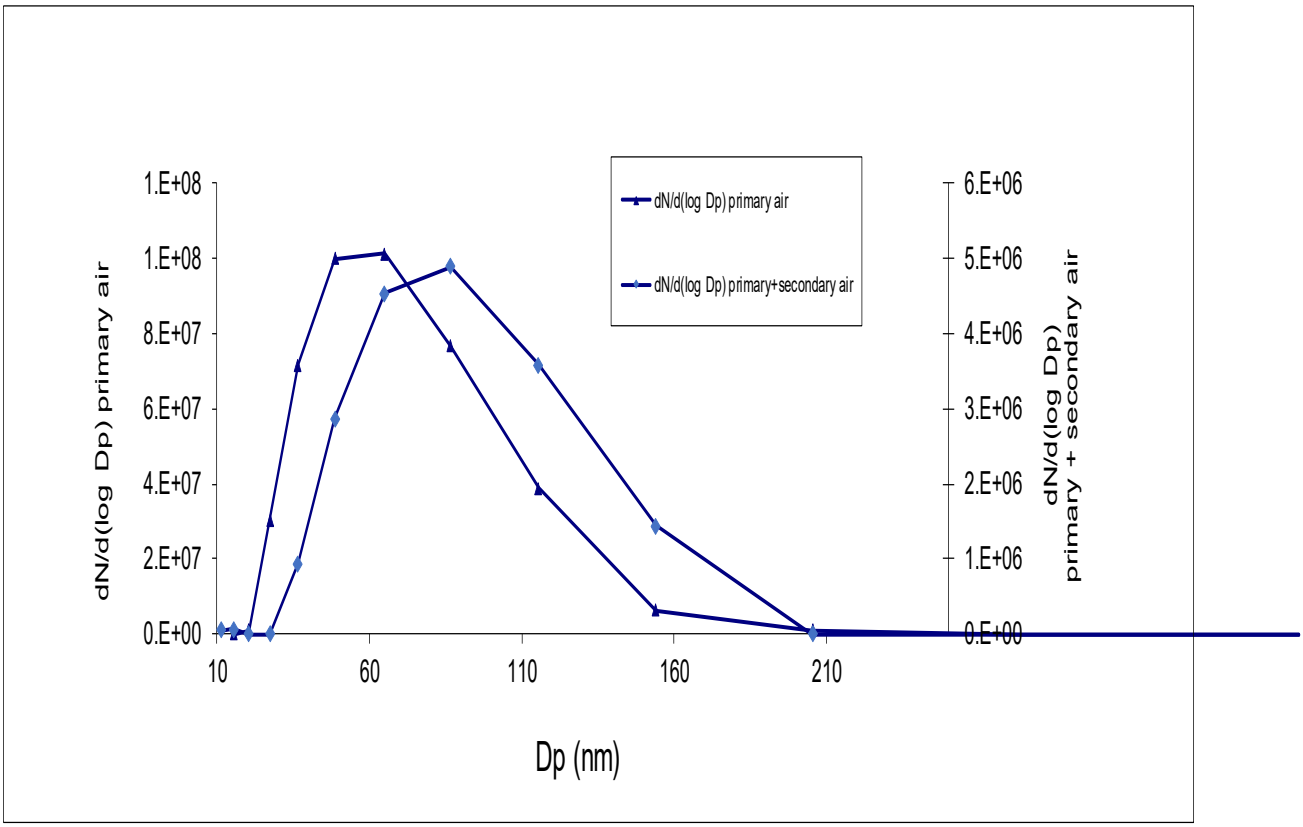

Figure 4-27 Particle diameter distribution curves for nanoparticle diameter

4.5 Chapter summary

For gaseous pollutant emissions, first the nominal performance of the boiler was studied. In comparing the pollution emissions inside the chimney in the ignition phase, steady state and extinguishing phase, it was found that the THC

emission in the steady state is the lowest, but no similar conclusions have been drawn for CO. It may be because CO can be produced under both lean and eutrophic combustion. During the combustion of biomass, CO may be released directly as a volatile compound or form intermediates in heterogeneous reactions involving char oxidation or homogeneous reactions in the gas phase. Next, the steady-state flue gas temperature (at the exit of the boiler) and gaseous pollutant emissions under the nominal conditions of the boiler were analyzed.

Now, regarding the effect of secondary air on the emission of gaseous pollutants with the maximum total air flow rate, it was found that under the condition of with secondary air supply, the mole fractions of CO and THC emissions both in the flame and in the chimney increased because the equivalence ratio (C/O) is higher meaning an incomplete combustion.

Regarding the effect of primary air flow rate on gaseous pollutant emissions, increasing primary air flow rate reduced the measured CO and THC mole fractions in the flame, but no significant correlation was observed for final CO and THC emissions in the chimney. This may be related to high air dilution for the gaseous emissions in the chimney.

For particulate matter emissions, a qualitative analysis is first carried out using a one-color LII method. It was found that the decay time of the signal was significantly longer with the secondary air present, indicating a larger particle size due to a more incomplete combustion because of a lower primary air flow. In addition, the peak of the LII signal exhibits instability, and the greatest instability is observed when the primary air flow rate is lowest, which indicates that the soot volume fraction fluctuates with time.

Second, the particulate matter emissions from the flames with backward LII were measured. It was found the strongest LII signal near the burner plate and the LII signal decreased with distance from the burner plate, indicating the highest soot concentration near the burner plate. At the point of injection of the secondary air, no strong drop in the LII signal was clearly observed.

Finally, the absolute volume fraction of soot was measure with a two-color LII method. It was found that under the condition of maximum primary air flow rate and no secondary air supply, the decay time of the LII signal is stable, which indicates that the soot size tends to be stable when the boiler enters a steady state. But the volume fraction of soot fluctuates irregularly with time, which may be related to the flame's turbulence which could observe directly by the transparent

window at the top of the boiler. Reducing the primary air flow rate cause the soot volume fraction to rise sharply.

It was also observed similar conclusions when using SMPS to observe the particle size distribution of soot. The size of particulate matter under the condition of secondary air supply is larger, but the overall number of particulate matters is lower. So, no post-combustion of soot could be highlighted due to injection of secondary air.

Chapter 5

Conclusions and Perspectives

Conclusions

The purpose of this PhD work is to study the effect of different operating parameters of a domestic pellet boiler on pollutant emissions for gaseous (CO, CO2 and TCH by commercial analyzers) and particulate emissions by Laser Induced Incandescence. To study the effect of several operating parameters on pollution emissions, the boiler used was modified:

- to allow manual control of the total air intake,

- to manually block the injection of secondary air,

- to take benefit of transparent windows for optical detection in the flame and in the chimney.

For gaseous pollutant emissions, the analysis of the results in chimney showed that when comparing the pollutant emissions in the ignition phase, steady state and extinguishment phase, it was found the lowest THC emissions in the steady state, but no similar conclusions were drawn for CO.

Reduction of the primary air flow rate increased the CO and THC mole fractions in the flame, but no significant correlation was observed for final CO and THC emissions. This may be related to high air dilution for the gaseous emissions in the chimney by the secondary air.

The mole fractions of CO and THC emissions in the flame and chimney were higher with the secondary air supply. This may be due to the fact that the cold secondary air reduce the temperature in the combustion chamber. There is no effective post combustion to reduce pollutant emissions. The primary air and the secondary air share an intake pipe. When secondary air is present, the primary airflow rate is lower although the total airflow rate into the boiler is higher. Therefore, the equivalence ratio (C/O) leads to incomplete combustion during the initial stages of combustion.

For particulate matter emissions, the analysis of the experimental results shows that the soot volume fraction in the boiler exhibits a strong instability, which may be related to the turbulence of the flame observed in the boiler. In contrast, the soot particle size tends to stabilize when the boiler enters steady state. The greatest soot volume fraction instability was observed at the lowest primary air flow rate and decreasing primary air flow rate resulted in a sharp rise in soot volume fraction. At the injection point of the secondary air, no strong drop in the LII signal is clearly observed, i.e. there is no evidence that the soot volume fraction

decreases here. However, the decay time of the LII signal and the SMPS results corroborate each other, showing that the average particle size is larger in the presence of secondary air. SMPS results also indicated that the boiler's total particulate matter emissions were reduced with secondary air. This may be related to high air dilution in the chimney with the presence of secondary air. This one could have also an influence on the combustion.

Perspectives

Some topics addressed in this work remain to be explored. The first is about the impact of secondary air on pollutant emissions. Due to constraints in this work, the secondary air was not preheated. Air is injected directly into the combustion chamber and there is no better designed post-combustion space. In the next work, it should try to to modify the secondary air injection equipment and boiler, so that the injection of preheated secondary air can be achieved to improve the efficiency of post-combustion. In addition, the restriction that the primary air and secondary air share one intake pipe should be modified so that the flow rates of primary air and secondary air can be controlled separately. It is then convenient to study the influence of different parameters on combustion and pollutant emissions.

Regarding the choice of biomass pellets, according to the original idea, it should compare and analyze the experimental results of wood pellets and black pellets. However, due to the limited planning, there is only obtained a shot of experimental data on the combustion of black pellets. First of all, it will be necessary to analyze black pellets to know diameter, length, density, LHV, moisture and chemical composition. Due to the lack of replicated experiments on the combustion of black pellets, the analysis of black pellets was put in Appendices 1 and 2. Reasonable suggestions for the use of biomass fuels could be given by comparing the two biomass materials.

Regarding the modification of the boiler, temperature sensors should be installed at key points inside the combustion chamber. The real-time data of the combustion chamber temperature can be used to assist in the analysis of the impact of the primary and secondary air on the combustion process and pollutant emissions.Another modification will be to measure the pellet mass flow rate.

Finally, to visualize them better, the combustion of biomass will be modeled later. First, individual pellet combustion will be modeled to understand the physics of the pellet combustion process, in particular mass and heat transfers within the

pellet, but also a pyrolysis scheme will be used to reproduce the observed phenomena.

References

[1] Enerdata,“https://yearbook.enerdata.net/total-energy/world consumption-statistics.html,” 2020.

[2] R. W. Bentley, “Global oil and gas depletion: An overview,” *Energy Policy*, vol. 30, no. 3, pp. 189–205, 2002, doi: 10.1016/S0301-4215(01)00144-6.

[3] O. Ellabban, H. Abu-rub, and F. Blaabjerg, “Renewable energy resources : Current status , future prospects and their enabling technology,” *Renew. Sustain. Energy Rev.*, vol. 39, pp. 748–764, 2014, doi: 10.1016/j.rser.2014.07.113.

[4] OurWorldInData,“https://ourworldindata.org/renewable-energy,” *OurWorldInData*, 2020. .

[5] K. Stephen, L. Kusum, and S. T. Coelho, “Traditional biomass energy: Improving its use and moving to modern energy use,” *Renew. energies*, pp. 258–289, 2012.

[6] P. McKendry, “Energy production from biomass (part 1): Overview of biomass,” *Bioresour. Technol.*, vol. 83, no. 1, pp. 37–46, 2002, doi: 10.1016/S0960-8524(01)00118-3.

[7] European Commission COM (97), “Energy for the Future: Renewable Energy Sources – White Paper for a Community Strategy and Action Plan.,” *Commun. from Comm. 599*, 1997.

[8] R. Saidur, E. A. Abdelaziz, A. Demirbas, M. S. Hossain, and S. Mekhilef, “A review on biomass as a fuel for boilers,” *Renew. Sustain. Energy Rev.*, vol. 15, no. 5, pp. 2262–2289, 2011, doi: 10.1016/j.rser.2011.02.015.

[9] A. C. Caputo, M. Palumbo, P. M. Pelagagge, and F. Scacchia, “Economics of biomass energy utilization in combustion and gasification plants: Effects of logistic variables,” *Biomass and Bioenergy*, vol. 28, no. 1, pp. 35–51, 2005, doi: 10.1016/j.biombioe.2004.04.009.

[10] P. Mckendry, “Energy production from biomass (part 2): conversion technologies,” *Bioresour. Technol.*, vol. 83, pp. 47–54, 2002.

[11] V. S. Sikarwar, M. Zhao, P. S. Fennell, N. Shah, and E. J. Anthony, “Progress in biofuel production from gasificatio,” vol. 61, pp. 189–248, 2017, doi: 10.1016/j.pecs.2017.04.001.

[12] A. Molino, V. Larocca, S. Chianese, and D. Musmarra, “Biofuels Production by Biomass Gasification : A Review,” *Energies*, vol. 11, no. 4, pp. 1–31, 2018, doi: 10.3390/en11040811.

[13] S. Pourkarimi, A. Hallajisani, A. Alizadehdakhel, and A. Nouralishahi, “Biofuel production through micro-and macroalgae pyrolysis–A review of

pyrolysis methods and process parameters," *J. Anal. Appl. Pyrolysis*, vol. 142, no. 104559, 2019, doi: 10.1016/j.jaap.2019.04.015.

[14] A. Demirbas, "Yields of hydrogen-rich gaseous products via pyrolysis from selected biomass samples," vol. 80, 2001.

[15] P. Adams, T. Bridgwater, A. Ross, and I. Watson, *Biomass Conversion Technologies*. Elsevier Inc., 2018.

[16] R. A. Lee and J. Lavoie, "From first- to third-generation biofuels : Challenges of producing a commodity from a biomass of increasing complexity," *Anim. Front.*, vol. 3, no. 2, pp. 6–11, 2013, doi: 10.2527/af.2013-0010.

[17] J. Porteiro, J. L. Míguez, E. Granada, and J. C. Moran, "Mathematical modelling of the combustion of a single wood particle," *Fuel Process. Technol.*, vol. 87, no. 2, pp. 169–175, 2006, doi: 10.1016/j.fuproc.2005.08.012.

[18] A. N. Hayhurst, "The kinetics of the pyrolysis or devolatilisation of sewage sludge and other solid fuels," *Combust. Flame*, vol. 160, no. 1, pp. 138–144, 2013, doi: 10.1016/j.combustflame.2012.09.003.

[19] G. T. Marangwanda, D. M. Madyira, and T. O. Babarinde, "Combustion models for biomass: A review," *Energy Reports*, vol. 6, pp. 664–672, 2020, doi: 10.1016/j.egyr.2019.11.135.

[20] D. Kühnemuth, F. Normann, K. Andersson, and F. Johnsson, "On the carbon monoxide formation in oxy-fuel combustion—Contribution by homogenous and heterogeneous reactions," *Int. J. Greenh. Gas Control*, vol. 25, pp. 33–41, 2014, doi: 10.1016/j.ijggc.2014.02.014.

[21] S. Feldmeier, M. Schwarz, E. Wopienka, and C. Pfeifer, "Categorization of small-scale biomass combustion appliances by characteristic numbers," *Renew. Energy*, vol. 163, pp. 2128–2136, 2021, doi: 10.1016/j.renene.2020.10.111.

[22] E. Vakkilainen, "Large-scale biomass combustion plants: an overview," *Biomass Combust. Sci. Technol. Eng.*, pp. 189–224, 2013, doi: 10.1533/9780857097439.3.189.

[23] I. Obernberger, "State-of-the-art of small-scale biomass combustion in boilers," *IEA Task 32 Bioenergy Work.*, pp. 10–16, 2011.

[24] M. Sami, K. Annamalai, and M. Wooldridge, "Co-firing of coal and biomass fuel blends," *Prog. Energy Combust. Sci.*, vol. 27, pp. 171–214, 2001, doi: 10.1016/S0360-1285(00)00020-4.

[25] R. Saidur, E. A. Abdelaziz, A. Demirbas, M. S. Hossain, and S. Mekhilef, "A review on biomass as a fuel for boilers," *Renew. Sustain. Energy Rev.*, vol. 15, no. 5, pp. 2262–2289, 2011, doi: 10.1016/j.rser.2011.02.015.

[26] T. Miranda, I. Montero, F. J. Sepúlveda, J. I. Arranz, C. V. Rojas, and

S. Nogales, “A Review of Pellets from Different Sources,” *Materials (Basel).*, pp. 1413–1427, 2015, doi: 10.3390/ma8041413.

[27] J. Sá, D. Curt, and M. Sanz, “A proposal for pellet production from residual woody biomass in the island of Majorca (Spain),” *AIMS Energy*, vol. 3, no. July, pp. 480–504, 2015, doi: 10.3439/energy.2015.3.480.

[28] R. Picchio, F. Latterini, R. Venanzi, and W. Stefanoni, “Pellet Production from Woody and Non-Woody Feedstocks : A Review on Biomass Quality Evaluation,” *Energies*, vol. 13, p. 2937, 2020.

[29] C. Whittaker and I. Shield, “Factors affecting wood, energy grass and straw pellet durability – A review,” *Renew. Sustain. Energy Rev.*, vol. 71, pp. 1–11, 2017, doi: 10.1016/j.rser.2016.12.119.

[30] B. Jun, H. Chang, S. Min, and D. Ha, “Effect of binders on the durability of wood pellets fabricated from Larix kaemferi C . and Liriodendron tulipifera L . sawdust,” *Renew. Energy*, vol. 62, pp. 18–23, 2014, doi: 10.1016/j.renene.2013.06.038.

[31] L. J. R. Nunes, J. C. O. Matias, and J. P. S. Catalão, “A review on torrefied biomass pellets as a sustainable alternative to coal in power generation,” *Renew. Sustain. Energy Rev.*, vol. 40, pp. 153–160, 2014, doi: 10.1016/j.rser.2014.07.181.

[32] Z. Liu, A. Quek, and R. Balasubramanian, “Preparation and characterization of fuel pellets from woody biomass , agro-residues and their corresponding hydrochars,” *Appl. Energy*, vol. 113, pp. 1315–1322, 2014, doi: 10.1016/j.apenergy.2013.08.087.

[33] S. Ren, H. Lei, L. Wang, Q. Bu, S. Chen, and J. Wu, “Thermal behaviour and kinetic study for woody biomass torrefaction and torrefied biomass pyrolysis by TGA,” *Biosyst. Eng.*, vol. 116, no. 4, pp. 420–426, 2013, doi: 10.1016/j.biosystemseng.2013.10.003.

[34] W. H. Chen and P. C. Kuo, “A study on torrefaction of various biomass materials and its impact on lignocellulosic structure simulated by a thermogravimetry,” *Energy*, vol. 35, no. 6, pp. 2580–2586, 2010, doi: 10.1016/j.energy.2010.02.054.

[35] D. Medic, M. Darr, B. Potter, and A. Shah, “Effect of torrefaction process parameters on biomass feedstock upgrading,” *Am. Soc. Agric. Biol. Eng. Annu.*, vol. 5, pp. 4277–4294, 2010, doi: 10.13031/2013.29898.

[36] W. Chen, S. Liu, T. Juang, C. Tsai, and Y. Zhuang, “Characterization of solid and liquid products from bamboo torrefaction,” *Appl. Energy*, vol. 160, pp. 829–835, 2015, doi: 10.1016/j.apenergy.2015.03.022.

[37] L. Wang, E. Barta-rajnai, Ø. Skreiberg, and R. Khalil, “Effect of torrefaction on physiochemical characteristics and grindability of stem wood ,

stump and bark," *Appl. Energy*, vol. 227, pp. 137–148, 2018, doi: 10.1016/j.apenergy.2017.07.024.

[38] L. Kumar, A. A. Koukoulas, S. Mani, and J. Satyavolu, "Integrating Torrefaction in the Wood Pellet Industry: A Critical Review," *Energy & Fuels*, vol. 31(1), pp. 37–54, 2017, doi: 10.1021/acs.energyfuels.6b02803.

[39] T. O. Olugbade, "Biomass Torrefaction for the Production of High-Grade Solid Biofuels : a Review," *BioEnergy Res.*, vol. 13, pp. 999–1015, 2020.

[40] A. K. Sarker, T. R., Nanda, S., Dalai, "A Review of Torrefaction Technology for Upgrading Lignocellulosic Biomass to Solid Biofuels," *BioEnergy Res.*, vol. 14, pp. 645–669, 2021.

[41] M. N. Cahyanti, T. Rama, K. C. Doddapaneni, and T. Kikas, "Bioresource Technology Biomass torrefaction : An overview on process parameters , economic and environmental aspects and recent advancements," *Bioresour. Technol.*, vol. 301, p. 122737, 2020, doi: 10.1016/j.biortech.2020.122737.

[42] A. Toptas, Y. Yildirim, G. Duman, and J. Yanik, "Bioresource Technology Combustion behavior of different kinds of torrefied biomass and their blends with lignite," *Bioresour. Technol.*, vol. 177, pp. 328–336, 2015, doi: 10.1016/j.biortech.2014.11.072.

[43] A. Pimchuai, A. Dutta, and P. Basu, "Torrefaction of Agriculture Residue To Enhance Combustible Properties," *Energy*, vol. 24, pp. 4638–4645, 2010, doi: 10.1021/ef901168f.

[44] P. Mcnamee, L. I. Darvell, J. M. Jones, and A. Williams, "The combustion characteristics of high-heating-rate chars from untreated and torrefied biomass fuels," *Biomass and Bioenergy*, vol. 82, pp. 63–72, 2015, doi: 10.1016/j.biombioe.2015.05.016.

[45] T. Botelho, M. Costa, and A. Magdziarz, "Evaluation of the combustion characteristics of raw and torrefied grape pomace in a thermogravimetric analyzer and in a drop tube furnace," *Fuel*, vol. 212, pp. 95–100, 2018, doi: 10.1016/j.fuel.2017.09.118.

[46] M. Janusz, A. Iluk, J. A. Lasek, and M. Kopczy, "Combustion properties of torrefied biomass obtained from flue gas-enhanced reactor," *Fuel*, vol. 119, pp. 362–368, 2017, doi: 10.1016/j.energy.2016.12.079.

[47] X. Ren, R. Sun, X. Meng, N. Vorobiev, M. Schiemann, and Y. A. Levendis, "Carbon, sulfur and nitrogen oxide emissions from combustion of pulverized raw and torrefied biomass," *Fuel*, vol. 188, pp. 310–323, 2017, doi: 10.1016/j.fuel.2016.10.017.

[48] J. A. Lasek, A. Iluk, and C. Processing, "The co-combustion of hard coal with raw and torrefied biomasses (willow (Salix viminalis), olive oil residue

and waste wood from furniture manufacturing)," *Energy*, pp. 1–10, 2017, doi: 10.1016/j.energy.2017.04.036.

[49] D. Jaffe, I. Bertschi, L. Jaeglé, and P. Novelli, "Long-range transport of Siberian biomass burning emissions and impact on surface ozone in western North America," *Geophys. Res. Lett.*, vol. 31, no. 16, pp. 6–9, 2004, doi: 10.1029/2004GL020093.

[50] J. P. Greenberg, P. R. Zimmerman, L. Heidt, and W. Pollock, "Hydrocarbon and Carbon Monoxide Emissions from Biomass Burning in Brazil," *J. Geophys. Res.*, vol. 89, pp. 1350–1354, 1984.

[51] X. LE Roux, "Nitrogen compound emission from biomass burning in tropical African savanna FOS/DECAFE 1991 experiment (Lamto, Ivory Coast)," *J. Atmos. Chem.*, vol. 22, pp. 175–193, 1991.

[52] A. Mukherjee and M. Agrawal, "World air particulate matter : sources , distribution and health effects," *Environ. Chem. Lett.*, vol. 15, pp. 283–309, 2017, doi: 10.1007/s10311-017-0611-9.

[53] M. Amann and M. Lutz, "The revision of the air quality legislation in the European Union related to ground-level ozone," *J. Hazard. Mater.*, vol. 78, pp. 1–3, 2000.

[54] D. Jaffe, I. Bertschi, L. Jaegle, and P. Novelli, "Long-range transport of Siberian biomass burning emissions and impact on surface ozone in western North America Long-range transport of Siberian biomass burning emissions and impact on surface ozone in western North America," vol. 31, 2004, doi: 10.1029/2004GL020093.

[55] E. D. Vicente, A. M. Vicente, and B. A. M. Bandowe, "Particulate phase emission of parent polycyclic aromatic hydrocarbons (PAHs) and their derivatives (alkyl-PAHs, oxygenated-PAHs, azaarenes and nitrated PAHs) from manually and automatically fired combustion appliances," *Air Qual. Atmos. Heal.*, vol. 9, pp. 653–668, 2016, doi: 10.1007/s11869-015-0364-1.

[56] A. Bari, G. Baumbach, J. Brodbeck, and M. Struschka, "Characterisation of particulates and carcinogenic polycyclic aromatic hydrocarbons in wintertime wood-fired heating in residential areas," *Atmos. Environ.*, vol. 45, no. 40, pp. 7627–7634, 2011, doi: 10.1016/j.atmosenv.2010.11.053.

[57] H. Yu, "Environmental carcinogenic polycyclic aromatic hydrocarbons: photochemistry and phototoxicity," *J. Environ. Sci. Heal.*, vol. 20, no. 2, pp. 149–183, 2002, doi: 10.1081/GNC-120016203.

[58] M. Kistler, C. Schmidl, E. Padouvas, and H. Giebl, "Odor , gaseous and PM 10 emissions from small scale combustion of wood types indigenous to Central Europe," *Atmos. Environ.*, vol. 51, pp. 86–93, 2012, doi:

10.1016/j.atmosenv.2012.01.044.

[59] N. W. Tame, B. Z. Dlugogorski, and E. M. Kennedy, "Formation of dioxins and furans during combustion of treated wood," *Prog. Energy Combust. Sci.*, vol. 33, no. 4, pp. 384–408, 2007, doi: 10.1016/j.pecs.2007.01.001.

[60] T. Zhang, J. Huang, S. Deng, and G. Yu, "In fl uence of pesticides contamination on the emission of PCDD / PCDF to the land from open burning of corn straws," *Environ. Pollut.*, vol. 159, no. 6, pp. 1744–1748, 2011, doi: 10.1016/j.envpol.2011.01.042.

[61] A. I. Calvo, L. A. C. Tarelho, C. A. Alves, M. Duarte, and T. Nunes, "Characterization of operating conditions of two residential wood combustion appliances," *Fuel Process. Technol.*, vol. 126, pp. 222–232, 2014, doi: 10.1016/j.fuproc.2014.05.001.

[62] S. Seddighi and F. Johnsson, "Carbon monoxide formation during oxy-fuel-fired fluidized bed combustion," vol. 27, no. 4, pp. 2275–2282, 2013, doi: 10.1021/ef3021393.

[63] M. B. Toftegaard, J. Brix, P. A. Jensen, P. Glarborg, and A. D. Jensen, "Oxy-fuel combustion of solid fuels," *Prog. Energy Combust. Sci.*, vol. 36, no. 5, pp. 581–625, 2010, doi: 10.1016/j.pecs.2010.02.001.

[64] P. Glarborg, A. D. Jensen, and J. E. Johnsson, "Fuel nitrogen conversion in solid fuel fired systems," *Prog. energy Combust. Sci.*, vol. 29, pp. 89–113, 2003, doi: 10.1016/S0360-1285(02)00031-X.

[65] T. Nussbaumer, "Combustion and Co-combustion of Biomass: Fundamentals, Technologies, and Primary Measures for Emission Reduction," *Energy and Fuels*, vol. 17, no. 6, pp. 1510–1521, 2003, doi: 10.1021/ef030031q.

[66] O. Karlström, M. Perander, N. Demartini, A. Brink, and M. Hupa, "Role of ash on the NO formation during char oxidation of biomass," *Fuel*, vol. 190, pp. 274–280, 2017, doi: 10.1016/j.fuel.2016.11.013.

[67] K. P. Shrestha, L. Seidel, T. Zeuch, and F. Mauss, "Kinetic Modeling of NOx Formation and Consumption during Methanol and Ethanol Oxidation," *Combust. Sci. Technol.*, vol. 191, no. 9, pp. 1627–1659, 2019, doi: 10.1080/00102202.2019.1606804.

[68] H. Liu, J. Chaney, J. Li, and C. Sun, "Control of NOx emissions of a domestic / small-scale biomass pellet boiler by air staging," *Fuel*, vol. 103, pp. 792–798, 2013, doi: 10.1016/j.fuel.2012.10.028.

[69] C. T. Bowman, "Control of combustion-generated nitrogen oxide emissions: Technology driven by regulation," *Symp. Combust.*, vol. 24, pp. 859–878, 1992, doi: 10.1016/s0082-0784(06)80104-9.

[70] X. Liu, Z. Luo, and C. Yu, "Conversion of char-N into NOx and N2O during combustion of biomass char," *Fuel*, vol. 242, pp. 389–397, 2019, doi:

10.1016/j.fuel.2019.01.061.

[71] E. G. Garijo, A. D. Jensen, and P. Glarborg, "Kinetic Study of NO Reduction over Biomass Char under Dynamic Conditions," *Energy and Fuels*, vol. 17, no. 6, pp. 1429–1436, 2003, doi: 10.1021/ef020276n.

[72] E. C. Zabetta, M. Hupa, and K. Saviharju, "Reducing NOx emissions using fuel staging, air staging, and selective noncatalytic reduction in synergy," *Ind. Eng. Chem. Res.*, vol. 44, no. 13, pp. 4552–4561, 2005, doi: 10.1021/ie050051a.

[73] M. Obaidullah, S. Bram, V. K. Verma, and J. De Ruyck, "A Review on Particle Emissions from Small Scale Biomass Combustion," *Int. J. Renew. energy Res.*, vol. 2, no. 1, pp. 147–159, 2012, doi: 10.20508/ijrer.15633.

[74] H. M. M. Kamal M S, Razzak S A, "Catalytic oxidation of volatile organic compounds (VOCs) - A review," *Atmos. Environ.*, vol. 140, pp. 117–134, 2016.

[75] J. Cheng, Y. Zhang, T. Wang, H. Xu, P. Norris, and W. Pan, "Emission of volatile organic compounds (VOCs) during coal combustion at di ff erent heating rates," *Fuel*, vol. 225, pp. 554–562, 2018, doi: 10.1016/j.fuel.2018.03.185.

[76] C. Pham, Y. Boongla, T. Nghiem, and H. Le, "Emission Characteristics of Polycyclic Aromatic Hydrocarbons and Nitro-Polycyclic Aromatic Hydrocarbons from Open Burning of Rice Straw in the North of Vietnam," *Int. J. Environ. Res. Public Health*, vol. 16, p. 2343, 2019.

[77] L. T. Fleming, P. Lin, J. M. Roberts, and V. Selimovic, "Molecular composition and photochemical lifetimes of brown carbon chromophores in biomass burning organic aerosol," *Atmos. Chem. Phys.*, vol. 20, pp. 1105–1129, 2020, doi: 10.5194/acp-20-1105-2020.

[78] J. C. Chiu, Y. H. Shen, H. W. Li, S. S. Chang, L. C. Wang, and P. Guo, "Toxic / Hazardous Substances and Environmental Engineering Effect of biomass open burning on particulate matter and polycyclic aromatic hydrocarbon concentration levels and PAH dry deposition in ambient air Effect of biomass open burning on particulate ma," *J. Environ. Sci. Heal. Part A*, vol. 46, no. 2, pp. 188–197, 2011, doi: 10.1080/10934529.2011.532438.

[79] H. Zhang, X. Zhang, Y. Wang, P. Bai, and K. Hayakawa, "Characteristics and Influencing Factors of Polycyclic Aromatic Hydrocarbons Emitted from Open Burning and Stove Burning of Biomass : A Brief Review," *Int. J. Environ. Res. Public Health*, vol. 19, no. 7, p. 3944, 2022, doi: 10.3390/ ijerph19073944.

[80] C. Wang, Y. Wang, and H. M. S. K. Herath, "Organic Geochemistry Polycyclic aromatic hydrocarbons (PAHs) in biochar – Their formation , occurrence and analysis : A review," *Org. Geochem.*, vol. 114, pp. 1–11, 2017, doi:

10.1016/j.orggeochem.2017.09.001.

[81] N. Guha *et al.*, "Outdoor Particulate Matter Exposure and Lung Cancer : A Systematic Review and Meta-Analysis," *Environ. Health Perspect.*, pp. 3–10, 2014, doi: 10.1289/ehp/1408092.

[82] G. Cadelis, R. Tourres, and J. Molinie, "Short-term effects of the particulate pollutants contained in Saharan dust on the visits of children to the emergency department due to asthmatic conditions in Guadeloupe (French archipelago of the Caribbean)," *PLoS One*, vol. 9, no. 3, p. e91136, 2014, doi: 10.1371/journal.pone.0091136.

[83] *Climate Change 2013: The Physical Science Basis : Working Group I contribution to the Fifth assessment report of the Intergovernmental Panel on Climate Change*. 2014.

[84] J. E. Penner, L. Xu, and M. Wang, "Satellite methods underestimate indirect climate forcing by aerosols," *Proc. Natl. Acad. Sci. U. S. A.*, vol. 108, no. 33, pp. 13404–13408, 2011, doi: 10.1073/pnas.1018526108.

[85] E. J. T. Levin, G. R. McMeeking, C. M. Carrico, L. E. Mack, and S. M. Kreidenweis, "Biomass burning smoke aerosol properties measured during Fire Laboratory at Missoula Experiments (FLAME)," *J. Geophys. Res. Atmos.*, vol. 115, no. 18, pp. 1–15, 2010, doi: 10.1029/2009JD013601.

[86] R. Esworthy, "Air Quality: EPA's 2013 Changes to the Particulate Matter (PM) Standard," *Washington, DC, USA Congr. Res. Serv.*, 2013.

[87] C. A. Pope, D. W. Dockery, J. D. Spengler, and M. E. Raizenne, "Respiratory Health and PM 10 Pollution," *Am. Rev. Respir. Dis.*, vol. 144, pp. 668–674, 1991, doi: https://doi.org/10.1164/ajrccm/144.3_Pt_1.668.

[88] S. Feng, D. Gao, F. Liao, F. Zhou, and X. Wang, "Ecotoxicology and Environmental Safety The health effects of ambient PM 2 . 5 and potential mechanisms," *Ecotoxicol. Environ. Saf.*, vol. 128, pp. 67–74, 2016, doi: 10.1016/j.ecoenv.2016.01.030.

[89] R. Jan, R. Roy, S. Yadav, and P. G. Satsangi, "Exposure assessment of children to particulate matter and gaseous species in school environments of Pune , India concentration followed the similar pattern for both sized fraction of PM and the trend was," *Build. Environ.*, vol. 111, pp. 207–217, 2017, doi: 10.1016/j.buildenv.2016.11.008.

[90] W. Phairuang, P. Suwattiga, S. Hongtieab, and M. Inerb, "Characteristics, sources, and health risks of ambient nanoparticles (PM0.1) bound metal in Bangkok, Thailand," *Atmos. Environ. X*, vol. 12: 100141, 2021.

[91] R. M. Harrison, "Airborne particulate matter," *Philos. Trans. R. Soc. A*, vol. 378(2183), 2020.

[92] W. H. Organization, *Air quality guidelines: global update 2005:*

particulate matter, ozone, nitrogen dioxide, and sulfur dioxide. World Health Organization, 2006.

[93] T. Chen, Y. Liu, and Q. Ma, "Significant source of secondary aerosol: formation from gasoline evaporative emissions in the presence of SO2 and NH3," *Atmos. Chem. Phys.*, vol. 2005, pp. 8063–8081, 2019.

[94] P. J. Ziemann and R. Atkinson, "Kinetics, products, and mechanisms of secondary organic aerosol formation," *Chem. Soc. Rev.*, vol. 41(19), pp. 6582–6605, 2012, doi: 10.1039/c2cs35122f.

[95] M. Obaidullah, "Particle Emissions from Small Scale Biomass Combustion Appliences," *Belgium Vrije Univ. Brussels*, 2014, doi: 10.13140/RG.2.2.21908.35206.

[96] R. J. Olave, E. G. A. Forbes, C. R. Johnston, and J. Relf, "Particulate and gaseous emissions from different wood fuels during combustion in a small-scale biomass heating system," *Atmos. Environ.*, vol. 157, pp. 49–58, 2017, doi: 10.1016/j.atmosenv.2017.03.003.

[97] J. Sciare, R. Sarda-este, L. Martinon, and O. Favez, "Evidence for a significant contribution of wood burning aerosols to PM2.5 during the winter season in Paris, France Olivier," *Atmos. Environ.*, vol. 43, pp. 3640–3644, 2009, doi: 10.1016/j.atmosenv.2009.04.035.

[98] J. JCain, A. Laskin, and R. Kholghy M, "Molecular Characterization of Organic Content of Soot along the Centerline of a Coflow Diffusion Flame," *Phys. Chem. Chem. Phys.*, vol. 16(47), pp. 25862–25875, 2014.

[99] M. R. Kholghy, A. Veshkini, and M. J. Thomson, "The core-shell internal nanostructure of soot-A criterion to model soot maturity," *Carbon N. Y.*, vol. 100, pp. 508–536, 2016, doi: 10.1016/j.carbon.2016.01.022.

[100] M. Frenklach, "Reaction mechanism of soot formation in flames," *Phys. Chem. Chem. Phys.*, vol. 4(11), pp. 2028–2037, 2002, doi: 10.1039/b110045a.

[101] M. Frenklach and H. A. I. Wang, "Detailed soot modelling in laminar and turbulent reacting flows," *Symp. Combust.*, vol. 23(1), pp. 1559–1566, 1991.

[102] M. Obaidullah, S. Bram, and J. De Ruyck, "An Overview of PM Formation Mechanisms from Residential Biomass Combustion and Instruments Using in PM Measurements," *Int. J. Energy Environ.*, vol. 12, pp. 41–50, 2018.

[103] D. R. Tree and K. I. Svensson, "Soot processes in compression ignition engines," *Prog. energy Combust. Sci.*, vol. 33, pp. 272–309, 2007, doi: 10.1016/j.pecs.2006.03.002.

[104] M. M. Maricq, "Coagulation dynamics of fractal-like soot aggregates," *J. Aerosol Sci.*, vol. 38, pp. 141–156, 2007, doi: 10.1016/j.jaerosci.2006.11.004.

[105] K. Dewa, K. Ono, A. Watanabe, and K. Takahashi, "Evolution of size

distribution and morphology of carbon nanoparticles during ethylene pyrolysis," *Combust. Flame*, vol. 163, pp. 115–121, 2016, doi: 10.1016/j.combustflame.2015.09.007.

[106] C. Boman, A. Nordin, D. Bostro, and O. Marcus, "Characterization of Inorganic Particulate Matter from Residential Combustion of Pelletized Biomass Fuels," *Energy & Fuels*, vol. 48, no. 1, pp. 338–348, 2004.

[107] I. Obernberger, T. Brunner, and G. Ba, "Chemical properties of solid biofuels — significance and impact," *Biomass and Bioenergy*, vol. 30, pp. 973–982, 2006, doi: 10.1016/j.biombioe.2006.06.011.

[108] C. Boman, "Particulate and gaseous emissions from residential biomass combustion," 2005.

[109] O. Sippula, J. Hokkinen, H. Puustinen, P. Yli-pirila, and J. Jokiniemi, "Comparison of particle emissions from small heavy fuel oil and wood-fired boilers," *Atmos. Environ.*, vol. 43, no. 32, pp. 4855–4864, 2009, doi: 10.1016/j.atmosenv.2009.07.022.

[110] B. F. Carroll J P, Finnan J M, "Air staging to reduce emissions from energy crop combustion in small scale applications," *Fuel*, vol. 155, pp. 37–43, 2015.

[111] H. Khodaei, F. Guzzomi, D. Patiño, B. Rashidian, and G. H. Yeoh, "Air staging strategies in biomass combustion-gaseous and particulate emission reduction potentials," *Fuel Process. Technol.*, vol. 157, pp. 29–41, 2017, doi: 10.1016/j.fuproc.2016.11.007.

[112] T. Zadravec, B. Rajh, F. Kokalj, and N. Samec, "Influence of air staging strategies on flue gas sensible heat losses and gaseous emissions of a wood pellet boiler_ An experimental study," *Renew. Energy*, vol. 178, pp. 532–548, 2021.

[113] O. Skreiberg, P. Glarborgb, A. Jensenb, and K. Dam-johansenb, "Kinetic NO , modeling and experimental results from single wood particle combustion," *Fuel*, vol. 76, no. 7, pp. 671–682, 1997.

[114] T. R. Saastamoinen J J, "NO x formation in grate combustion of wood," *Int. J. Energy a Clean Environ.*, vol. 4, no. 3, pp. 1–29, 2003.

[115] H. Lamberg, O. Sippula, J. Tissari, and J. Jokiniemi, "Effects of air staging and load on fine-particle and gaseous emissions from a small-scale pellet boiler," *Energy and Fuels*, vol. 25, no. 11, pp. 4952–4960, 2011, doi: 10.1021/ef2010578.

[116] S. Ø. Houshfar E, Løvås T, "Experimental investigation on NOx reduction by primary measures in biomass combustion: straw, peat, sewage sludge, forest residues and wood pellets," *Energies*, vol. 5, pp. 270–290, 2012, doi: 10.3390/en5020270.

[117] G. Qiu, "Testing of fl ue gas emissions of a biomass pellet boiler and

abatement of particle emissions," *Renew. Energy*, vol. 50, pp. 94–102, 2013, doi: 10.1016/j.renene.2012.06.045.

[118] G. Caposciutti, F. Barontini, M. Antonelli, L. Tognotti, and U. Desideri, "Experimental investigation on the air excess and air displacement in fl uence on early stage and complete combustion gaseous emissions of a small scale fi xed bed biomass boiler," *Appl. Energy*, vol. 216, pp. 576–587, 2018, doi: 10.1016/j.apenergy.2018.02.125.

[119] Y. Li, Y. Lin, J. Zhao, B. Liu, and T. Wang, "Control of NOx emissions by air staging in small- and medium-scale biomass pellet boilers Control of NOx emissions by air staging in small-and medium-scale biomass pellet boilers," *Environ. Sci. Pollut. Res.*, vol. 26, no. 10, pp. 9717–9729, 2019, doi: 10.1007/s11356-019-04396-8.

[120] J. P. Carroll, J. M. Finnan, F. Biedermann, T. Brunner, and I. Obernberger, "Air staging to reduce emissions from energy crop combustion in small scale applications," *Fuel*, vol. 155, pp. 37–43, 2015, doi: 10.1016/j.fuel.2015.04.008.

[121] F. Biedermann, T. Brunner, I. Obernberger, and O. Sippula, "Summary and Evaluation of Existing Data on Air Staging Strategies," 2012.

[122] H. Wiinikka and R. Gebart, "Critical parameters for particle emissions in small-scale fixed-bed combustion of wood pellets," *Energy and Fuels*, vol. 18, no. 4, pp. 897–907, 2004, doi: 10.1021/ef030173k.

[123] P. M. Fine, G. R. Cass, and B. R. T. Simoneit, "Chemical Characterization of Fine Particle Emissions from the Wood Stove Combustion of Prevalent United States Tree Species," *Environ. Eng. Sci.*, vol. 21, no. 6, pp. 705–721, 2004.

[124] R. W. Weeks and W. W. Duley, "Aerosol-particle sizes from light emission during excitation by TEA CO 2 laser pulses," *J. Appl. Phys.*, vol. 45, no. 10, pp. 4661–4662, 1974, doi: 10.1063/1.1663111.

[125] A. C. Eckbreth, *Laser Diagnostics for combustion temperature and species measurements*. Gordon and Breach Publishers, 1989.

[126] L. A. Melton, "Soot Diagnostics Based on Laser Heating.," *Chem. Phys. Process. Combust. Fall Tech. Meet. East. States Sect.*, vol. 23, no. 13, 1983, doi: 10.1364/ao.23.002201.

[127] P. Desgroux, X. Mercier, and K. A. Thomson, "Study of the formation of soot and its precursors in flames using optical diagnostics," *Proc. Combust. Inst.*, vol. 34, no. 1, pp. 1713–1738, 2013, doi: 10.1016/j.proci.2012.09.004.

[128] H. A. Michelsen, C. Schulz, G. J. Smallwood, and S. Will, "Laser-induced incandescence: Particulate diagnostics for combustion, atmospheric, and industrial applications," *Prog. Energy Combust. Sci.*, vol. 51, pp. 2–48, 2015, doi:

10.1016/j.pecs.2015.07.001.

[129]H. A. Michelsen, F. Liu, B. F. Kock, and H. Bladh, “Modeling laser-induced incandescence of soot: A summary and comparison of LII models,” *Appl. Phys. B Lasers Opt.*, vol. 87, no. 3, pp. 503–521, 2007, doi: 10.1007/s00340-007-2619-5.

[130]B. J. Mccoy and C. Y. Cha, “Transport phenomena in the rarefied gas transition regime,” *Chem. Eng. Sci.*, vol. 29, no. 4, pp. 381–388, 1974.

[131]NGO Thi Linh Dan, “Characterization of soot particles and their precursors produced during the combustion of conventional and alternative fuels : an in-situ laser diagnostics and ex-situ mass spectrometry investigation,” University of Lille, 2019.

[132]T. Ni, J. A. Pinson, S. Gupta, and R. J. Santoro, “Two-dimensional imaging of soot volume fraction by the use of laser-induced incandescence,” *Appl. Opt.*, vol. 34, no. 30, p. 7083, 1995, doi: 10.1364/ao.34.007083.

[133]K. C. Shaddix, C. R., Harrington, J.E., Smyth, “Quantitative measurements of enhanced soot production in a flikering methane air diffusion flame,” *Combust. Flame*, vol. 99, pp. 723–732, 1994.

[134]B. Axelsson, R. Collin, and P. E. Bengtsson, “Laser-induced incandescence for soot particle size and volume fraction measurements using on-line extinction calibration,” *Appl. Phys. B Laser Opt.*, vol. 372, pp. 367–372, 2001.

[135]R. L. Vander Wal and B. Park, “Laser-Induced Incandescence Calibration via Gravimetric Sampling,” *Combust. Flame*, no. June, pp. 426–470, 1996.

[136]M. X. Schoemaecker Moreau C, Therssen E, “Two-color laser-induced incandescence and cavity ring-down spectroscopy for sensitive and quantitative imaging of soot and PAHs in flames,” *Appl. Phys. B Laser Opt.*, vol. 492, pp. 485–492, 2004, doi: 10.1007/s00340-003-1370-9.

[137]R. L. Vander Wal, “Laser-induced incandescence : excitation and detection conditions , material transformations and calibration,” *Appl. Phys. B Laser Opt.*, vol. 96, pp. 601–611, 2009, doi: 10.1007/s00340-009-3521-0.

[138]C. H. Jeong and G. J. Evans, “Inter-comparison of a fast mobility particle sizer and a scanning mobility particle sizer incorporating an ultrafine water-based condensation particle counter,” *Aerosol Sci. Technol.*, vol. 43, no. 4, pp. 364–373, 2009, doi: 10.1080/02786820802662939.

[139]F. Liu and G. J. Smallwood, “The effect of particle aggregation on the absorption and emission properties of mono- and polydisperse soot aggregates,” *Appl. Phys. B Lasers Opt.*, vol. 104, no. 2, pp. 343–355, 2011, doi: 10.1007/s00340-011-4382-x.

[140]J. Yon, E. Therssen, F. Liu, S. Bejaoui, and D. Hebert, “Influence of

soot aggregate size and internal multiple scattering on LII signal and the absorption function variation with wavelength determined by the TEW-LII method," *Appl. Phys. B Lasers Opt.*, vol. 119, no. 4, pp. 643–655, 2015, doi: 10.1007/s00340-015-6116-y.

[141] C. Boman, E. Pettersson, R. Westerholm, D. Boström, and A. Nordin, "Stove performance and emission characteristics in residential wood log and pellet combustion, part 1: Pellet stoves," *Energy and Fuels*, vol. 25, no. 1, pp. 307–314, 2011, doi: 10.1021/ef100774x.

[142] S. Ozgen *et al.*, "Emission factors from small scale appliances burning wood and pellets," *Atmos. Environ.*, vol. 94, pp. 144–153, 2014, doi: 10.1016/j.atmosenv.2014.05.032.

[143] K. M. Win, T. Persson, and C. Bales, "Particles and gaseous emissions from realistic operation of residential wood pellet heating systems," *Atmos. Environ.*, vol. 59, pp. 320–327, 2012, doi: 10.1016/j.atmosenv.2012.05.016.

[144] G. R. Wiinikka H, "The influence of air distribution rate on particle emissions in fixed bed combustion of biomass," *Combust. Sci. Technol.*, vol. 177, no. 9, pp. 1747-1766., 2005.

Appendices

Appendix 1 Gaseous emissions produced by black pellets combustion

In this part, all the results obtained from the combustion of black pellets were presented and analyzed. Emissions of CO and THC were studied for experiments based on changes in primary airflow rate. For particle emissions, the emissions from the combustion of the black pellets are also analyzed by the LII method and by SMPS.

1. Analysis of nominal boiler operation

Experiments were performed under the same experimental conditions. That is the full power operation with the primary air outlet completely open and no secondary air supply. The temperature at the furnace outlet (point 1) was measured when the boiler is thermally stable and take samples from the chimney to measure the pollutant mole fraction (CO, CO_2 and THC). The following measurements are started after the boiler has reached a steady state (30 minutes later). Then sample in the chimney was analyzed for at least 20 minutes. This series of tests ensure the repeatability of the operation of the system.

Figure 1 (A) shows the average temperatures for the 4 tests at the furnace outlet (point 1). The data obtained were statistically analyzed by calculating the means and the standard deviations, the standard deviations are represented by the error bars. Just like the results of wood pellets, the temperatures obtained from each test are not repeatable, the maximum difference between them is as much as 10 °C, but the standard deviation of each test is less than one degree. Therefore, the system can be also considered thermally stable after entering a steady state.

Figure 1 (B) shows the means and standard deviations of flue gas mole fractions for the 4 tests (CO and THC corrected to 10% O_2) in the chimney. It was observed larger standard deviations for CO and THC in the experimental results for black pellets than for wood pellets. It has achieved 51% and 63% of the mean value, higher than wood pellets at 23% and 50%. The standard deviation of CO_2 and O_2 is relatively small, only 4.6% and 15% of the mean value. But still higher than wood pellets at 3.8% and 11.4%.

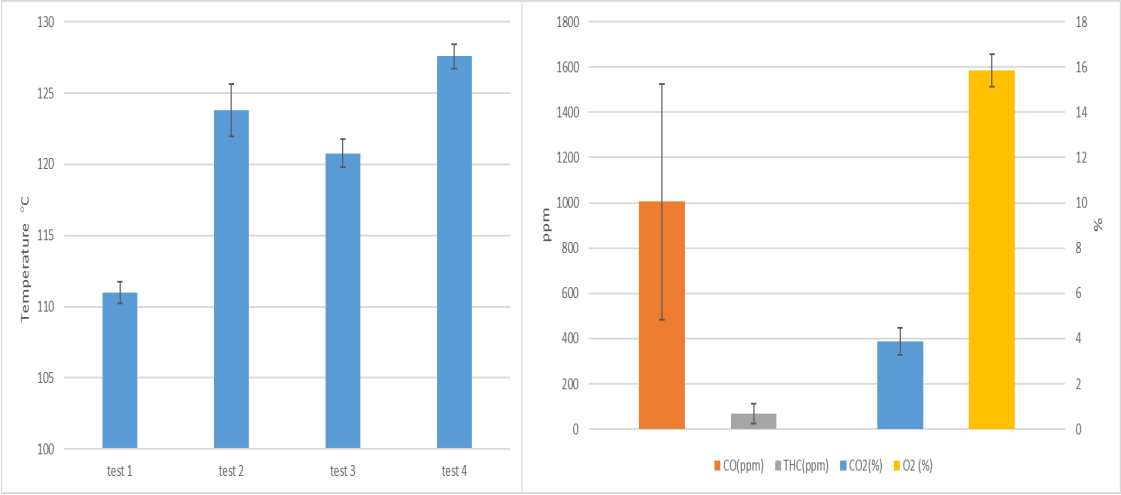

(A) **(B)**

Figure A1-1 (A) Average temperatures for the 4 tests at the furnace outlet (point 1), (B) Average flue gas mole fractions for the 4 tests (CO, THC corrected to 10% O_2)

The conversion of the mole fraction values into emission factors is done by equation 4-2. Figure 2 shows the average value of the emission factor of CO and THC for black pellets.

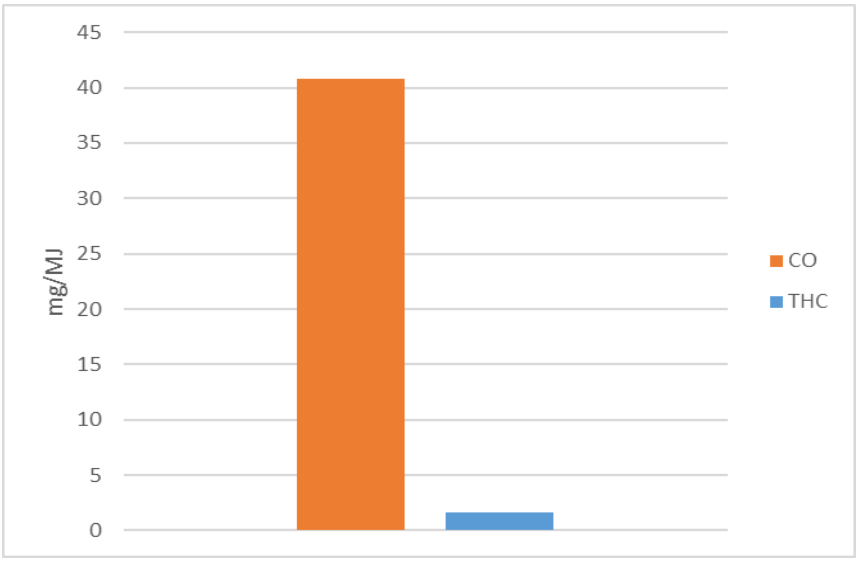

Figure A1-2 Averages value of the emission factor of CO and THC for black pellets.

2. Influence of primary airflows rate on gases emissions

In this subsection, the effect of the primary airflow rate on the emission of gaseous pollutants from the combustion of black particles were investigated. As in the wood pellet experiments, the inlet airflow rate was adjusted by manually adjusting the coverage cross-sectional area. During the experiments, the secondary air inlet was blocked and tested the boiler under the condition of only the primary airflow supply.

The pollutant mole fractions of different primary air flow rates were measured on different test days to compare the effects of primary air flow rate on gaseous pollutants. Gaseous pollutant mole fractions in the flame and the chimney were simultaneously sampled for at least 20 minutes after the boiler has reached a steady state. The mole fraction of gaseous pollutants in the chimney are the average values of the measurements corrected to 10% O_2.

Consider the results in terms of the final pollutant mole fraction, having observed the evolution of the gaseous emission mole fraction in the flame with the primary air flow rate. Due to the limitations of instrumentation here, there are only the data on the mole fraction of CO and THC in the chimney. These results are from different test days, and each value is an average of at least 20 minutes of measurements.

From Figure 3, it presented the results of black pellets showing that the mole fraction of both CO and THC decreases with the increase of primary airflow rate. The lowest point of CO mole fraction occurs at the highest point of the primary gas flow rate. When the primary air flow rate is equal to 5.3g/s, the CO mole fraction is 5304 ppm. Afterward, with the increase of the primary gas flow rate, the CO mole fraction decreased rapidly. The lowest value of CO mole fraction as 531ppm when the primary air flow rate is equal to 7.5g/s (the maximum value of the primary air flow rate in the measurement). It was found that the highest CO mole fraction values were almost ten times higher than the lowest values.

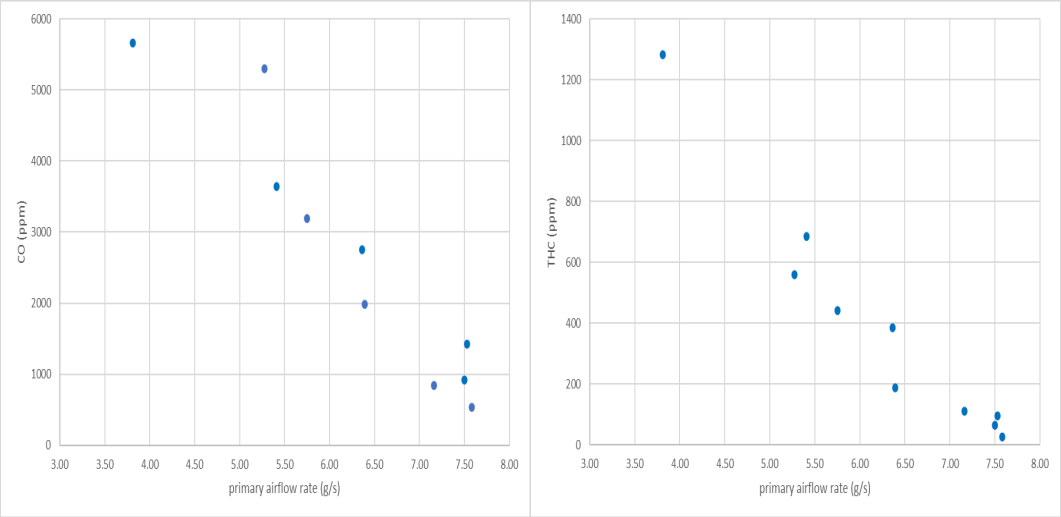

Figure A1-3 Evolution of gaseous emissions (CO, THC) in the chimney as a function of the primary airflow rate in the condition without secondary air supply (corrected to 10% O_2)

It was also observed similar results for THC. The lowest point of THC mole fraction is still when the primary air volume is 7.5 g/s, and the THC mole fraction measured at this time is 26 ppm. The highest THC mole fraction is when the primary air flow rate is also equal to 5.3 g/s, and the THC mole fraction at this time is about 560ppm. It was still observed that the mole fraction of THC decreased rapidly with the increase in primary air intake, and the highest THC mole fraction value was almost 21 times that of the lowest value.

Such results show that, for black particles, keeping the maximum airflow rate without blocking the air inlet is an effective way to reduce the two pollutants of CO and THC. Since the growth of pollutants is very fast after reducing the primary airflow rate, any measure of reducing the primary air supply is unwise for pollutant emissions.

Appendix 2 Particulate emissions produced by black pellets combustion

1. Particulate emissions by LII

- **Decay time**

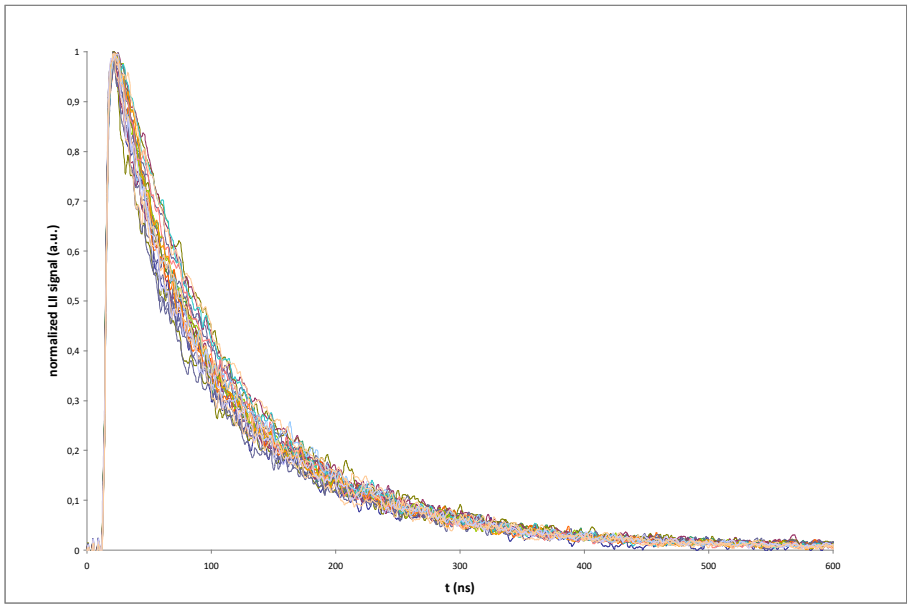

Figure A2-1 LII decay during a test of 30 min (30 signals each integrated during around 1 min of 512 laser shots). The black pellets are burning with the maximum primary air flow.

Figure 4 shows the decay of the LII signal during the 30 minutes test under the condition of black particles burning with maximum primary airflow. It was found that the decay time is really reproducible. This shows that the particle diameter is stable during this test.

The decay time (for the reference of 1/e2 of the LII peak) is around 200 ns very shorter than the one for wood pellets (chapter 4), meaning that the soot produced by black pellets combustion are smaller.

- **LII Soot Temperature**

The soot temperature for black pellet combustion can be calculated using equations 4-30 and the two LII signals at different wavelengths (750 and 850 nm).

Figure 5 shows the evolution of the soot temperature within 60 minutes, and each point in the figure is the average temperature of the soot temperature within 1 minute. It was found that the soot temperature of black pellets is unstable with time. The relative temperature variation ($\Delta T/\overline{T}$) is around 20%. But in fact, for each point in this figure, the soot volume fraction is calculated.

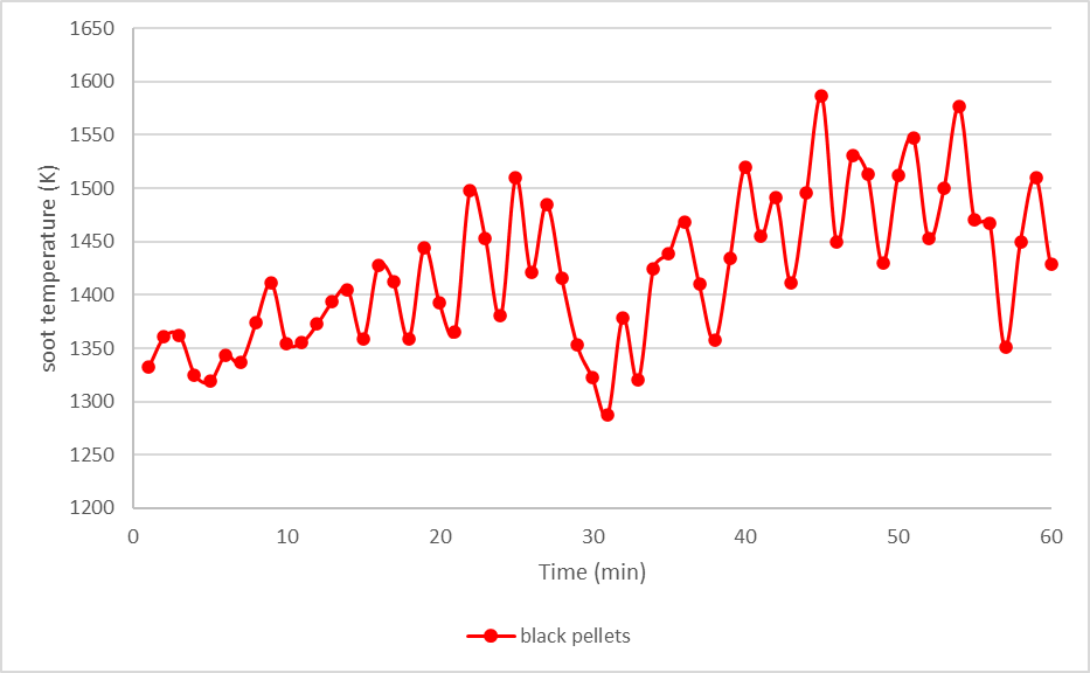

Figure A2-2 Evolution of soot temperature over 60 minutes

- **Soot volume fraction**

Figure 6 shows the evolution of soot volume fraction within 60 minutes under the condition of maximum primary airflow rate.

Again, for black pellets (comparing wood pellets in chapter 4), it is not difficult to observe that the volume fraction of soot produced by the combustion is not stable, that is, it fluctuates irregularly with time. The reason for the relatively high fluctuation may be that the flame of the boiler is unstable. For this test, the average value is 79 ppb over 60 minutes.

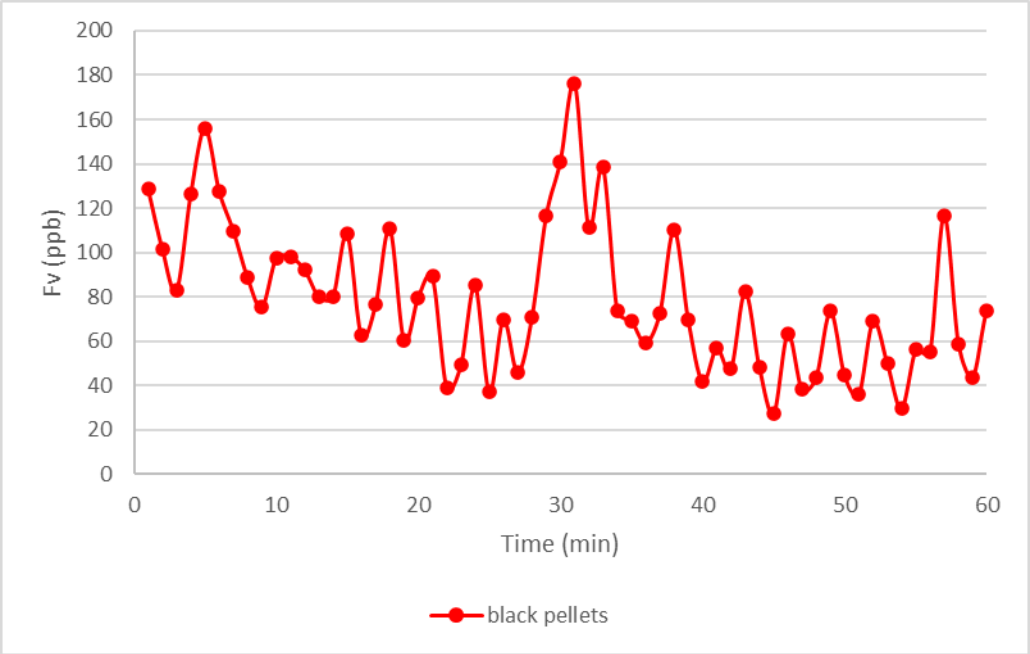

Figure A2-3 Evolution of soot temperature over 60 minutes for black pellets

Figure 7 shows the variation of soot volume fraction in the chimney with the primary airflow rate in the absence of secondary air supply. There is a similar curve to wood pellets. With the increase in primary air flow rate, the volume fraction of soot decreased significantly. The soot volume fraction at the minimum airflow rate (5.2 g/s) is 800 times higher than that at the maximum airflow rate (7.5 g/s). Even when the primary gas flow rate is reduced from 7.5 g/s to 7.2 g/s, the soot volume fraction increases significantly. The primary airflow rate has a great influence on the volume fraction of soot. Reducing the primary airflow rate can greatly increase chimney emissions.

Again, equation 4-2 converts the soot volume fraction into an emission factor. The emission factor of black pellets is 12.8 mg/MJ. The data is the average value within 60 minutes under the maximum condition of the primary airflow rate.

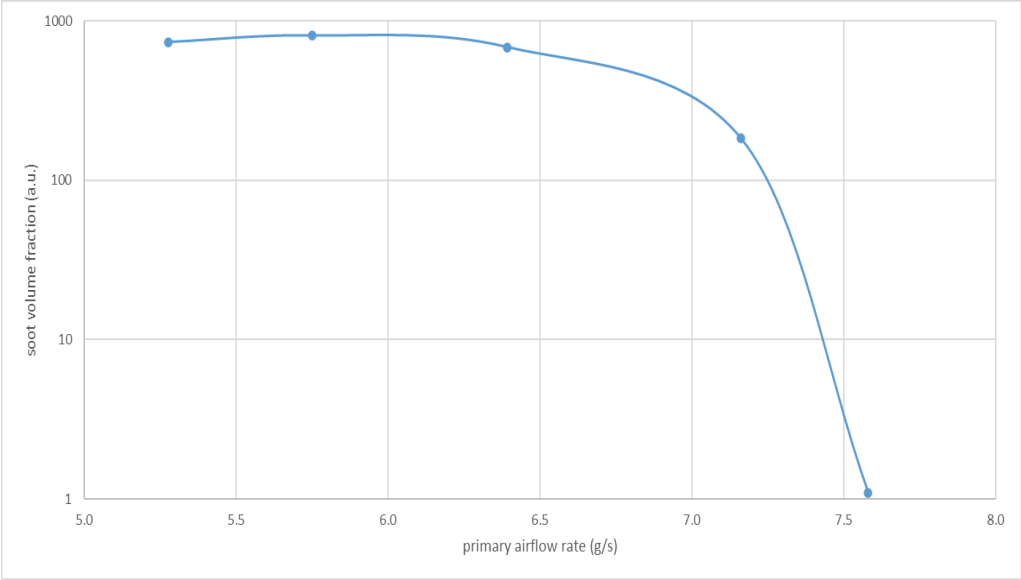

Figure A2-4 The evolution of soot volume fraction as a function of the primary airflow rate (corrected to 10% O_2)

2. Particulate emissions by SMPS

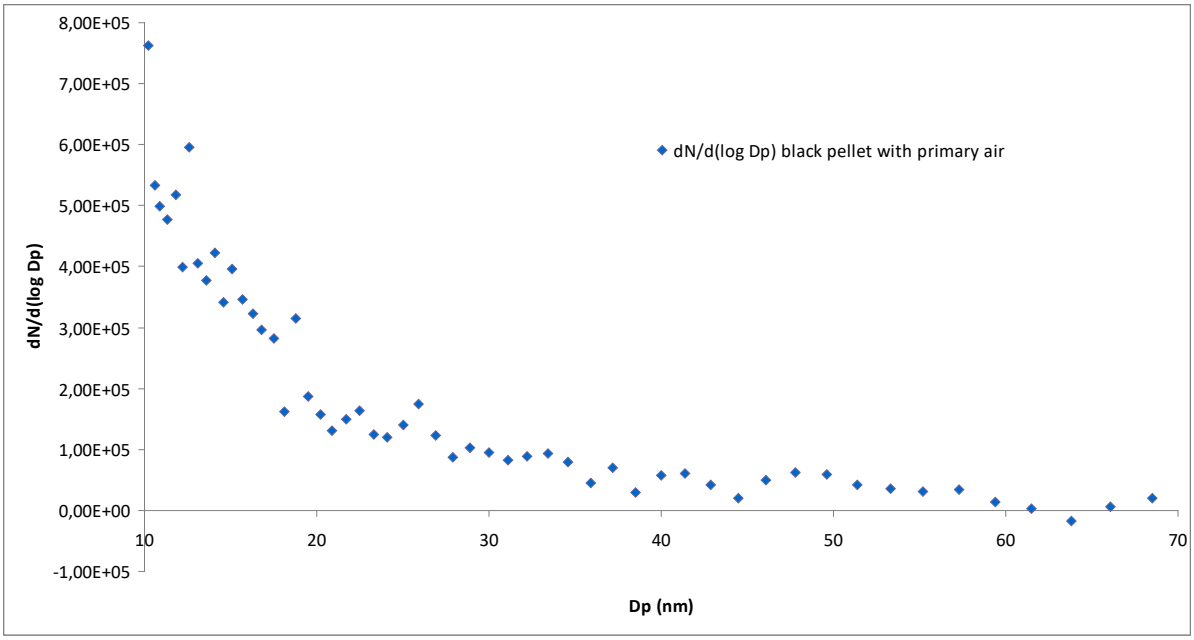

Figure A2-5 Particle diameter distribution curves for black pellets

Figure 8 shows the particle diameter distribution curves for black pellets. It is the non-modal distribution due to the sensitivity of SMPS (10 nm).

Appendix 3 Typical evolution of combustion gases during a full test

Figure 9 and figure 10 show the evolution of CO_2, O_2, CO and THC during a full test. The evolution of the measured gases at steady state is relatively stable. Emissions of pollutants CO and THC vary drastically during ignition and extinguishing phases. When ignition is complete, oxygen is consumed and the concentration decreases, and CO_2 is produced and the concentration increases. The extinguishing phase is the opposite.

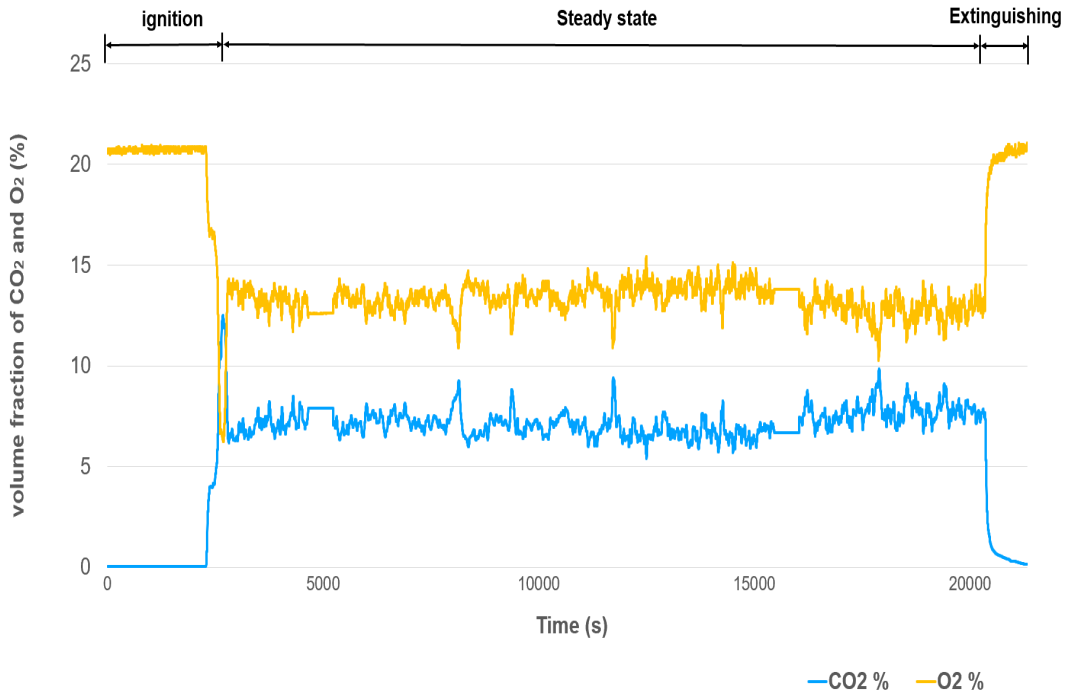

Figure A3-1 Evolution of CO_2 and O_2 during a full test

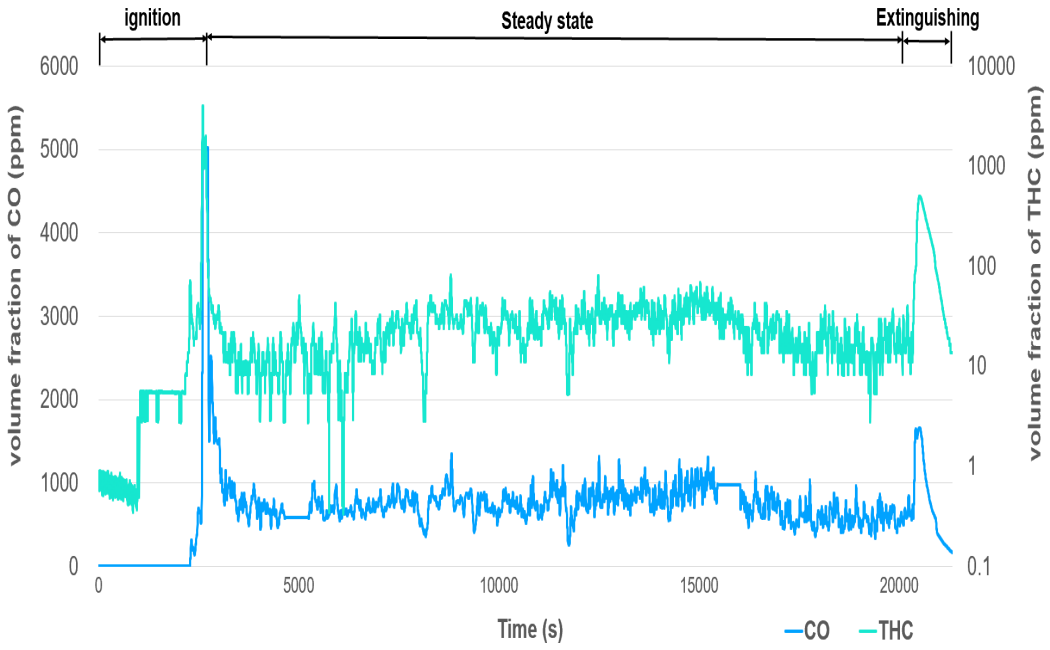

Figure A3-2 Evolution of CO and THC during a full test